

**CROSS-SHORE NUMERICAL MODEL CSHORE FOR
WAVES, CURRENTS, SEDIMENT TRANSPORT
AND BEACH PROFILE EVOLUTION**

by

Nobuhisa Kobayashi and Ali Farhadzadeh

**Sponsored by
U. S. Army Corps of Engineers
Engineering Research and Development Center**

RESEARCH REPORT NO. CACR-08-01

SEPTEMBER, 2008



CENTER FOR APPLIED COASTAL RESEARCH

Ocean Engineering Laboratory
University of Delaware
Newark, Delaware 19716

ACKNOWLEDGEMENT

This study has been supported by the U.S. Army Corps of Engineers under Contract Nos. W912BU-08-C-0014, W912HZ-07-P-0311 and W912HZ-08-P-0342.

The authors would like to thank the researchers who participated in the development of the computer program CSHORE.

TABLE OF CONTENTS

Abstract

1. Introduction.....	5
2. History of CSHORE Development.....	7
3. Wave and Current Models	13
4. Combined Wave and Current Model CSHORE	20
5. Sediment Transport Model	28
6. Permeable Layer Model.....	35
7. Irregular Wave Runup and Overtopping.....	40
8. Probabilistic Model for Intermittently Wet Zone	46
8.1 Water depth and velocity	46
8.2 Sediment transport	53
9. Wave Overtopping and Overflow on Levees.....	57
9.1 Wave overtopping and overflow experiments	58
9.2 Comparison of EurOtop formulas with experiments	61
9.3 Comparison of CSHORE empirical formulas with experiments.....	64
9.4 Comparison of CSHORE wet and dry model with experiments	67
9.5 Comparisons with Dutch experiments.....	71
9.6 Representative wave periods $T_{m-1,0}$ and T_p	82
10. Computer Program CSHORE.....	88
10.1 Main program.....	89
10.2 Subroutines	91

10.3 Input	97
10.4 Output	103
11. Conclusions.....	115
References.....	116

ABSTRACT

The majority of the world shoreline is currently suffering from erosion. Beach erosion will become more serious if the mean sea level rise accelerates because of the greenhouse effect. Nourishment and maintenance of wide sand beaches for developed coastal communities will become more expensive unless the present nourishment design method is improved by the development of a reliable morphological model. Concurrently, the recent increase of coastal storm damage demands the development of numerical models for predicting the damage progression and breaching of coastal stone structures and earthen levees during extreme storms. This report summarizes our continuing effort to improve our quantitative understanding of beach morphology and structural damage progression with the goal to develop simple and robust models that are suited for engineering applications. Our effort for the last 10 years has produced the cross-shore numerical model CSHORE which is presently limited to the case of alongshore uniformity. CSHORE consists of the following components: a combined wave and current model based on time-averaged continuity, cross-shore and longshore momentum, wave action, and roller energy equations; a sediment transport model for suspended sand and bedload; a permeable layer model to account for porous flow and energy dissipation; empirical formulas for irregular wave runup, overtopping and seepage; and a probabilistic model for an intermittently wet and dry zone for the purpose of predicting wave overwash and structural damage progression. The wet and dry model, which is the latest addition to CSHORE, is calibrated and verified using our 107 small-scale tests for irregular wave overtopping and overflow on a levee as well as 118 Dutch tests for low-exceedance wave overtopping in which velocities and water depths were measured on the crest and landward (inner) slope of dikes. Finally, the computer program CSHORE is explained so that a user of CSHORE will be able to use it effectively and modify it if necessary. In the near future, CSHORE will be compared with wave overwash experiments and structural damage progression experiments.

1. Introduction

A sand beach with a wide berm and a high dune provides storm protection and damage reduction, recreational and economical benefits and biological habitats for plants and animals. Most sandy beaches are eroding partly due to sea level rise. Beach nourishment is widely adopted to maintain a wide beach for a developed coastal community if a suitable beachfill is available in the vicinity of an eroding beach. Empirical methods based on field data have been developed for the design of beach fills (Coastal Engineering Manual 2003). The design of the cross-shore beachfill profile is normally based on the concept of an equilibrium beach profile. The alongshore spreading of the beachfill is generally predicted using a one-line model coupled with the CERC formula or the formula by Kamphuis (1991) for the longshore sediment transport rate. These simple beachfill design methods have been criticized and a number of more process-based models have been proposed. However, the process-based models may not necessarily be more accurate at present.

Sediment transport is caused by the combined action of waves and currents. Our capabilities of predicting wave and current fields have improved steadily for the last 30 years. However, the predictive capability of sediment transport on beaches has not improved much. The major reason for this discrepancy is that no dynamic equation is available to describe the motion of a large number of sediment particles. Consequently, sediment transport models are essentially empirical and dependent on reliable sediment transport data. Unfortunately, sediment dynamics on beaches are highly complex and involve wide ranges of morphological scales in time and space. Correspondingly, available sediment transport models have become more complex and less transparent. We have tried to synthesize available data and formulas in order to develop

simple and transparent formulas for the cross-shore and longshore transport rates of suspended sand and bedload on beaches. The simple formulas need to include basic sediment dynamics sufficiently so that the formulas will be applicable to small-scale and large-scale laboratory beaches and eventually prototype beaches. Furthermore, the morphological model should be very efficient computationally because the model will need to be calibrated and verified using extensive data sets. The hydrodynamic input required for the morphological model should be limited to the quantities that can be predicted routinely and reliably. These considerations have guided our development of the cross-shore model CSHORE presented in this report.

Coastal storm damage has been increasing mostly due to the recent growth of coastal population and assets and possibly due to the intensification of hurricanes caused by global warming. Coastal structures including earthen levees (dikes) have been designed conventionally for no storm surge overflow and minor wave overtopping during a design storm. Empirical formulas for wave overtopping rates are used for a preliminary design where EurOtop Manual (2007) recommends the latest formulas. Physical model testing is normally conducted in a wave flume or basin for a detailed design. Various numerical models have also been developed to predict detailed hydrodynamics that are difficult to measure even in a laboratory (Kobayashi and Otta 1987; Kobayashi 1999; van Gent 2001). The latest numerical models for hydrodynamics are reviewed by Losada et al. (2008) and Neves et al. (2008). However, our improved predictive capabilities for the hydrodynamics have not really improved our predictive capability for damage progression partly because damage to a coastal structure is cumulative (Melby and Kobayashi 1998). As a result, a performance or risk-based design of a coastal structure relies on empirical formulas for damage (e.g., Kobayashi et al. 2003). This practical difficulty is similar to that for

sediment transport on beaches. Alternatively, the computationally-efficient CSHORE calibrated with extensive data sets has been developed for the design of inclined structures with relatively small wave reflection where damage progression models for stone structures and earthen levees will be developed by modifying the sediment transport model in this report. The eventual goal is to predict the performance of an inclined structure located on a movable bottom.

2. History of CSHORE Development

The history of the cross-shore model CSHORE is summarized to provide an overview of CSHORE and acknowledge a number of graduate students and visiting scientists who contributed to the development of CSHORE. The present version of CSHORE includes the various capabilities added to the initial CSHORE developed in 1998. The different stages of the CSHORE development are summarized in the following where the detail of each stage can be found in the listed publications.

The cross-shore model CSHORE was initially developed to predict the cross-shore transformation of irregular nonlinear waves using the time-averaged continuity, momentum and wave energy equations together with a non-Gaussian probability distribution of the free surface elevation. However, empirical formulas of limited generality were required to parameterize the wave nonlinearity. The present version of CSHORE is based on linear wave theory and the Gaussian probability distribution to reduce the degree of empiricism.

- Kobayashi, N., Herrman, M.N., Johnson, B.D., and Orzech, M.D. (1998). “Probability distribution of surface elevation in surf and swash zones.” *J. Waterway, Port, Coastal and Ocean Eng.*, 124(3), 99-107.

- Kobayashi, N., and Johnson, B.D. (1998). “Computer program CSHORE for predicting cross-shore transformation of irregular breaking waves.” Res. Rep. No. CACR-98-04, Center for Applied Coastal Research, Univ. of Delaware, Newark, Del.
- Johnson, B.D., and Kobayashi, N. (1998). “Nonlinear time-averaged model in surf and swash zones.” Proc. 26th Coastal Eng. Conf., ASCE, 2785-2798.
- Kearney, P.G., and Kobayashi, N. (2000). “Time-averaged probabilistic model for irregular wave runup on coastal structures.” Proc. 27th Coastal Eng. Conf., ASCE, 2004-2017.
- Johnson, B.D., and Kobayashi, N. (2000). “Free surface statistics and probabilities in surf zones on beaches.” Proc. 27th Coastal Eng. Conf., ASCE, 1022-1035.

The next stage of the CSHORE development was motivated by the need of a computationally-efficient time-averaged model that can be used for the design of porous coastal structures. The linear-wave version of the initial CSHORE was modified to account for the effects of a permeable layer for the case of normally incident waves. The permeable version of CSHORE was called CSHOREP. The impermeable and permeable versions of CSHORE have been merged in the present CSHORE in order to expand the range of practical applications. The permeability effects are extended to obliquely incident waves in the present CSHORE.

- Meigs, L.E., and Kobayashi, N. (2004). “Time-averaged model for irregular breaking waves on porous structures and beaches.” Res. Rep. No. CACR-04-02, Center for Applied Coastal Res., Univ. of Delaware, Newark, Del.
- Meigs, L.E., Kobayashi, N., and Melby, J.A. (2004). “Cobble beaches and revetments.” Proc. 29th Coastal Eng. Conf., World Scientific, 3865-3877.

- de los Santos, F.J., and Kobayashi, N. (2005). “Irregular wave setup and runup on cobble beaches and revetments.” Res. Rep. No. CACR-05-06. Center for Applied Coastal Res., Univ. of Delaware, Newark, Del.
- Ota, T., Kobayashi, N., and Kimura, A. (2006). “Irregular wave transformation over deforming submerged structures.” Proc. 30th Coastal Eng. Conf., World Scientific, 4945-4956.
- de los Santos, F.J., Kobayashi, N., and Losada, M. (2006). “Irregular wave runup and overtopping on revetments and cobble beaches.” Proc. 30th Coastal Eng. Conf., World Scientific, 4667-4679.
- de los Santos, F.J., and Kobayashi, N. (2006). “Irregular wave seepage and overtopping of cobble beaches and revetments.” Res. Rep. No. CACR-06-01, Center for Applied Coastal Res., Univ. of Delaware, Newark, Del.
- Kobayashi, N., Meigs, L.E., Ota, T., and Melby, J.A. (2007). “Irregular breaking wave transmission over submerged porous breakwaters.” J. Waterway, Port, Coastal, Ocean Eng., 133(2), 104-116.
- Kobayashi, N., and de los Santos, F.J. (2007). “Irregular wave seepage and overtopping of permeable slopes.” J. Waterway, Port, Coastal, Ocean Eng., 133(4), 245-254.
- Ota, T., Matsumi, Y., Kobayashi, N., and Kimura, A. (2007). “Influence of damage progression on performance of rubble mound breakwaters.” Proc. Coastal Structures’2007, Venice, Italy.
- Kobayashi, N., de los Santos, F.J., and Kearney, P.G. (2008). “Time-averaged probabilistic model for irregular wave runup on permeable slopes.” J. Waterway, Port, Coastal, Ocean Eng., 134(2), 88-96.

Concurrently, the impermeable version of CSHORE was extended to predict the cross-shore and longshore transport rates of suspended sand and bedload on beaches as a part of the MORPHOS project of the U.S. Army Engineer Research and Development Center. MORPHOS is the world's first attempt at developing an open-source, physics-based computer model of coastal storms and their impact that can be used by the broad coastal community. A series of extensions were made in the following publications to make CSHORE more versatile and better verified.

- Zhao, H., and Kobayashi, N. (2005). "Suspended sand transport in surf zones on equilibrium beaches." Res. Rep. No. CACR-05-01, Center for Applied Coastal Res., Univ. of Delaware, Newark, Del.
- Kobayashi, N., Zhao, H., and Tega, Y. (2005). "Suspended sand transport in surf zone." *J. Geophys. Res.*, 110, C12009, doi:10.1029/2004JC002853.
- Agarwal, A., and Kobayashi, N. (2005). "Time-averaged model for longshore current and sediment transport in surf and swash zones." Res. Rep. No. CACR-05-07, Center for Applied Coastal Res., Univ. of Delaware, Newark, Del.
- Schmied, L., Kobayashi, N., Payo, A., and Puleo, J.A. (2006). "Cross-shore sediment transport and beach profile change." Res. Rep. No. CACR-06-03, Center for Applied Coastal Res., Univ. of Delaware, Newark, Del.
- Schmied, L.D., Kobayashi, N., Puleo, J.A., and Payo, A. (2006). "Cross-shore suspended sand transport on beaches." *Proc. 30th Coastal Eng. Conf.*, World Scientific, 2511-2523.
- Agarwal, A., Kobayashi, N., and Johnson, B.D. (2006). "Longshore suspended sediment transport in surf and swash zones." *Proc. 30th Coastal Eng. Conf.*, World Scientific, 2498-2510.

- Payo, A., Kobayashi, N., and Kim, K.H. (2006). “Beach nourishment strategies.” Proc. 30th Coastal Eng. Conf., World Scientific, 4129-4140.
- Kobayashi, N., Agarwal, A., and Johnson, B.D. (2007). “Longshore current and sediment transport on beaches.” J. Waterway, Port, Coastal, Ocean Eng., 133(4), 296-304.
- Buck, M., Kobayashi, N., Payo, A., and Johnson, B.D. (2007). “Experiments and numerical model for berm and dune erosion.” Res. Rep. No. CACR-07-03, Center for Applied Coastal Res., Univ. of Delaware, Newark, Del.
- Gencarelli, R., Johnson, B.D., Kobayashi, N. and Tomasicchio, G.R. (2007). “Dune erosion and breaching.” Proc. Coastal Structures’2007, Venice, Italy.
- Kobayashi, N., Payo, A., and Schmied, L. (2008). “Cross-shore suspended sand and bedload transport on beaches.” J. Geophys. Res., 113, C07001, doi:10.1029/2007JC004203.
- Kobayashi, N., Buck, M., Payo, A., and Johnson, B.D. (2008). “Berm and dune erosion during a storm.” J. Waterway, Port, Coastal, Ocean Eng., 134 (in press).
- Kobayashi, N., Payo, A., and Johnson, B.D. (2008). “Suspended sand and bedload transport on beaches.” Handbook of Coastal and Ocean Engineering, World Scientific, Singapore (in press).
- Payo, A., Kobayashi, N., and Yamada, F. (2008). “Suspended sand transport along pier depression.” J. Waterway, Port, Coastal, Ocean Eng. (submitted).
- Buck, M., Kobayashi, N., Payo, A., and Johnson, B.D. (2008). “Berm and dune erosion.” Proc. 31th Coastal Eng. Conf., World Scientific (accepted).
- Gencarelli, R., Tomasicchio, G.R., Kobayashi, N., and Johnson, B.D. (2008). “Beach profile evolution and dune erosion due to the impact of Hurricane Isabel.” Proc. 31th Coastal Eng. Conf., World Scientific (accepted).

- Gencarelli, R., Tomasicchio, G.R., Kobayashi, N., and Johnson, B.D. (2008). “Effects of Hurricane Isabel along the North Carolina coastline: Beach profile evolution and dune erosion.” Proc. 3rd International Short Conf. on Applied Coastal Res., Lecce, Italy (accepted).

The following papers summarized the progress of the CSHORE development concisely.

- Kobayashi, N. (2006). “Time-averaged wave models for coastal structures and sediments.” Proc. 2nd International Short Course and Workshop on Coastal Processes and Port Eng., Cosenza, Italy, 61-75.
- Kobayashi, N. (2008). “Efficient wave and current models for coastal structures and sediments.” Nonlinear Wave Dynamics. World Scientific, Singapore, 1-21.
- Kobayashi, N., Figlus, J., and Buck, M. (2008). “Beach nourishment and dune erosion.” Proc. 3rd Internal Short Conf. on Applied Coastal Res., Lecce, Italy (in press).

The ongoing extension of CSHORE includes the prediction of the combined wave overtopping and overflow on levees and dunes, and eventually the erosion and breaching prediction of earthen levees and sand dunes. The initial results are presented in the following publications:

- Farhadzadeh, A., Kobayashi, N., Melby, J.A., and Ricottilli, C. (2007). “Experiments and numerical modeling of wave overtopping and overflow on dikes.” Res. Rep. No. CACR-07-02, Center for Applied Coastal Res., Univ. of Delaware, Newark, Del.
- Kobayashi, N., Farhadzadeh, A., and Melby, J.A. (2007). “Structures of storm surge disaster prevention.” Proc. 4th International Workshop on Coastal Disaster Prevention, Yokohama, Japan, 41-49.

- Farhadzadeh, A., Kobayashi, N., and Melby, J.A. (2008). “Wave overtopping and overflow on inclined structures.” Proc. 31st Coastal Eng. Conf., World Scientific (accepted).
- Kobayashi, N., Farhadzadeh, A., and Melby, J.A. (2008). “Combined wave overtopping and overflow on levees.” J. Waterway, Port, Coastal, Ocean Eng. (submitted).

In addition, CSHORE will be extended to predict the long-term (seasonal and yearly) cross-shore and longshore sediment transport rates on natural and nourished beaches. The field data required for the calibration and verification for the long-term morphological model CSHORE has been obtained and analyzed in the following publications:

- Figlus, J., and Kobayashi, N. (2007). “Seasonal and yearly profile changes of Delaware beaches.” Res. Rep. No. CACR-07-01, Center for Applied Coastal Res., Univ. of Delaware, Newark, Del.
- Figlus, J., and Kobayashi, N. (2008). “Inverse estimation of sand transport rates on nourished Delaware beaches.” J. Waterway, Port, Coastal, Ocean Eng., 134(4), 218-225.
- Figlus, J., and Kobayashi, N. (2008). “Two-line model for inverse estimation of cross-shore and longshore transport rates on nourished beaches.” 31st Coastal Eng. Conf., World Scientific (accepted).

3. Wave and Current Models

Cross-shore sediment transport on beaches has been investigated extensively (e.g., Kriebel and Dean 1985; van Rijn et al. 2003) but we still cannot predict beach profile evolution accurately. In order to improve our predictive capabilities, sediment transport models have become more sophisticated but less transparent. For example, Thornton et al. (1996) and Gallagher et al.

(1998) used the energetics-based total load model of Bailard (1981) to explain the offshore movement of a bar at Duck, North Carolina during storms. The onshore bar migration on the same beach was predicted by both Hoefel and Elgar (2003), using the skewed acceleration effect on bedload, and Henderson et al. (2004), using a suspended sediment model. The roles of bedload and suspended load are not clear at present. Kobayashi et al. (2008a) made an attempt to synthesize and simplify existing cross-shore sediment transport models with the aim of developing a simple and robust model that is suited for engineering applications including the berm and dune erosion. This model has been extended to predict the cross-shore and longshore transport rates of bedload and suspended load under the combined wave and current action predicted by the time-averaged, probabilistic model by Kobayashi et al. (2007a). The latest version of the numerical model CSHORE is explained in the following.

Sediment transport on beaches is caused by the combined action of waves and currents. The hydrodynamic input required for a sediment transport model depends on whether the sediment transport model is time-dependent (phase-resolving) or time-averaged over a number of waves. A time-dependent sediment transport model such as that by Kobayashi and Johnson (2001) is physically appealing because it predicts intense but intermittent sand suspension under irregular breaking waves (Kobayashi and Tega 2002). However, the time-dependent model requires considerable computation time and is not necessarily more accurate in predicting slow morphological changes than the corresponding time-averaged model presented in the following. Horizontally two-dimensional wave and current models are presented first before the cross-shore model CSHORE based on the assumption of alongshore uniformity.

Fig. 1 shows obliquely incident irregular waves on an essentially straight shoreline where the cross-shore coordinate x is positive onshore and the longshore coordinate y is positive in the downwave direction. The beach is assumed to be impermeable. The depth-averaged cross-shore and longshore velocities are denoted by U and V , respectively. Incident waves are assumed to be unidirectional with $\theta =$ incident angle relative to the shore normal. The height and period of the irregular waves are represented by the root-mean-square wave height H_{rms} and the spectral peak period T_p specified at the seaward boundary located at $x = 0$. The wave angle θ is assumed to be in the range of $|\theta| < 90^\circ$ to ensure that the incident waves propagate landward. The wind speed and direction at the elevation of 10 m above the sea surface are denoted by W_{10} and θ_w , respectively.

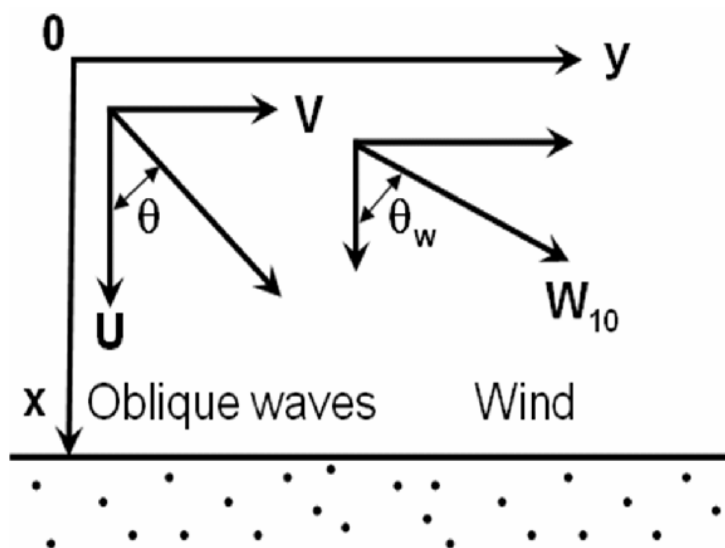


Fig. 1. Definition sketch for incident irregular waves and wind on beach.

The mean water depth \bar{h} is given by

$$\bar{h} = (\bar{\eta} + S - z_b) \quad (1)$$

where $\bar{\eta}$ = wave setup above the still water level (SWL); and S = storm tide above the datum $z = 0$ which is assumed to be uniform in the computation domain. Linear wave and current theory for wave refraction (e.g., Phillips 1977; Mei 1989; Dalrymple 1988) is used to predict the spatial variations of H_{rms} and θ . The dispersion relation for linear waves is expressed as

$$\omega^2 = kg \tanh(k\bar{h}) \quad ; \quad \omega_p = \omega + k(Q_x \cos \theta + Q_y \sin \theta) / \bar{h} \quad (2)$$

where ω = intrinsic angular frequency; k = wave number; g = gravitational acceleration; \bar{h} = mean water depth with the overbar indicating time-averaging; ω_p = absolute angular frequency given by $\omega_p = 2\pi/T_p$; Q_x and Q_y = time-averaged volume flux per unit width in the x and y directions, respectively, and θ = incident wave angle. Eq. (2) can be solved iteratively to obtain k and ω for known $\omega_p, \bar{h}, \theta, Q_x$ and Q_y . The phase velocity C and the group velocity C_g are given by

$$C = \omega / k \quad ; \quad C_g = nC \quad ; \quad n = \frac{1}{2} \left[1 + \frac{2k\bar{h}}{\sinh(2k\bar{h})} \right] \quad (3)$$

The wave angle θ is computed using the irrotationality of the wave number

$$\frac{\partial}{\partial x}(k \sin \theta) - \frac{\partial}{\partial y}(k \cos \theta) = 0 \quad (4)$$

The root-mean-square wave height H_{rms} defined as $H_{rms} = \sqrt{8} \sigma_\eta$ with σ_η = standard deviation of the free surface elevation η is computed using the wave action equation

$$\frac{\partial}{\partial x} \left[\frac{E}{\omega} \left(C_g \cos \theta + \frac{Q_x}{\bar{h}} \right) \right] + \frac{\partial}{\partial y} \left[\frac{E}{\omega} \left(C_g \sin \theta + \frac{Q_y}{\bar{h}} \right) \right] = - \frac{D_B + D_f}{\omega} \quad (5)$$

with

$$E = \rho g \sigma_{\eta}^2 = \frac{1}{8} \rho g H_{rms}^2 \quad (6)$$

where E = specific wave energy; ρ = fluid density; and D_B and D_f = wave energy dissipation rate per unit horizontal area due to wave breaking and bottom friction, respectively. The formulas for D_B and D_f are presented later in relation to the cross-shore model CSHORE.

The time-averaged volume fluxes Q_x and Q_y in Eq. (2) are expressed as

$$Q_x = \bar{h}\bar{U} + Q_{wx} \quad ; \quad Q_y = \bar{h}\bar{V} + Q_{wy} \quad (7)$$

with

$$Q_{wx} = \frac{g\sigma_{\eta}^2 \cos \theta}{C} + q_r \cos \theta \quad ; \quad Q_{wy} = \frac{g\sigma_{\eta}^2 \sin \theta}{C} + q_r \sin \theta \quad (8)$$

where \bar{U} and \bar{V} = time-averaged, depth-averaged velocities in the x and y directions; Q_{wx} and Q_{wy} = wave-induced volume fluxes in the x and y directions; $(g\sigma_{\eta}^2/C)$ = volume flux due to linear waves propagating in the direction of θ ; and q_r = volume flux of a roller on the front of a breaking wave. The roller volume flux q_r is estimated using the roller energy equation as explained by Kobayashi et al. (2005,2007a)

$$\frac{\partial}{\partial x}(\rho C^2 q_r \cos \theta) + \frac{\partial}{\partial y}(\rho C^2 q_r \sin \theta) = D_B - D_r \quad (9)$$

with

$$D_r = \rho g \beta_r q_r \quad ; \quad \beta_r = (0.1 + S_b) \geq 0.1 \quad (10)$$

$$S_b = \frac{\partial z_b}{\partial x} \cos \theta + \frac{\partial z_b}{\partial y} \sin \theta \quad (11)$$

where D_r = roller dissipation rate; β_r = wave-front slope; S_b = bottom slope in the direction of wave propagation; and z_b = bottom elevation relative to the datum $z = 0$ with z = vertical coordinate taken to be positive upward. The wave front slope β_r is assumed to be 0.1 unless it is increased by the positive bottom slope S_b .

The mean water depth \bar{h} and the current velocities \bar{U} and \bar{V} are computed using the time-averaged continuity and momentum equations (Phillips 1977; Svendsen et al. 2002).

$$\frac{\partial}{\partial x}(\bar{Q}_x) + \frac{\partial}{\partial y}(\bar{Q}_y) = 0 \quad (12)$$

$$\frac{\partial}{\partial x} \left(\frac{\bar{Q}_x^2}{\bar{h}} \right) + \frac{\partial}{\partial y} \left(\frac{\bar{Q}_x \bar{Q}_y}{\bar{h}} \right) + g \bar{h} \frac{\partial \bar{\eta}}{\partial x} + \frac{\tau_{bx}}{\rho} = \tau_{wx} + \frac{\tau_{sx}}{\rho} \quad (13)$$

$$\frac{\partial}{\partial x} \left(\frac{\bar{Q}_x \bar{Q}_y}{\bar{h}} \right) + \frac{\partial}{\partial y} \left(\frac{\bar{Q}_y^2}{\bar{h}} \right) + g \bar{h} \frac{\partial \bar{\eta}}{\partial y} + \frac{\tau_{by}}{\rho} = \tau_{wy} + \frac{\tau_{sy}}{\rho} \quad (14)$$

with

$$\tau_{wx} = -\frac{\partial}{\partial x} \left(\frac{S_{xx}}{\rho} - \frac{\bar{Q}_{wx}^2}{\bar{h}} \right) - \frac{\partial}{\partial y} \left(\frac{S_{xy}}{\rho} - \frac{\bar{Q}_{wx} \bar{Q}_{wy}}{\bar{h}} \right) \quad (15)$$

$$\tau_{wy} = -\frac{\partial}{\partial x} \left(\frac{S_{xy}}{\rho} - \frac{\bar{Q}_{wx} \bar{Q}_{wy}}{\bar{h}} \right) - \frac{\partial}{\partial y} \left(\frac{S_{yy}}{\rho} - \frac{\bar{Q}_{wy}^2}{\bar{h}} \right) \quad (16)$$

$$S_{xx} = (nE + M_r) \cos^2 \theta + E \left(n - \frac{1}{2} \right) \quad ; \quad M_r = \rho C q_r \quad (17)$$

$$S_{xy} = (nE + M_r) \cos \theta \sin \theta \quad ; \quad S_{yy} = (nE + M_r) \sin^2 \theta + E \left(n - \frac{1}{2} \right) \quad (18)$$

where τ_{bx} and τ_{by} = bottom shear stresses in the x and y directions; τ_{sx} and τ_{sy} = wind stresses on the sea surface in the x and y directions; and S_{xx} , S_{xy} and S_{yy} = radiation stresses including the momentum flux M_r of a roller propagating with the phase speed C . It is noted that the terms Q_{wx}^2 , $Q_{wx}Q_{wy}$ and Q_{wy}^2 in Eqs. (15) and (16) included by Phillips (1977) are of 4-th order in terms of the wave height and normally neglected. The present circulation model based on Eqs. (12) – (18) is a simplified version of SHORECIRC (Svendsen et al. 2002) for irregular waves where SHORECIRC assumes monochromatic waves. The formulas for τ_{bx} , τ_{by} , τ_{sx} and τ_{sy} are presented later in relation to the cross-shore model CSHORE.

A horizontally two-dimensional model C2SHORE has been developed in the MORPHOS project (Shi et al. 2008). The directional spectral wave model STWAVE (Smith et al. 2001) is used to predict the wave transformation. The wave-induced fluxes Q_{wx} and Q_{wy} and the radiation stresses S_{xx} , S_{xy} and S_{yy} are computed from the predicted directional wave spectra. The roller effects included in Eqs. (8), (17) and (18) are neglected. The circulation model is based on Eqs. (12)–(16) with the formulas for τ_{bx} , τ_{by} , τ_{sx} and τ_{sy} used in CSHORE. The wave and circulation models are coupled and run iteratively for several times. The wave field is computed to estimate τ_{wx} and τ_{wy} given by Eqs. (15) and (16) for the circulation model which computes the wave setup and wave-induced currents. An efficient finite difference method is used to solve Eqs. (12) – (14) and reduce the computation time considerably (Shi et al. 2007). The iteration between the wave and circulation models is necessary in the region near and landward of the still water shoreline

where wave setup determines the mean water depth \bar{h} for the wave model. Shi et al. (2008) compared C2SHORE with the morphological change data at the U.S. Army Corps of Engineers Field Research Facility (FRF) during Hurricane Isabel and found the need to model the effects of the FRF piling.

4. Combined Wave and Current Model CSHORE

The cross-shore model CSHORE assumes alongshore uniformity but computes the wave and current fields simultaneously. The depth-integrated continuity equation of water given by Eq. (12) requires that the cross-shore volume flux Q_x is constant and equal to the wave overtopping rate q_o at the landward end of the computation domain. Eqs. (7) and (8) yield

$$Q_x = \bar{h}\bar{U} + \frac{g\sigma_\eta^2}{C} \cos \theta + q_r \cos \theta = q_o \quad (19)$$

$$Q_y = \bar{h}\bar{V} + \frac{g\sigma_\eta^2}{C} \sin \theta + q_r \sin \theta \quad (20)$$

where \bar{h} = mean water depth; \bar{U} = mean cross-shore velocity; which is negative and offshore because $\cos \theta > 0$ if $q_o = 0$ (no wave overtopping); g = gravitational acceleration; σ_η = standard deviation of the free surface elevation η ; C = linear wave phase velocity in the mean water depth \bar{h} corresponding to the spectral peak period T_p ; and q_r = volume flux of a roller on the front of a breaking wave. If the incident wave angle θ is small, Eq. (20) can be approximated by $Q_y \approx \bar{h}\bar{V}$ for most applications.

For the case of alongshore uniformity, Eq. (4) reduces to Snell's law which is used to obtain the wave direction θ

$$k \sin \theta = \text{constant} \quad (21)$$

The constant value is obtained from the values of θ , \bar{h} and T_p specified at the seaward boundary $x = 0$ located outside the surf zone where ω can be approximated by ω_p in Eq. (2). Reflected waves are neglected in this model.

The cross-shore and longshore momentum equations (13) and (14) are simplified as

$$\frac{d}{dx} \left(S_{xx} + \rho \frac{Q_x^2}{h} \right) = -\rho g \bar{h} \frac{d\bar{\eta}}{dx} - \tau_{bx} + \tau_{sx} \quad (22)$$

$$\frac{d}{dx} \left(S_{xy} + \rho \frac{Q_x Q_y}{h} \right) = -\tau_{by} + \tau_{sy} \quad (23)$$

where S_{xx} = cross-shore radiation stress; ρ = water density; τ_{bx} = cross-shore bottom stress; τ_{sx} = cross-shore wind stress on the sea surface; S_{xy} = shear component of the radiation stress; τ_{by} = longshore bottom stress; and τ_{sy} = longshore wind stress on the sea surface. The wind shear stresses may not be negligible especially outside surf zones on natural beaches (Lentz et al. 1999). Linear wave theory for progressive waves is used to estimate S_{xx} and S_{xy} as in Eqs. (17) and (18)

$$S_{xx} = (nE + M_r) \cos^2 \theta + E \left(n - \frac{1}{2} \right) ; S_{xy} = (nE + M_r) \cos \theta \sin \theta \quad (24)$$

with

$$n = C_g / C \quad ; \quad E = \rho g \sigma_\eta^2 \quad ; \quad M_r = \rho C q_r \quad (25)$$

where C_g = linear wave group velocity; E = specific wave energy with the root-mean-square wave height defined as $H_{rms} = \sqrt{8} \sigma_\eta$; and M_r = momentum flux of a roller propagating with the phase velocity C . It is noted that the equations used in CSHORE are presented again for clarity.

The time-averaged bottom shear stresses in Eqs. (22) and (23) are written as

$$\tau_{bx} = \frac{1}{2} \rho f_b \overline{UU_a} \quad ; \quad \tau_{by} = \frac{1}{2} \rho f_b \overline{VU_a} \quad ; \quad U_a = (U^2 + V^2)^{0.5} \quad (26)$$

where U = depth-averaged cross-shore velocity; V = depth-averaged longshore velocity; f_b = bottom friction factor; and the overbar indicates time averaging. The bottom friction factor f_b is of the order of 0.015 but should be calibrated using longshore current data because of the sensitivity of longshore currents to f_b . The equivalency of the time and probabilistic averaging is assumed to express τ_{bx} and τ_{by} in terms of the mean and standard deviation of the depth-averaged velocities U and V expressed as

$$U = \sigma_T F_U \quad ; \quad V = \sigma_T F_V \quad ; \quad U_a = \sigma_T F_a \quad ; \quad F_a = (F_U^2 + F_V^2)^{0.5} \quad (27)$$

with

$$F_U = U_* + r \cos \theta \quad ; \quad F_V = V_* + r \sin \theta \quad ; \quad U_* = \frac{\bar{U}}{\sigma_T} \quad ; \quad V_* = \frac{\bar{V}}{\sigma_T} \quad (28)$$

where \bar{U} and \bar{V} = depth-averaged cross-shore and longshore currents; σ_T = standard deviation of the oscillatory (assumed Gaussian) depth-averaged velocity U_T with zero mean; and r = Gaussian variable defined as $r = U_T / \sigma_T$ whose probability density function is given by

$$f(r) = \frac{1}{\sqrt{2\pi}} \exp\left(-\frac{r^2}{2}\right) \quad (29)$$

Linear progressive wave theory is used locally to express U_T in terms of the oscillatory free surface elevation $(\eta - \bar{\eta})$

$$U_T = \frac{C}{h} (\eta - \bar{\eta}) \quad (30)$$

which yields the standard deviation σ_T of the oscillatory velocity U_T

$$\sigma_T = C \sigma_* \quad ; \quad \sigma_* = \sigma_\eta / \bar{h} \quad (31)$$

It is noted that that $U_* = \bar{U} / \sigma_T$ and $V_* = \bar{V} / \sigma_T$ are of the order of unity or less. The standard deviations of U and V are given by

$$\sigma_U = \sigma_T \cos \theta \quad ; \quad \sigma_V = \sigma_T |\sin \theta| \quad (32)$$

where $\cos \theta > 0$ but $\sin \theta$ can be negative. Substitution of Eq. (27) into Eq. (26) yields

$$\tau_{bx} = \frac{1}{2} \rho f_b \sigma_T^2 G_{bx} \quad ; \quad \tau_{by} = \frac{1}{2} \rho f_b \sigma_T^2 G_{by} \quad (33)$$

with

$$G_{bx} = \int_{-\infty}^{\infty} F_U F_a f(r) dr \quad ; \quad G_{by} = \int_{-\infty}^{\infty} F_V F_a f(r) dr \quad (34)$$

which must be integrated numerically.

The wind shear stress in Eqs. (22) and (23) are expressed as

$$\tau_{sx} = \rho_a C_D W_{10}^2 \cos \theta_w \quad ; \quad \tau_{sy} = \rho_a C_D W_{10}^2 \sin \theta_w \quad (35)$$

where ρ_a = air density ($\rho_a \approx 1.225 \text{ kg/m}^3$); C_D = drag coefficient, W_{10} = 10-m wind speed; and θ_w = wind direction defined in Fig. 1. The formula by Large and Pond (1981) is used to estimate C_D where $C_D = 0.0012$ for $W_{10} < 11 \text{ m/s}$ and $C_D = (0.00049 + 0.000065 W_{10})$ for $W_{10} \geq 11 \text{ m/s}$. It is noted that the measured values of C_D during tropical cyclones by Powell et al. (2003) indicated no increase of C_D with the increase of W_{10} much above 25 m/s. In short, available data is insufficient to estimate C_D for extreme wind conditions.

The wave action equation (5) for the case of alongshore uniformity becomes

$$\frac{d}{dx} \left[\frac{E}{\omega} \left(C_g \cos \theta + \frac{Q_x}{h} \right) \right] = - \frac{D_B + D_f}{\omega} \quad (36)$$

which reduces to the wave energy equation if ω is constant and $Q_x=0$.

$$\frac{dF_x}{dx} = -D_B - D_f \quad ; \quad F_x = EC_g \cos \theta \quad (37)$$

where F_x = cross-shore energy flux based on linear progressive wave theory; and D_B and D_f = energy dissipation rates due to wave breaking and bottom friction, respectively. The energy dissipation rate D_B due to wave breaking in Eq. (36) is estimated using the formula by Battjes and Stive (1985), which was modified by Kobayashi et al. (2005) to account for the local bottom slope and to extend the computation to the lower swash zone. The modified formula is expressed as

$$D_B = \frac{\rho g a Q H_B^2}{4T} ; \quad \frac{Q-1}{\ln Q} = \left(\frac{H_{rms}}{H_m} \right)^2 ; \quad (38)$$

$$H_m = \frac{0.88}{k} \tanh \left(\frac{\gamma k \bar{h}}{0.88} \right) ; \quad a = \frac{2\pi S_b}{3k\bar{h}} \geq 1$$

where a = slope effect parameter; Q = fraction of breaking waves; H_B = breaker height used to estimate D_B ; T = intrinsic wave period given by $T = 2\pi/\omega$ with ω obtained using Eq. (2); $H_{rms} = \sqrt{8}\sigma_\eta$ = local root-mean-square wave height; H_m = local depth-limited wave height; k = wave number; \bar{h} = mean water depth including wave setup; γ = empirical breaker ratio parameter; and S_b = local bottom slope given by Eq. (11). The parameter a is the ratio between the wave length ($2\pi/k$) and the horizontal length ($3\bar{h}/S_b$) imposed by the small depth and relatively steep slope where the lower limit of $a = 1$ corresponds to the formula by Battjes and Stive (1985) who also assumed $H_B = H_m$. The fraction Q is zero for no wave breaking and unity when all waves break. The requirement of $0 \leq Q \leq 1$ implies $H_{rms} \leq H_m$ but H_{rms} can become larger than H_m in very shallow water. When $H_{rms} > H_m$, use is made of $Q = 1$ and $H_B = H_{rms}$. In addition, the upper limit of $\sigma_* = \sigma_\eta / \bar{h}$ is imposed as $\sigma_* \leq 1$ in very shallow water (Kobayashi et al. 1998). The breaker ratio parameter γ in Eq. (38) is typically in the range of $\gamma = 0.5 - 1.0$ (Kobayashi et al. 2007a) but should be calibrated to obtain a good agreement with the measured cross-shore variation of σ_η if such data is available. On the other hand, the energy dissipation rate D_f due to bottom friction in Eq. (36) is expressed as

$$D_f = \frac{1}{2} \rho f_b \overline{U_a^3} \quad (39)$$

Substitution of U_a given in Eq. (27) into Eq. (39) yields

$$D_f = \frac{1}{2} \rho f_b \sigma_r^3 G_f \quad ; \quad G_f = \int_{-\infty}^{\infty} F_a^3 f(r) dr \quad (40)$$

where $f(r)$ is given by Eq. (29).

The energy equation for the roller given by Eq. (9) reduces to that used by Ruessink et al. (2001) for the case of alongshore uniformity

$$\frac{d}{dx} (\rho C^2 q_r \cos \theta) = D_B - D_r \quad ; \quad D_r = \rho g \beta_r q_r \quad (41)$$

where the roller dissipation rate D_r is assumed to equal the rate of work to maintain the roller on the wave-front slope β_r of the order of 0.1. Use is made of the empirical formula given by Eq. (10) proposed by Kobayashi et al. (2005) who included the local bottom slope effect. If the roller is neglected, $q_r = 0$ and Eq. (41) yields $D_r = D_B$. The roller effect improves the agreement for the longshore current (Kobayashi et al. 2007a).

Eqs. (19) – (41) are the same as those used by Kobayashi et al. (2007a) who assumed $Q_x = q_o = 0$ in Eq. (19) and neglected the wind shear stresses in Eqs. (22) and (23), and used linear shallow-water wave theory with $C = (g \bar{h})^{0.5}$ in Eq. (30). Substitution of Eqs. (31) and (32) into Eq. (19) yields

$$\bar{U} = -\frac{g \bar{h}}{C^2} \sigma_U \sigma_* \left(1 + \frac{C q_r}{g \sigma_\eta^2} \right) + \frac{Q_x}{\bar{h}} \quad (42)$$

The landward-marching computation starting from $x = 0$ outside the surf zone is the same as that of Kobayashi et al. (2007a).

Approximate analytical equations of G_{bx} , G_{by} and G_f given by Eqs. (34) and (40) are obtained by Kobayashi (2008b) to reduce the computation time and improve the numerical stability. The function F_a given in Eq. (27) with Eq. (28) is rewritten as

$$F_a = \left[(r - r_m)^2 + F_m^2 \right]^{0.5} \quad (43)$$

with

$$r_m = -(U_* \cos \theta + V_* \sin \theta) \quad ; \quad F_m = V_* \cos \theta - U_* \sin \theta \quad (44)$$

Eq. (43) is approximated as

$$\begin{aligned} F_a &= (r - r_m) + |F_m| \quad \text{for } r \geq 0 \\ F_a &= -(r - r_m) + |F_m| \quad \text{for } r < 0 \end{aligned} \quad (45)$$

Substituting Eq. (45) into Eqs. (34) and (40) and integrating the resulting equations analytically, we obtain approximate expressions for G_{bx} , G_{by} and G_f

$$G_{bx} = \sqrt{\frac{2}{\pi}} (U_* - r_m \cos \theta) + U_* |F_m| \quad (46)$$

$$G_{by} = \sqrt{\frac{2}{\pi}} (V_* - r_m \sin \theta) + V_* |F_m| \quad (47)$$

$$G_f = 2\sqrt{\frac{2}{\pi}} + (1 + U_*^2 + V_*^2) |F_m| + \sqrt{\frac{2}{\pi}} (U_*^2 + V_*^2 + 2r_m^2) \quad (48)$$

which depends on $\sin \theta$ ($\cos \theta > 0$ assumed), r_m and F_m where Eq. (44) yields $U_* = -(r_m \cos \theta + F_m \sin \theta)$ and $V_* = (F_m \cos \theta - r_m \sin \theta)$.

For the case of normally incident waves with no wind, $\sin \theta = 0$ and $V_* = 0$. Eqs. (46) – (48) yield $G_{bx} = 1.6 U_*$, $G_{by} = 0$, and $G_f = (1.6 + 2.4 U_*^2)$. For this case, Eq. (23) requires $\tau_{by} = 0$ for $Q_x = 0$ (no wave overtopping) and Eq. (33) yields $G_{by} = 0$. As a result, Eq. (47) is exact. For $\sin \theta = 0$ and $V_* = 0$, G_{bx} and G_f given by Eqs. (34) and (40) can be integrated analytically as presented by Kobayashi et al. (2007b) who approximated the analytical expressions of G_{bx} and G_f as $G_{bx} = 1.64 U_*$ and $G_f = (1.6 + 2.6 U_*^2)$. These approximate equations are very similar to the above equations obtained from Eqs. (46) and (48). For the case of $|\sin \theta| \ll 1$ and $|U_*| \ll |V_*|$, Eq. (47) can be approximated as $G_{by} = V_* (0.8 + |V_*|)$. Using field data and probabilistic analyses, Feddersen et al. (2000) obtained $G_{by} = V_* (1.16^2 + V_*^2)^{0.5}$. The difference between these two approximate equations for G_{by} is less than 20% for $|V_*| < 1.4$, which is typically satisfied.

Kobayashi et al. (2008b) compared the approximate values of G_{bx} , G_{by} and G_f given by Eqs. (46) – (48) with the exact values of G_{bx} , G_{by} and G_f obtained by the numerical integration of Eqs. (34) and (40). The percentage error was typically about 10% and always less than 35% for the ranges of $|\sin \theta| < 1$, $|r_m| < 1$ and $|F_m| < 1$. This error is probably less than the uncertainty of the bottom friction factor f_b .

5. Sediment Transport Model

The combined wave and current model CSHORE predicts the spatial variations of the hydrodynamic variables used in the following sediment transport model for given beach profile, water level and seaward wave conditions at $x = 0$. The bottom sediment is assumed to be

uniform and characterized by d_{50} = median diameter; w_f = sediment fall velocity; and s = sediment specific gravity. The sediment transport model developed for CSHORE is modified slightly for the horizontally two-dimensional model C2SHORE.

First, the spatial variation of the degree of sediment movement is estimated using the critical Shields parameter ψ_c (Madsen and Grant 1976) which is taken as $\psi_c = 0.05$. The instantaneous bottom shear stress τ'_b is assumed to be given by $\tau'_b = 0.5 \rho f_b U_a^2$ with U_a given in Eq. (26). The sediment movement is assumed to occur when τ'_b exceeds the critical shear stress, $\rho g(s-1)d_{50} \psi_c$. The probability P_b of sediment movement can be shown to be the same as the probability of $(r-r_m)^2 > F_b^2 = (R_b^2 - F_m^2)$ where $R_b = [2 g (s-1) d_{50} \psi_c f_b^{-1}]^{0.5} / \sigma_T$ and r_m and F_m are defined in Eq. (44). For the Gaussian variable r given by Eq. (29), P_b is given by

$$P_b = \frac{1}{2} \operatorname{erfc} \left(\frac{F_b - r_m}{\sqrt{2}} \right) + \frac{1}{2} \operatorname{erfc} \left(\frac{F_b + r_m}{\sqrt{2}} \right) \quad \text{for } F_b^2 > 0 \quad (49)$$

and $P_b = 1$ for $F_b^2 \leq 0$ where erfc is the complementary error function. The value of P_b computed from $x = 0$ located outside the surf zone increases landward and fluctuates in the surf and swash zones, depending on the presence of a bar or a terrace that increases the local fluid velocity.

Second, the spatial variation of the degree of sediment suspension is estimated using the experimental finding of Kobayashi et al. (2005) who showed that the turbulent velocities measured in the vicinity of the bottom were related to the energy dissipation rate due to bottom friction. Representing the magnitude of the instantaneous turbulent velocity by $(D'_f/\rho)^{1/3}$ with

$D'_f = 0.5 \rho f_b U_a^3$ in light of Eq. (39), the probability P_s of sediment suspension is assumed to be the same as the probability of $(D'_f/\rho)^{1/3}$ exceeding the sediment fall velocity w_f . The probability P_s is then equal to the probability of $F_s^2 = (R_s^2 - F_m^2)$ with $R_s = [(2/f_b)^{1/3} w_f / \sigma_T]$ and is given by

$$P_s = \frac{1}{2} \operatorname{erfc} \left(\frac{F_s - r_m}{\sqrt{2}} \right) + \frac{1}{2} \operatorname{erfc} \left(\frac{F_s + r_m}{\sqrt{2}} \right) \quad \text{for } F_s^2 > 0 \quad (50)$$

and $P_s = 1$ for $F_s^2 \leq 0$. If $P_s > P_b$, use is made of $P_s = P_b$ assuming that sediment suspension occurs only when sediment movement occurs. Fine sands on beaches tend to be suspended once their movement is initiated.

Third, the suspended sediment volume V_s per unit horizontal bottom area is estimated by modifying the sediment suspension model by Kobayashi and Johnson (2001)

$$V_s = P_s \frac{e_B D_r + e_f D_f}{\rho g (s-1) w_f} (1 + S_{bx}^2)^{0.5} (1 + S_{by}^2)^{0.5} ; \quad S_{bx} = \frac{\partial z_b}{\partial x} ; \quad S_{by} = \frac{\partial z_b}{\partial y} \quad (51)$$

where S_{bx} = cross-shore bottom slope; S_{by} = longshore bottom slope; and e_B and e_f = suspension efficiencies for the energy dissipation rates D_r and D_f due to wave breaking and bottom friction, respectively. Use is made of $e_B = 0.005$ and $e_f = 0.01$ as typical values in the computation of berm and dune erosion but the value of e_B is uncertain and should be calibrated if V_s is measured (Kobayashi et al. 2007a). The sediment suspension probability P_s is added to Eq. (51) to ensure $V_s = 0$ if $P_s = 0$. The term involving S_{bx} and S_{by} is the actual bottom area per unit horizontal bottom area and essentially unity except for very steep slopes. For the case of alongshore uniformity, $S_{by} = 0$. The cross-shore and longshore suspended sediment transport rates q_{sx} and q_{sy} are expressed as

$$q_{sx} = a_x \bar{U} V_s \quad ; \quad q_{sy} = \bar{V} V_s \quad ; \quad a_x = \left[a + (S_{bx} / \tan \phi)^{0.5} \right] \geq a \quad (52)$$

where a = empirical suspended load parameter and ϕ = angle of internal friction of the sediment with $\tan \phi = 0.63$ for sand (Bailard 1981). The parameter a accounts for the onshore suspended sediment transport due to the positive correlation between the time-varying cross-shore velocity and suspended sediment concentration. The value of a increases to unity as the positive correlation decreases to zero. For the three small-scale equilibrium profile tests conducted by Kobayashi et al. (2005), a was of the order of 0.2. The effect of the cross-shore bottom slope on a_x was included by Kobayashi et al. (2008c) to increase berm and dune erosion. For $S_{bx} \leq 0$, $a_x = a$. The cross-shore suspended sediment transport rate q_{sx} is negative (offshore) because the return (undertow) current \bar{U} is negative (offshore). On the other hand, the longshore suspended sediment transport rate q_{sy} in Eq. (52) neglects the correlation between the time-varying longshore velocity and suspended sediment concentration, which appears to be very small if the longshore current \bar{V} is sufficiently large.

Fourth, the formulas for the cross-shore and longshore bedload transport rates q_{bx} and q_{by} are devised somewhat intuitively because bedload in the surf zone has never been measured. The time-averaged rates q_{bx} and q_{by} are tentatively expressed as

$$q_{bx} = B \overline{(U^2 + V^2)} U \quad ; \quad q_{by} = B \overline{(U^2 + V^2)} V \quad (53)$$

where B = empirical parameter. Eq. (53) may be regarded as a quasi-steady application of the formula of Meyer-Peter and Mueller (e.g., Ribberink 1998). Substitution of U and V given in Eq. (27) with Eqs. (28) and (29) into Eq. (53) yields

$$q_{bx} = B\sigma_T^3 \left(b_* + U_* V_*^2 + 2F_m \sin \theta \right) \quad (54)$$

$$q_{by} = B\sigma_T^3 \left[V_* (1 + U_*^2 + V_*^2) - 2r_m \sin \theta \right] \quad (55)$$

where $b_* = (3U_* + U_*^3)$ and F_m and r_m are defined in Eq. (44).

Eqs. (54) and (55) yield $q_{bx} = b_* B\sigma_T^3$ and $q_{by} = 0$ for normally incident waves with $\sin \theta = 0$ and $V_* = 0$. The expressions of B and b_* are obtained by requiring that $q_{bx} = b_* B\sigma_T^3$ reduces to the onshore bedload formula proposed by Kobayashi et al. (2008a) for normally incident waves, which synthesized existing data and simple formulas. The proposed formulas are written as

$$q_{bx} = \frac{bP_b}{g(s-1)} \sigma_T^3 (1 + U_* V_*^2 + 2F_m \sin \theta) G_s(S_{bx}) \quad (56)$$

$$q_{by} = \frac{bP_b}{g(s-1)} \sigma_T^3 \left[V_* (1 + U_*^2 + V_*^2) - 2r_m \sin \theta \right] G_s(S_{by}) \quad (57)$$

where b = empirical bedload parameter; and G_s = bottom slope function. The sediment movement probability P_b given in Eq. (49) accounts for the initiation of sediment movement. It is noted that $b_* = 1$ in Eq. (56) to compensate for the limitations of Eq. (53) and the Gaussian distribution of the horizontal velocity used in Eqs. (28) and (29) as discussed by Kobayashi et al. (2008a). They calibrated $b = 0.002$ using the 20 water tunnel tests of Ribberink and Al-Salem (1994), the 4 large-scale wave flume tests of Dohmen-Janssen and Hanes (2002), and the 24 sheet flow tests by Dohmen-Janssen et al. (2002). Furthermore, this simple bedload formula is consistent with the sheet flow model for onshore bar migration by Trowbridge and Young (1989) and the energetics-based bedload formula for steady flow by Bagnolds (1966) if the steady flow formula is applied in the time-averaged manner. The onshore bedload transport predicted by Eq.

(56) is consistent with the field observations of onshore ripple migration by Becker et al. (2007) and Masselink et al. (2007). The offshore suspended sediment transport predicted by Eq. (52) is consistent with the field measurement during a storm by Madsen et al. (1994). The condition of $(q_{bx} + q_{sx}) = 0$ for an equilibrium profile along with additional assumptions can be shown to yield the equilibrium profile popularized by Dean (1991).

The bottom slope function $G_s(S_{bx})$ was introduced by Kobayashi et al. (2008a) to account for the effect of the steep cross-shore slope S_{bx} on the bedload transport rate and is expressed as

$$G_s(S_{bx}) = \tan \phi / (\tan \phi + S_{bx}) \quad \text{for} \quad -\tan \phi < S_{bx} < 0 \quad (58)$$

$$G_s(S_{bx}) = (\tan \phi - 2S_{bx}) / (\tan \phi - S_{bx}) \quad \text{for} \quad 0 < S_{bx} < \tan \phi \quad (59)$$

where $G_s = 1$ for $S_{bx} = 0$. Eq. (58) corresponds to the functional form of G_s used by Bagnold (1966) for steady stream flow on a downward slope with $S_{bx} < 0$ where the downward slope increases q_{bx} . Eq. (59) ensures that G_s approaches negative infinity as the upward slope S_{bx} approaches $\tan \phi$. Eqs. (58) and (59) reduce to $G_s = (1 - S_{bx} / \tan \phi)$ for $|S_{bx}| \ll \tan \phi$. Eq. (56) with G_s given by Eqs. (58) and (59) implies that the bedload transport rate q_{bx} is positive (onshore) for $S_{bx} < (\tan \phi)/2$ and negative (offshore) for $S_{bx} > (\tan \phi)/2$. Use is made of $|G_s| < G_m = 10$ to avoid an infinite value in the computation. The computed profile change is not very sensitive to the assumed value of G_m because the beach profile changes in such a way to reduce a very steep slope except in the region of scarping (e.g., Seymour et al. 2005). The effect of the longshore bottom slope S_{by} is included in Eq. (57) using the same bottom slope function $G_s(S_{by})$ but has never been validated for lack of suitable data.

The landward marching computation of the present time-averaged model ends at the cross-shore location $x = x_m$ where the mean water depth \bar{h} is less than 1 cm. No reliable data exists for suspended sand and bedload transport rates in the zone which is wet and dry intermittently. Consequently, the following simple procedure was proposed by Kobayashi et al. (2008a) to deal with the zone with the bottom slope $S_{bx} > \tan \phi$. The cross-shore total sediment transport rate $q_x = (q_{sx} + q_{bx})$ at $x = x_m$ is denoted by q_{xm} . If q_{xm} is negative (offshore), q_x is extrapolated linearly to estimate q_x on the scarped face with $S_{bx} > \tan \phi$

$$q_x = q_{xm} (x_e - x) / (x_e - x_m) \quad \text{for } x_m < x < x_e \quad (60)$$

where x_e = landward limit of the scarping zone with $S_{bx} > \tan \phi$. The extrapolated q_x is in the range of $q_{xm} \leq q_x \leq 0$ and the scarping zone is eroded due to the offshore sediment transport. This simple procedure is effective for a high and wide dune, that is typical in the Netherlands (e.g., van Gent et al. 2006), but does not allow onshore sediment transport due to overwash. As a result, no wave overtopping has been allowed so far and $q_o = 0$ in Eq. (19).

Finally, the beach profile change is computed using the continuity equation of bottom sediment

$$(1 - n_p) \frac{\partial z_b}{\partial t} + \frac{\partial q_x}{\partial x} + \frac{\partial q_y}{\partial y} = 0 \quad (61)$$

where n_p = porosity of the bottom sediment which is normally taken as $n_p = 0.4$; t = slow morphological time for the change of the bottom elevation z_b ; and $q_y = (q_{sy} + q_{by})$ = longshore total sediment transport rate. For the case of alongshore uniformity, the third term in Eq. (61) is zero. Eq. (61) is solved using an explicit Lax-Wendroff numerical scheme (e.g., Nairn and Southgate 1993) to obtain the bottom elevation at the next time level. This computation

procedure is repeated starting from the initial bottom profile until the end of a profile evolution test. The computation time is of the order of 10^{-3} of the test duration.

6. Permeable Layer Model

The combined wave and current model CSHORE is extended to allow the presence of a permeable layer in the computation domain. Fig. 2 shows an example of irregular wave overtopping of a permeable slope where x = onshore coordinate; z = vertical coordinate, $\bar{\eta}$ = mean free surface elevation above SWL; S = storm tide above $z = 0$; z_b = bottom elevation; \bar{h} = mean water depth; U = instantaneous depth-averaged cross-shore velocity above the bottom; z_p = elevation of the lower boundary of the permeable layer; $h_p = (z_b - z_p)$ = vertical thickness of the permeable layer; and U_p = instantaneous cross-shore discharge velocity inside the permeable layer. The cross-shore profiles of $z_b(x)$ and $z_p(x)$ are specified as input where $h_p = 0$ in the zone of no permeable layer. The lower boundary located at $z = z_p$ is assumed to be impermeable for simplicity. It is noted that the profile change of the permeable slope such as a gravel beach has not been predicted so far.

0.01 – 0.05 (Kobayashi et al. 2007b). For the case of alongshore uniformity and negligible momentum fluxes into and out of the permeable layer, the time-averaged longshore discharge velocity \overline{V}_p is assumed to be zero because of no or negligible driving force to cause the longshore discharge inside the permeable layer. It is noted that the assumption of $\overline{V}_p = 0$ cannot be validated at present for lack of suitable data.

On the other hand, the wave action equation (36) is modified as

$$\frac{d}{dx} \left[\frac{E}{\omega} \left(C_g \cos \theta + \frac{Q_x}{h} \right) \right] = - \frac{D_B + D_f + D_p}{\omega} \quad (63)$$

where D_p = energy dissipation rate due to flow resistance in the permeable layer, assuming that the energy influx into the permeable layer equals the dissipation rate D_p per unit horizontal area.

The dissipation rate D_p is expressed as (Wurjanto and Kobayashi 1993)

$$D_p = \rho h_p \left[\alpha_p \left(\overline{U_p^2 + V_p^2} \right) + \beta_p \left(\overline{U_p^2 + V_p^2} \right)^{1.5} \right] \quad (64)$$

where α_p and β_p = laminar and turbulent flow resistance coefficients, respectively, and V_p = instantaneous longshore discharge velocity. Kobayashi et al. (2007b) modified the formulas for α_p and β_p proposed by van Gent (1995) as follows:

$$\alpha_p = \alpha_0 \frac{(1-n_p)^2}{n_p^2} \frac{\nu}{D_{n50}^2} \quad ; \quad \beta_p = \beta_1 + \frac{\beta_2}{\sigma_p} \quad (65)$$

with

$$\beta_1 = \frac{\beta_0 (1-n_p)}{n_p^3 D_{n50}} \quad ; \quad \beta_2 = \frac{7.5 \beta_0 (1-n_p)}{\sqrt{2} n_p^2 T} \quad (66)$$

where α_0 and β_0 = empirical parameters calibrated as $\alpha_0 = 1,000$ and $\beta_0 = 5$; n_p = porosity of the permeable layer consisting of stone; ν = kinematic viscosity of the fluid; D_{n50} = nominal stone diameter defined as $D_{n50} = (M_{50} / \rho_s)^{1/3}$ with M_{50} = median stone mass and ρ_s = stone density; σ_p = standard deviation of the instantaneous discharge velocity; and T = intrinsic wave period used in Eq. (38).

The discharge velocities U_p and V_p in Eq. (64) are assumed to be expressed as

$$U_p = \overline{U}_p + r \sigma_p \cos \theta \quad ; \quad V_p = r \sigma_p \sin \theta \quad (67)$$

where r = Gaussian variable whose probability density function is given by Eq. (29); and θ = incident wave angle for the oscillatory velocity direction above and inside the permeable layer.

The assumptions of the Gaussian velocity distribution and $\overline{V}_p = 0$ allow one to represent the discharge velocities by the mean cross-shore discharge velocity \overline{U}_p and the standard deviation σ_p . Substitution of Eq. (67) into Eq. (64) yields

$$D_p = \rho h_p \left\{ \alpha_p \left(\overline{U}_p^2 + \sigma_p^2 \right) + \sqrt{\frac{2}{\pi}} (\beta_2 + \beta_1 \sigma_p) \left[2\sigma_p^2 + \overline{U}_p^2 (1 + 2\cos^2 \theta) \right] \right\} \quad (68)$$

where use is made of the approximate expression of G_f given by Eq. (48) and the assumption of $|\overline{U}_p \sin \theta| \ll \sigma_p$ to simplify Eq. (68). Approximate equations for \overline{U}_p and σ_p are derived in the following.

Neglecting the inertia terms in the cross-shore momentum equation for the flow inside the permeable layer (Kobayashi and Wurjanto 1990), the local force balance between the cross-shore hydrostatic pressure gradient and flow resistance is assumed

$$g \frac{\partial \eta}{\partial x} + \alpha_p U_p + \beta_p U_p (U_p^2 + V_p^2)^{0.5} = 0 \quad (69)$$

Eq. (69) is averaged probabilistically using Eq. (67). For the case of alongshore uniformity, the averaged force balance equation is expressed as

$$g \frac{d\bar{\eta}}{dx} + \bar{U}_p \left[\alpha_p + \sqrt{\frac{2}{\pi}} (\beta_2 + \beta_1 \sigma_p) (1 + \cos^2 \theta) \right] = 0 \quad (70)$$

where use is made of the approximate expression of G_{bx} given by Eq. (46) and the assumption of

$|\bar{U}_p \sin \theta| \ll \sigma_p$ to simplify Eq. (70). It is noted that the local force balance between the

longshore hydrostatic pressure gradient and flow resistance yields $\bar{V}_p = 0$ for the case of

alongshore uniformity where $\bar{\eta}$ is independent of the longshore coordinate y . To derive an

equation σ_p , the approximate analytical method used by Kobayashi et al. (2007b) is adopted.

Eq. (69) is linearized as

$$g \frac{\partial \eta}{\partial x} + (\alpha_p + 1.9 \beta_p \sigma_p) U_p = 0 \quad (71)$$

which is used to obtain

$$\left[\alpha_p + 1.9 (\beta_2 + \beta_1 \sigma_p) \right] \sigma_p = g k \bar{h} \sigma_* \quad ; \quad \sigma_* = \sigma_\eta / \bar{h} \quad (72)$$

where the wave number k is computed using Eq. (2). Eq. (72) can be solved analytically to

obtain σ_p for known $k \bar{h} \sigma_*$. After σ_p is obtained, Eq. (70) is used to calculate \bar{U}_p for known

$d\bar{\eta}/dx$. The energy dissipation rate D_p is computed using Eq. (68). Eq. (62) for assumed q_o is used to obtain Q_x and \bar{U} where \bar{U} is expressed by Eq. (42).

7. Irregular Wave Runup and Overtopping

The time-averaged model CSHORE does not predict the shoreline oscillations on beaches and coastal structures unlike time-dependent models (e.g., Wurjanto and Kobayashi 1993). To compensate this shortcoming of CSHORE, Kobayashi et al. (2008d) proposed a probabilistic model for irregular wave runup as illustrated in Fig. 3. The shoreline oscillation is assumed to be measured by a runup wire (RW) placed parallel to the bottom elevation z_b at a vertical height of δ . The runup wire measures the instantaneous elevation η_r above SWL of the intersection between the wire and the free surface elevation. The mean $\bar{\eta}_r$ and standard deviation σ_r of η_r are estimated using the computed cross-shore variations of $\bar{\eta}(x)$ and $\sigma_\eta(x)$ of the free surface elevation η above SWL. The probabilities of η_r exceeding $(\bar{\eta}_r + \sigma_r)$, $\bar{\eta}_r$, and $(\bar{\eta}_r - \sigma_r)$ are assumed to be the same as the probabilities of η exceeding $(\bar{\eta} + \sigma_\eta)$, $\bar{\eta}$, and $(\bar{\eta} - \sigma_\eta)$, respectively. The elevations of Z_1 , Z_2 , and Z_3 of the intersections of $(\bar{\eta} + \sigma_\eta)$, $\bar{\eta}$, and $(\bar{\eta} - \sigma_\eta)$ with the runup wire are obtained for the given wire elevation ($z_b + \delta$). The obtained elevations are assumed to correspond to $Z_1 = [\bar{\eta}_r + \sigma_r]$, $Z_2 = \bar{\eta}_r$, and $Z_3 = (\bar{\eta}_r - \sigma_r)$. The mean and standard deviation of η_r are estimated as

$$\bar{\eta}_r = (Z_1 + Z_2 + Z_3) / 3 \quad ; \quad \sigma_r = (Z_1 - Z_3) / 2 \quad (73)$$

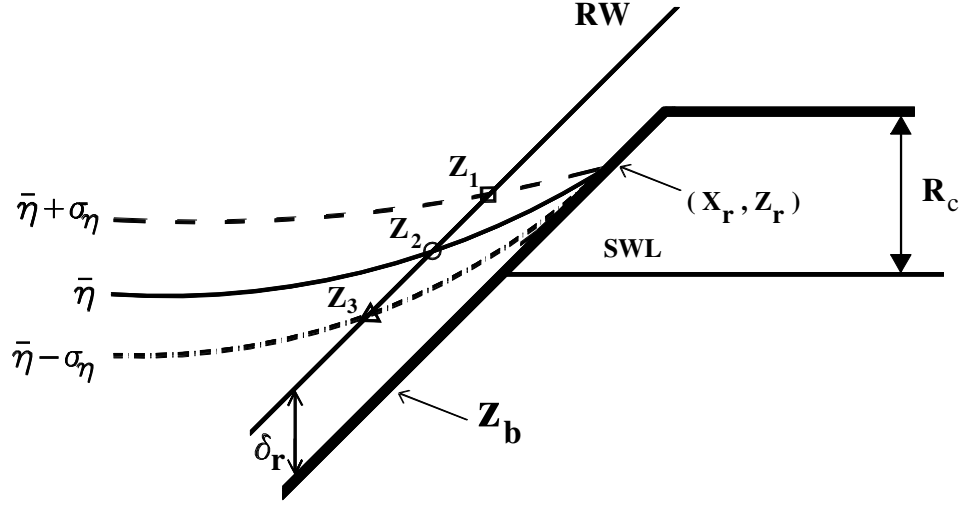


Fig. 3. Definition sketch for probabilistic model for irregular wave runup.

The runup height R is defined as the crest height above SWL of the temporal variation of η . The probability distribution of linear wave crests above the mean water level (MWL) is normally given by the Rayleigh distribution. For the case of no wave overtopping, the runup height $(R - \bar{\eta}_r)$ above the mean elevation $\bar{\eta}_r$ is assumed to be given by the Rayleigh distribution (Kobayashi et al. 2008d)

$$P(R) = \exp \left[-2 \left(\frac{R - \bar{\eta}_r}{R_{1/3} - \bar{\eta}_r} \right)^2 \right] \quad (74)$$

where $P(R)$ = exceedance probability of the runup height R above SWL; and $R_{1/3}$ = significant runup height defined as the average of 1/3 highest values of R . The mean $\bar{\eta}_r$ related to wave setup is normally neglected in Eq. (74) for the prediction of irregular wave runup on steep coastal structures. For the 1/5 and 1/2 permeable slope experiments conducted by Kobayashi et al. (2008d), $R_{1/3}$ was estimated as

$$R_{1/3} = \bar{\eta}_r + (2 + \tan \theta) \sigma_r \quad (75)$$

where θ = seaward slope angle from the horizontal and $\tan \theta = 1/5$ and $1/2$ in the experiments. It is cautioned that Eqs. (74) and (75) have been calibrated only for permeable slopes with $\tan \theta = 0.2 - 0.5$ in the absence of wave overtopping.

Wave overtopping occurs when the individual runup height R above SWL exceeds the structure crest height R_c above SWL as depicted in Fig. 3. Wave overtopping reduces R exceeding R_c because of overtopping flow on the crest. Kobayashi and de los Santos (2007) adopted the following Weibull distribution:

$$P(R) = \exp \left[-2 \left(\frac{R - \bar{\eta}_r}{R_{1/3} - \bar{\eta}_r} \right)^\kappa \right] \quad (76)$$

with

$$\kappa = 2 + 0.5 R_*^{-3} \quad ; \quad R_* = (R_c - \bar{\eta}_r) / (R_{1/3} - \bar{\eta}_r) \quad (77)$$

where κ = shape parameter with $\kappa = 2$ for the Rayleigh distribution given by Eq. (74); and R_* = normalized crest height related to the wave overtopping probability P_o . The probability P_o of R exceeding R_c in Eq. (76) is given by

$$P_o = \exp(-2R_*^\kappa) \quad (78)$$

It should be noted that the empirical formula for κ given by Eq. (77) has been calibrated using only 22 permeable slope tests so far. The formula for $R_{1/3}$ given by Eq. (75) has been found to be applicable to these 22 tests. The runup height $R_{2\%}$ for the 2% exceedance probability obtained using Eq. (76) is given by

$$R_{2\%} = \bar{\eta}_r + (1.40)^{2/\kappa} (R_{1/3} - \bar{\eta}_r) \quad (79)$$

where the shape parameter κ given by Eq. (77) accounts for the decrease of $R_{2\%}$ due to the decrease of the normalized crest height R_* and the resulting increase of the wave overtopping probability P_o given by Eq. (78).

The wave overtopping rate q_o in Eq. (19) for an impermeable slope and in Eq. (62) for a permeable slope needs to be estimated if wave overtopping occurs at the landward end of the computation domain located at $x = x_e$ in Fig. 2. For permeable slopes, Kobayashi and de los Santos (2007) proposed the following empirical formula:

$$q_o = a_* (P_o)^{b_*} q_{SWL} + q_s \quad (80)$$

with

$$q_{SWL} = \frac{g\sigma_\eta^2}{C} \cos\theta \quad \text{at } x = x_{SWL} \quad (81)$$

where a_* and b_* = empirical parameters; P_o = wave overtopping probability; q_{SWL} = wave-induced onshore flux in Eq. (62) evaluated at the still water shoreline located at $x = x_{SWL}$ with $z_b(x_{SWL}) = S$ in Fig. 2; and q_s = seepage rate through the permeable layer at $x = x_e$. It is noted that the roller effect has been neglected for permeable slopes because of its negligible effect and $q_r = 0$ in Eq. (62). The empirical parameters a_* and b_* are assumed to depend on the horizontal width L_h of the permeable surface above the upper limit of wave setup located at (x_r, z_r) in Fig. 3 where the infiltration of overtopped water is assumed to be vertical due to gravity. The empirical formulas based on 32 tests were expressed as

$$a_* = \exp(-0.1L_*) \quad ; \quad b_* = 1 + 0.1L_* \quad ; \quad L_* = L_h / D_{n50} \quad (82)$$

where L_s = infiltration width normalized by the nominal stone diameter D_{n50} , crudely representing the horizontal number of stones above the maximum wave setup.

On the other hand, Kobayashi and de los Santos (2007) estimated the seepage rate q_s for normally incident waves

$$q_s = 0.2(z_r - z_e)^{1.5} \left[\frac{g}{(x_e - x_r)\beta_1} \right]^{0.5} \quad \text{for } z_r > z_e \quad (83)$$

where z_e = elevation of the landward end of the impermeable surface z_p as shown in Fig. 2; and β_1 = turbulent flow resistance coefficient defined in Eq. (66). To derive Eq. (83), the seepage flow was assumed to be driven by the horizontal pressure gradient from the point (x_r, z_r) to the point (x_e, z_e) . Consequently, $q_s = 0$ if $z_r < z_e$. If $x_r = x_e$, the permeable layer is wet always and $q_s = h_p \bar{U}_p$ at $x = x_e$ where the water flux $h_p \bar{U}_p$ in the permeable layer is included in the continuity equation (62).

Kobayashi et al. (2007c) examined the transition from little wave overtopping to excessive wave overtopping and overflow on an impermeable smooth levee with a seaward slope of 1/5 in wave-flume experiments consisting of 107 tests. For the impermeable slope, Eqs. (75) and (77) for the permeable slope had to be modified as

$$R_{1/3} = \bar{\eta}_r + 4\sigma_r \quad ; \quad \kappa = 2 \quad (84)$$

The wave overtopping probability P_o is given by Eq. (78) with $\kappa = 2$ where the normalized crest height R_* above SWL is defined in Eq. (77) with $R_{1/3}$ given by Eq. (84). It is noted $P_o = 1$ if

$R_* < 0$. For the impermeable slope, the seepage rate $q_s = 0$ in Eq. (80) and Eq. (82) yields $a_* = 1$ and $b_* = 1$ for $L_h = 0$. As a result, the wave overtopping rate q_o is given by $q_o = P_o q_{SWL}$. For the case of combined wave overtopping and overflow, Kobayashi et al. (2007c) expressed the combined rate q_o as

$$q_o = P_o q_{SWL} + H_{SWL} \sqrt{g H_{SWL}} \quad \text{for } H_{SWL} > 0 \quad (85)$$

with

$$H_{SWL} = \bar{\eta} - R_c \quad \text{at } x = x_{SWL} \quad (86)$$

where H_{SWL} = head for the overflow; $\bar{\eta}$ = mean water level above SWL; and R_c = levee crest height above SWL. If $R_c < 0$, the levee crest is below SWL and x_{SWL} is chosen at the seaward edge of the levee crest. For $H_{SWL} > 0$, H_{SWL} is the mean water level above the levee crest and $\sqrt{g H_{SWL}}$ may be regarded as the water velocity on the crest.

In summary, Eqs. (73) – (86) are essentially empirical and used in the cross-shore model CSHORE to predict irregular wave runup, overtopping, seepage and overflow on permeable and impermeable structures. These equations have not been verified for irregular wave overtopping and overflow of dunes. These equations do not predict the spatial variations of the hydrodynamic variables required for the sediment model and the computation of dune profile evolution. Consequently, a hydrodynamic model for the intermittently wet zone landward of the maximum wave setup is developed in the following.

8. Probabilistic Model for Intermittently Wet Zone

Time-dependent numerical models such as the nonlinear shallow-water wave model by Kobayashi et al. (1989) can predict the water depth and horizontal velocity in the intermittently wet and dry (swash) zone on beaches and inclined structures. However, the time-dependent hydrodynamic computation requires considerable computation time and may not lead to an accurate prediction of dune profile evolution in view of the earlier attempt by Tega and Kobayashi (1996). A time-averaged probabilistic model is developed here to predict the cross-shore variations of the wet probability and the mean and standard deviation of the water depth and cross-shore velocity in the swash. The developed model is very efficient computationally and can be calibrated using a large number of data sets. The present model is limited to normally incident waves and alongshore uniformity. A sediment transport model in the swash zone is formulated by modifying the sediment transport model in the wet zone.

8.1 Water depth and velocity

For normally incident waves on impermeable beaches and inclined structures of alongshore uniformity, the time-averaged cross-shore continuity and momentum equations derived from the nonlinear shallow-water wave equations are expressed as

$$\overline{hU} = q_o \quad (87)$$

$$\frac{d}{dx} \left(\overline{hU^2} + \frac{g}{2} \overline{h^2} \right) = -gS_{bx} \bar{h} - \frac{1}{2} f_b \overline{|U|U} \quad ; \quad S_{bx} = \frac{dz_b}{dx} \quad (88)$$

where h and U = instantaneous water depth and cross-shore velocity, respectively; q_o = combined wave overtopping and overflow rate; g = gravitational acceleration; S_{bx} = cross-shore bottom slope; and f_b = bottom friction factor which is allowed to vary spatially. The wave

energy equation corresponding to Eqs. (87) and (88) was given by Kobayashi and Wurjanto (1992) who used it to estimate the rate of wave energy dissipation due to wave breaking which is neglected in the wet and dry zone.

The instantaneous water depth h depends on the cross-shore coordinate x and the swash hydrodynamic time t . The water depth h at given x is described probabilistically rather than in the time domain. Kobayashi et al. (1998) analyzed the probability distributions of the free surface elevations measured in the shoaling, surf and swash zones. The measured probability distributions were shown to be in agreement with the exponential gamma distribution which reduces to the Gaussian distribution and the exponential distribution when the skewness approaches zero offshore and two in the swash zone, respectively. The assumption for the Gaussian distribution assumed in Eq. (29) has simplified the cross-shore model CSHORE in the wet zone significantly. The assumption of the exponential distribution is made here to simplify the cross-shore model in the wet and dry zone. The probability density function $f(h)$ is expressed as

$$f(h) = \frac{P_w^2}{h} \exp\left(-P_w \frac{h}{h}\right) \quad \text{for } h > 0 \quad (89)$$

with

$$P_w = \int_0^{\infty} f(h) dh \quad ; \quad \bar{h} = \int_0^{\infty} hf(h) dh \quad (90)$$

where P_w = wet probability for the water depth $h > 0$; and \bar{h} = mean water depth for the wet duration. The dry probability of $h = 0$ is equal to $(1 - P_w)$. The mean water depth for the entire duration is equal to $P_w \bar{h}$. The overbar in Eqs. (87) and (88) indicates averaging for the wet

duration only. The free surface elevation $(\eta - \bar{\eta})$ above MWL is equal to $(h - \bar{h})$. The standard deviations of η and h are the same and given by

$$\frac{\sigma_{\eta}}{\bar{h}} = \left(\frac{2}{P_w} - 2 + P_w \right)^{0.5} \quad (91)$$

which yields $\sigma_{\eta} = \bar{h}$ for $P_w = 1$. This equality was supported by the depth measurements in the lower swash zone by Kobayashi et al. (1998), but the scatter was large due to the difficulty in measuring the very small depth accurately.

The cross-shore velocity U depends on x and t and is related to the depth h in the swash zone. The following relationship between U and h may be assumed to express U as a function of h

$$U = \alpha \sqrt{gh} + U_s \quad (92)$$

where α = positive constant; and U_s = steady velocity which is allowed to vary with x . The steady velocity U_s is intended to account for offshore return flow on the seaward slope and the downward velocity increase on the landward slope. Holland et al. (1991) measured the bore speed and flow depth on a barrier island using video techniques and obtained $\alpha \approx 2$ where the celerity and fluid velocity of the bore are assumed to be approximately the same. Tega and Kobayashi (1996) computed wave overtopping of dunes using the nonlinear shallow-water wave equations and showed $\alpha \approx 2$ for the computed U and h . As a result, use may be made of $\alpha = 2$ as a first approximation. Eq. (92) implies that the cross-shore velocity U increases monotonically with the increase of h at given x . Eq. (92) yields $U = U_s$ when $h = 0$, which

may be acceptable in view of the very small depth in the wet and dry zone. Using Eqs. (89) and (92), the mean \bar{U} and standard deviation σ_U of the cross-shore velocity U can be expressed as

$$\bar{U} = \frac{\sqrt{\pi}}{2} \alpha (P_w g \bar{h})^{0.5} + P_w U_s \quad (93)$$

$$\sigma_U^2 = \alpha^2 g \bar{h} - 2(\bar{U} - U_s)(\bar{U} - P_w U_s) + P_w (\bar{U} - U_s)^2 \quad (94)$$

Eq. (92) is substituted into Eqs. (87) and (88) which are averaged for the wet duration using Eq. (89). The continuity equation (87) yields

$$\frac{3\sqrt{\pi}\alpha}{4} \bar{h} \left(\frac{g\bar{h}}{P_w} \right)^{0.5} + U_s \bar{h} = q_o \quad (95)$$

After lengthy algebra, the cross-shore momentum equation (88) is expressed as

$$\frac{d}{dx} \left(B \frac{g\bar{h}^2}{P_w} + \frac{q_o^2}{\bar{h}} \right) = -g S_{bx} \bar{h} - \frac{f_b}{2} \alpha^2 g \bar{h} G_b(r_s) \quad (96)$$

with

$$B = \left(2 - \frac{9\pi}{16} \right) \alpha^2 + 1 \quad ; \quad r_s = \frac{3\sqrt{\pi}}{4} \frac{U_s \bar{h}}{q_o - U_s \bar{h}} \quad (97)$$

The function $G_b(r_s)$ in Eq. (96) with $r = r_s$ for simplicity is given by

$$G_b(r) = 1 + \sqrt{\pi} r + r^2 \quad \text{for } r \geq 0 \quad (98)$$

$$G_b(r) = 2 \exp(-r^2) - r^2 - 1 + \sqrt{\pi} r [2 \operatorname{erf}(r) + 1] \quad \text{for } r < 0 \quad (99)$$

where erf is the error function. The function G_b increases monotonically with the increase of r and $G_b = 0$ and 1 for $r = -0.94$ and 0.0, respectively, as shown in Fig. 4. For $r < -1.5$, $G_b \approx -(1 + \sqrt{\pi}r + r^2)$.

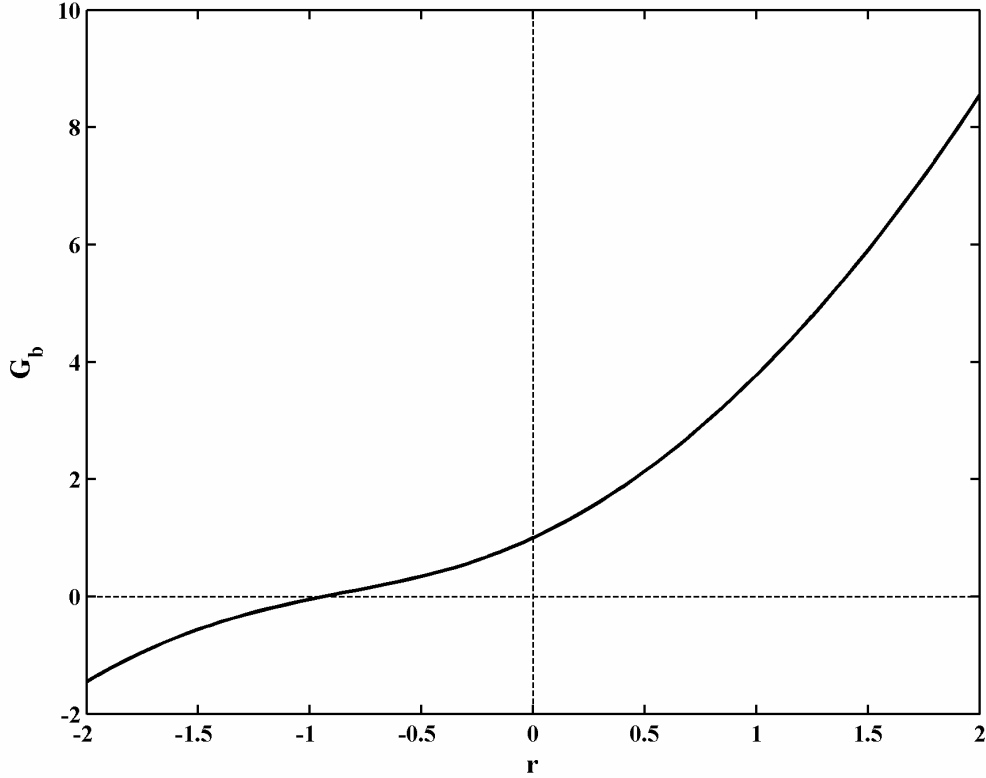


Fig. 4. Function $G_b(r)$ for wet and dry zone.

Eqs. (95) and (96) are used to predict the cross-shore variation of \bar{h} and U_s for assumed q_o where σ_η, \bar{U} and σ_U are computed using Eqs. (91), (93) and (94), respectively. It is necessary to estimate the wet probability P_w empirically. To simplify the integration of the momentum equation (96), the following formula is adopted:

$$P_w = \left[(1+A) \left(\frac{\bar{h}_1}{\bar{h}} \right)^n - A \left(\frac{\bar{h}_1}{\bar{h}} \right)^3 \right]^{-1} ; \quad A = \frac{q_o^2}{Bg\bar{h}_1^3} \quad \text{for } x \leq x_c \quad (100)$$

where \bar{h}_1 = mean water depth at the location of $P_w = 1$; n = empirical parameter for P_w ; A = parameter related to the wave overtopping and overflow rate q_o normalized by the depth \bar{h}_1 where water is present always. The transition from the wet ($P_w = 1$ always) zone to the wet and dry ($P_w < 1$) zone may be taken at $x = x_{SWL}$ where x_{SWL} is the cross-shore location of the still water shoreline of an emerged slope (see Fig. 5) or the seaward edge of a submerged crest as discussed in relation to Eqs. (85) and (86). Eq. (100) is assumed to be valid on the seaward slope and crest in the region of $x \leq x_c$ where x_c = landward end of the horizontal crest in Fig. 5.

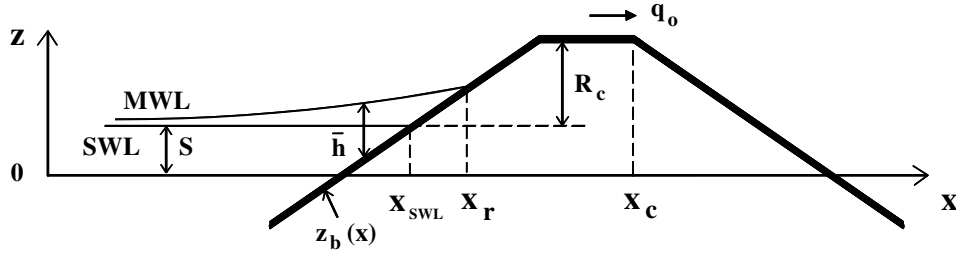


Fig. 5. Transition from wet model ($x < x_r$) to wet and dry model ($x > x_{SWL}$) for emerged structure ($R_c > 0$).

Integration of Eq. (96) for P_w given by Eq. (100) with $\bar{h} = \bar{h}_1$ at $x = x_1$ yields $\bar{h}(x)$ for $x_1 \leq x \leq x_c$

$$B_n (1+A) \bar{h}_1 \left[\left(\frac{\bar{h}_1}{\bar{h}} \right)^{n-1} - 1 \right] = z_b(x) - z_b(x_1) + \frac{\alpha^2}{2} \int_{x_1}^x f_b G_b dx \quad (101)$$

where $B_n = B(2-n)/(n-1)$; and $z_b(x)$ = bottom elevation at the cross-shore location x . The mean water depth \bar{h} at given x is computed by solving Eq. (101) iteratively where the bottom

friction factor f_b is allowed to vary with x and the function G_b given by Eqs. (98) and (99) depends on r_s defined in Eq. (97). The empirical parameter n is taken to be in the range of $1 < n < 2$ so that $B_n > 0$. The formula for n calibrated using the 107 tests of wave overtopping and overflow on a dike by Farhadzadeh et al. (2007) is expressed as $n = 1.01 + 0.98 [\tanh(A)]^{0.3}$ where $1.01 \leq n \leq 1.99$.

The wave overtopping and overflow rate q_o is predicted by imposing $U_s = 0$ in Eq. (95) at the location of x_c

$$q_o = \frac{3\sqrt{\pi}\alpha}{4} \bar{h}_c \left(\frac{g\bar{h}_c}{P_c} \right)^{0.5} \quad \text{at } x = x_c \quad (102)$$

where \bar{h}_c and P_c are the computed mean depth \bar{h} and wet probability P_w at x_c . The wave overtopping probability P_o may be related to the wet probability P_c at $x = x_c$ where both P_o and P_c are in the range of 0.0 – 1.0. The empirical relation of $P_o = [P_c^{0.6} + 0.6P_c(1 - P_c)]$ is fitted for the 107 tests by Farhadzadeh et al. (2007).

On the slope landward of the crest, the wet probability P_w is assumed to be constant and equal to P_c

$$P_w = P_c \quad \text{for } x \geq x_c \quad (103)$$

Substituting Eq. (103) into Eq. (96) and integrating the resulting equation from x_c to x , the mean depth $\bar{h}(x)$ on the landward slope in the region of $x > x_c$ is expressed as

$$\frac{\bar{h}}{\bar{h}_c} - 1 + \frac{9\pi\alpha^2}{64B} \left[\left(\frac{\bar{h}_c}{\bar{h}} \right)^2 - 1 \right] = \frac{P_c}{2B\bar{h}_c} \left[z_b(x_c) - z_b(x) - \frac{\alpha^2}{2} \int_{x_c}^x f_b G_b dx \right] \quad (104)$$

where the bottom elevation $z_b(x)$ decreases with the landward increase of x in the region of $x > x_c$. Eq. (104) is solved iteratively to compute \bar{h} at given x .

For assumed q_o , the landward marching computation of \bar{h} , σ_η , \bar{U} and σ_U is initiated using the wet model in section 4 from the seaward boundary $x=0$ to the landward limit located at $x=x_r$ which corresponds to the location where the computed \bar{h} or σ_η becomes negative in the region of \bar{h} less than 1 cm for an emerged crest as shown in Fig. 5. For a submerged crest, the landward limit of x_r is taken as x_c . The landward marching computation is continued using the wet and dry model in this section from the location of $x=x_{SWL}$ where $\bar{h}=\bar{h}_1$ in Eq. (101) to the landward end of the computation domain or until the mean depth \bar{h} becomes less than 0.001 cm. Then, the rate q_o is computed using Eq. (102). This landward computation starting from $q_o=0$ is repeated until the difference between the computed and assumed values of q_o is less than 1%. This convergency is normally obtained after several iterations. The computed values of $\bar{h}, \sigma_\eta, \bar{U}$ and σ_U by the two different models in the overlapping zone of $x_{SWL} < x < x_r$ (see Fig. 5) are averaged to smooth the transition from the wet zone to the wet and dry zone.

8.2 Sediment transport

The sediment transport model for the wet zone in section 5 is adjusted for the wet and dry zone. Normally incident waves and alongshore uniformity are assumed here. The Gaussian velocity

distribution has been assumed in section 5, whereas U in the wet and dry zone is expressed as Eq. (92) along with the exponential distribution of h given by Eq. (89).

First, the movement of sediment particles is assumed to occur when the instantaneous bottom shear stress given by $0.5\rho f_b U^2$ exceeds the critical shear stress $\rho g(s-1)d_{50}\psi_c$ as has been assumed for Eq. (49). The probability P_b of sediment movement is then the same as the probability of $|U| > U_{cb}$ where $U_{cb} = [2g(s-1)d_{50}\psi_c f_b^{-1}]^{0.5}$. Using Eqs. (89) and (92), P_b can be shown to be given by

$$P_b = P_w \quad \text{for } U_s > U_{cb} \quad (105)$$

$$P_b = P_w \exp\left[-\frac{P_w (U_{cb} - U_s)^2}{\alpha^2 g \bar{h}}\right] \quad \text{for } |U_s| \leq U_{cb} \quad (106)$$

$$P_b = P_w \left\{ 1 - \exp\left[-\frac{P_w (U_{cb} + U_s)^2}{\alpha^2 g \bar{h}}\right] + \exp\left[-\frac{P_w (U_{cb} - U_s)^2}{\alpha^2 g \bar{h}}\right] \right\} \quad \text{for } -U_s > U_{cb} \quad (107)$$

where the upper limit of P_b is the wet probability P_w because no sediment movement occurs during the dry duration.

Second, sediment suspension is assumed to occur when the instantaneous turbulent velocity estimated as $(f_b/2)^{1/3}|U|$ exceeds the sediment fall velocity w_f as has been assumed for Eq. (50). The probability P_s of sediment suspension is then the same as the probability of $|U| > U_{cs}$

where $U_{cs} = w_f (2/f_b)^{1/3}$. The probability P_s is then given by

$$P_s = P_w \quad \text{for } U_s > U_{cs} \quad (108)$$

$$P_s = P_w \exp\left[-\frac{P_w (U_{cs} - U_s)^2}{\alpha^2 g \bar{h}}\right] \quad \text{for } |U_s| \leq U_{cs} \quad (109)$$

$$P_s = P_w \left\{ 1 - \exp\left[-\frac{P_w (U_{cs} + U_s)^2}{\alpha^2 g \bar{h}}\right] + \exp\left[-\frac{P_w (U_{cs} - U_s)^2}{\alpha^2 g \bar{h}}\right] \right\} \quad \text{for } -U_s > U_{cs} \quad (110)$$

which reduces to Eqs. (105) – (107) if U_{cs} is replaced by U_{cb} . If $P_s > P_b$, use is made of $P_s = P_b$ because sediment suspension occurs only when sediment movement occurs.

Third, the suspended sediment volume V_s per unit horizontal bottom area is estimated using Eq. (51) with $S_{by} = 0$ for alongshore uniformity where wave breaking may be neglected in the wet and dry zone of very small water depth. Consequently, V_s is assumed to be given by

$$V_s = P_s \frac{e_f D_f}{\rho g (s-1) w_f} (1 + S_{bx}^2)^{0.5} \quad (111)$$

where the energy dissipation rate due to bottom friction is given by $D_f = 0.5 \rho f_b \overline{|U|^3}$. Using Eqs. (89) and (92) for the wet and dry zone, D_f can be shown to be expressed as

$$D_f = \frac{1}{2} \rho f_b \frac{\alpha^3 (g \bar{h})^{1.5}}{\sqrt{P_w}} G_d(r_s) \quad ; \quad r_s = \frac{3\sqrt{\pi}}{4} \frac{U_s \bar{h}}{q_o - U_s \bar{h}} \quad (112)$$

where the function $G_d(r_s)$ with $r = r_s$ for simplicity is given by

$$G_d(r) = \frac{3\sqrt{\pi}}{4} + 3r + \frac{3\sqrt{\pi}}{2} r^2 + r^3 \quad \text{for } r \geq 0 \quad (113)$$

$$G_d(r) = \frac{3\sqrt{\pi}}{4} (1 + 2r^2) [1 - 2\text{erf}(r)] - 3r - r^3 + (16r^3 + 9r) \exp(-r^2) \quad \text{for } r < 0 \quad (114)$$

The cross-shore suspended sediment transport rate q_{sx} is estimated using Eq. (52).

$$q_{sx} = a_x \bar{U} V_s \quad ; \quad a_x = \left[a + (S_{bx} / \tan \phi)^{0.5} \right] \geq a \quad (115)$$

where \bar{U} is given by Eq. (93).

Fourth, the cross-shore bedload transport rate q_{bx} is estimated using Eq. (56) for the case of normally incident waves ($\sin \theta = 0$) and no longshore current ($\bar{V} = 0$) where $\sigma_T = \sigma_U$ for $\sin \theta = 0$ in Eq. (32). For this case, q_{bx} is given by

$$q_{bx} = \frac{b P_b \sigma_U^3}{g(s-1)} G_s(S_{bx}) \quad (116)$$

where the bottom slope function $G_s(S_{bx})$ is given by Eqs. (58) and (59), and the standard deviation σ_U is given by Eq. (94) for the wet and dry zone.

Finally, the cross-shore sediment transport rates q_{sx} and q_{bx} computed for the wet zone and the wet and dry zone are averaged in the overlapping zone of $x_{SWL} < x < x_r$ for the smooth transition between the two zones in the same way as the smooth transition of $\bar{h}, \sigma_\eta, \bar{U}$ and σ_U as explained at the end of section 8.1. The linear extrapolation for the case of no overwash given by Eq. (60) for scarping is not applied now that the sediment transport in the wet and dry zone is predicted. The continuity equation of bottom sediment given by Eq. (61) with $q_y = 0$ is solved numerically to obtain the bottom elevation at the next time level. It must be emphasized that the sediment transport model in this section has not been validated yet.

9. Wave Overtopping and Overflow on Levees

Coastal levees (dikes) have been designed for no storm surge overflow and limited wave overtopping during a design storm. Efforts have been made to improve our understanding and capability in predicting wave runup (van Gent 2001), wave overtopping flow (Schüttrumpf 2001; van Gent 2002a; Schüttrumpf and van Gent 2003; Schüttrumpf and Oumeraci 2005), and earthen levee breaching (D'Eliso et al. 2006). A wave overtopping simulator has also been developed to investigate the effect of wave overtopping on prototype dikes (van der Meer et al. 2006).

However, very limited data is available for the transition from limited wave overtopping to overflow due to storm surge and waves. Existing formulas (e.g., EurOtop Manual 2007) for wave overtopping are not verified for the cases of excessive wave overtopping and overflow. Storm surge and wind waves can exceed the design conditions in view of Hurricane Katrina's devastation of the U.S. Gulf Coast. Time-dependent numerical models are already available to predict wave overtopping and overflow for relatively short durations where Neves et al. (2008) reviewed a number of existing models. The aim of this study is to develop a computationally efficient model that is suited for the prediction of levee erosion and breaching during an entire storm.

The transition from little wave overtopping to combined wave overtopping and overflow on a levee is investigated in small-scale laboratory experiments. A total of 107 tests were conducted on an impermeable smooth levee of a 1/5 slope located on a beach of a 1/34.2 slope. The measured overtopping and overflow rates are compared with the formulas in EurOtop Manual (2007) which are found to predict the rates of excessive wave overtopping and overflow within a factor of about 2. The numerical model developed by Kobayashi and de los Santos (2007) for

wave overtopping is modified to include wave and current interactions. A time-averaged probabilistic model is developed to predict the water depth and velocity in the wet and dry zone on the levee. The numerical model extended to the wet and dry zone is calibrated to predict the measured overtopping and overflow rates for the 107 tests within the factor of 2. The model is also compared with the 118 tests conducted by van Gent (2002b) who measured the water depths and velocities on the crest and landward (inner) slope of dikes.

9.1 Wave overtopping and overflow experiments

Experiments were conducted in a wave flume that was 33 m long, 0.6 m wide, and 1.5 m high as shown in Fig. 6. An impermeable smooth beach with a $1/34.2$ slope was installed in the flume. A $1/14.8$ slope of horizontal length 1.29 m was installed between the horizontal flume bottom and the $1/34.2$ slope but is not shown in Fig. 6 for brevity. An impermeable levee was constructed of plywood. The seaward slope and crest width of the levee were $1/5$ and 30 cm, respectively. A tank was built landward of the levee crest to collect overtopped and overflowed water. The horizontal length and width of the tank were 1.85 m and 0.6 m, respectively.

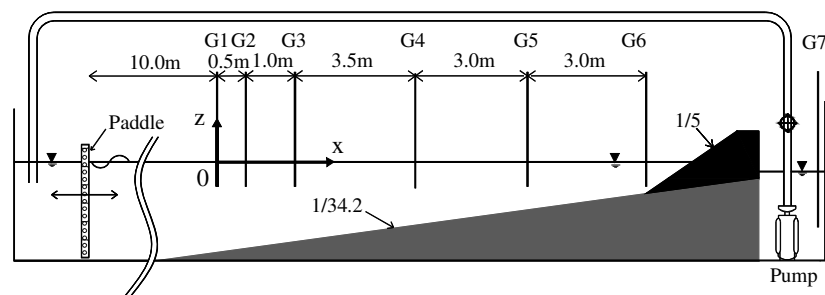


Fig. 6. Experimental setup for wave overtopping and overflow.

Seven capacitance wave gauges (G1 to G7) were placed as shown in Fig. 6. Wave gauges G1 – G3 were used to separate the incident and reflected waves and estimate the average reflection coefficient R outside the surf zone (Kobayashi et al. 1990). Wave gauges G4 – G6 measured the wave transformation on the 1/34.2 slope. Wave gauge G7 measured the water level and corresponding water volume in the tank. A pump-pipe system was used to circulate water from the tank to the zone behind the piston-type perforated wave paddle. A flow meter in the pipe was installed to measure the discharge and corresponding water volume pumped during a specified duration. The flow meter was calibrated by pumping water from the tank at a constant rate and measuring the constant rate of decrease of the water level in the tank.

In the following, the cross-shore coordinate x is taken to be positive landward with $x=0$ at wave gauge G1. The vertical coordinate z is taken to be positive upward with $z=0$ at the lowest still water level (SWL) used in the wave overtopping experiment. The bottom elevation is denoted by $z_b(x)$. For the experimental setup shown in Fig. 6, $z_b = -45.6$ cm at $x=0$, $z_b = -12.0$ cm at the toe of the 1/5 slope located at $x = 11.0$ m, and $z_b = 16.5$ cm on the levee crest located at $x = 12.5 - 12.8$ m. The still water level S above $z=0$ was varied in the range of $S = 0.0 - 16.5$ cm for the wave overtopping experiment. The levee crest height R_c above SWL is given by $R_c = (16.5 - S)$ cm. Irregular waves, based on the TMA spectrum, were generated using the wave paddle in a burst of 400 s. The water depth at the wave paddle was $(52 + S)$ cm. The initial transient of 40 s in each burst was removed from the measured time series sampled at a rate of 50 Hz. The time series of the free surface elevation η above SWL for the remaining 360-s duration were used to obtain the mean $\bar{\eta}$ and the standard deviation σ_η for wave gauges G1—G6, as well as the spectral peak period T_p , the spectral wave period $T_{m-1,0}$ (van Gent 2001), and the average

reflection coefficient R at wave gauge G1. Table 1 lists the ranges of S , T_p , $T_{m-1,0}$, σ_η and R for the 78 wave overtopping (WO) tests conducted in the experiment. The root-mean-square (RMS) wave height H_{rms} and the significant wave height H_{mo} are defined as $H_{rms} = \sqrt{8} \sigma_\eta$ and $H_{mo} = 4\sigma_\eta$. The difference between T_p and $T_{m-1,0}$ was small at wave gauge G1 located outside the surf zone.

For the overflow experiment, the water level was raised above the levee crest. The overflowed water was pumped. The pumping of about 800 s was required to establish the steady flow in the wave flume. The still water level S is taken as the water level at wave gauge G1 before the generation of irregular waves. The generated waves were measured and analyzed in the same way as in the wave overtopping experiment. The measured free surface elevation above SWL included the combined effects of the current and waves. Table 1 lists the ranges of S , T_p , $T_{m-1,0}$, σ_η and R for the 29 overflow (OF) tests. Irregular waves with larger values of σ_η could not be tested in the overflow experiment because of the limited space between the water level and the carriage supporting the wave gauge. The wave reflection coefficient R decreased somewhat with the increase of wave overtopping and overflow because the landward mass flux accompanies the landward energy flux.

Table 1 also lists the ranges of the measured variables related to wave overtopping and overflow for the WO and OF tests where N_i = number of incident waves for the 360-s duration; P_o = overtopping probability estimated as $P_o = N_o/N_i$ with N_o = number of overtopped waves, which were counted visually; and q_o = combined overtopping and overflow rate calculated from the pumped water volume and the volume change in the tank during the 360-s duration. It is noted

that the measured values for all the tests were tabulated in the report by Farhadzadeh et al. (2007).

Table 1: Wave Conditions at Wave Gauge G1 and Ranges of Wave Overtopping Measurements for Wave Overtopping (WO) and Overflow (OF) Tests

Test	Number of tests	S (cm)	T_p (s)	$T_{m-1,0}$ (s)	σ_η (cm)	R	N_i	P_o	q_o (cm ² /s)
WO	78	0.0-16.5	1.32-2.50	1.47-2.31	0.84-4.58	0.20-0.46	197-274	0.0-1.0	0.0-71.6
OF	29	17.2-19.4	1.56-2.06	1.47-1.89	0.73-1.89	0.09-0.34	206-271	1.0	26.3-107.5

9.2 Comparison of EurOtop formulas with experiments

The measured values of q_o for the 107 tests are compared with the formulas in the EurOtop Manual (2007). For the smooth seaward slope $\tan \theta = 0.2$, the formula for the emerged crest is expressed as

$$q_* = \frac{0.067}{\sqrt{\tan \theta}} \xi \exp\left(-4.75 \frac{R_*}{\xi}\right) \leq 0.2 \exp(-2.6R_*) \quad \text{for } R_* > 0 \quad (117)$$

with

$$q_* = \frac{q_o}{\sqrt{gH_{mo}^3}} \quad ; \quad \xi = \tan \theta \left(\frac{gT_{m-1,0}^2}{2\pi H_{mo}} \right)^{0.5} \quad ; \quad R_* = \frac{R_c - \bar{\eta}}{H_{mo}} \quad (118)$$

where g = gravitational acceleration; q_* = normalized overtopping rate; ξ = surf similarity parameter; and R_* = normalized crest height. Eq. (117) implies that the upper limit of q_* for given R_* is given by $0.2\exp(-2.6R_*)$. Use is made of the measured values of $H_{mo}, T_{m-1,0}$ and $\bar{\eta}$ at wave gauge G6 located at the toe of the 1/5 slope where the measured values included the effect of reflected waves. The original formula does not include the mean water level $\bar{\eta}$ but its effect is examined in the following. Eq. (117) was obtained for $R_* > 0.4$ but is extrapolated to $R_* > 0$, corresponding to excessive wave overtopping. For the submerged crest with $R_* \leq 0$, q_* may be expressed as

$$q_* = 0.6|R_*|^{1.5} + 0.0537\xi \quad \text{for } \xi < 2 \quad (119)$$

$$q_* = 0.6|R_*|^{1.5} + 0.136 - 0.226\xi^{-3} \quad \text{for } \xi \geq 2$$

For $R_* = 0$, Eq. (119) reduces to the formula proposed by Schüttrumpf (2001). The term, $0.6|R_*|^{1.5}$, is based on the weir formula for a broad crested structure in the absence of waves. Eq. (119) simply adds the two formulas. Eqs. (117) and (119) do not yield the same value of q_* at $R_* = 0$ but Eq. (117) is extrapolated to $R_* = 0$ because it was based on extensive data sets. The difference of q_* at $R_* = 0$ is less than a factor of 2 for the 107 tests with $-1.1 < R_* < 2.6$ and $1.8 < \xi < 67$.

Fig. 7 compares the measured and empirical values of q_* for the 107 tests. The solid and dashed lines in this and subsequent figures indicate the perfect agreement and deviation of a factor of 2,

respectively. Most of the data points fall within the deviation of the factor of 2. Eqs. (117) and (119) are applicable to the cases of excessive wave overtopping and overflow in these tests. Fig. 7 indicates that the agreement for $q_* \geq 0.1$ is slightly better if the normalized crest height R_* is based on the crest height $(R_c - \bar{\eta})$ above the mean water level (MWL) at the toe of the 1/5 slope. The mean water level $\bar{\eta}$ is affected by wave set-down and setup on the beach seaward of the levee as well as onshore flow due to wave overtopping and overflow. The use of MWL instead of SWL for the design of coastal structures may eventually become standard because the coupled predictions of wind waves and storm surge in shallow water are now common.

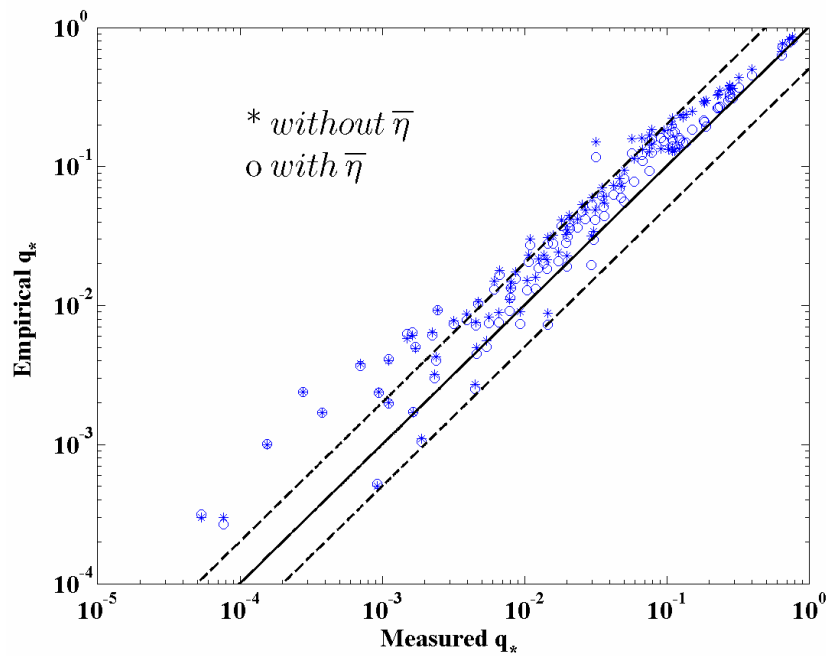


Fig. 7. Measured and empirical wave overtopping and overflow rates for 107 tests.

9.3 Comparison of CSHORE empirical formulas with experiments

The probabilistic model for the wet and dry zone in section 8.1, which has been added in the present version of CSHORE, eliminates the need to rely on the empirical formulas given by Eqs. (78), (84) and (85) for irregular wave runup and overtopping on the impermeable levee. These formulas were calibrated by Kobayashi et al. (2007c) for the previous CSHORE with no wet and dry zone using the present experiments in section 9.1. The comparison made by Kobayashi et al. (2007c) is repeated here using the present CSHORE with the wet and dry zone. All the empirical formulas in section 7 are included in the present CSHORE mainly because the wet and dry model is presently limited to impermeable structures. No additional computation was necessary for the following comparison because the present CSHORE computes both the empirical values using section 7 and the values computed using the wet and dry model in section 8.1. The computational input was explained by Kobayashi et al. (2007c) and is summarized in section 9.4 where the computed results using the wet and dry model are presented.

The runup wire placed parallel to the seaward slope and crest of the levee in Fig. 6 was used to measure the shoreline oscillation $\eta_r(t)$ above SWL for each of the 107 tests. The vertical height δ_r of the wire was approximately 2 cm. The measured mean $\bar{\eta}_r$ and standard deviation σ_r are compared with the values computed in Eq. (73). Fig. 8 compares the measured and computed water level $(\bar{\eta}_r + S)$ above the datum $z = 0$ for the 107 tests. The agreement appears excellent because $\bar{\eta}_r$ due to waves and overflow is small relative to the still water level increase S due to storm surge and tides in the experiments where the crest height above $z = 0$ is 16.5 cm. The numerical model underpredicts $(\bar{\eta}_r + S)$ for the data points with $(\bar{\eta}_r + S)$ exceeding 18 cm

perhaps because Eq. (73) developed for the inclined slope is not really applicable to the horizontal crest. Fig. 9 compares the measured and computed standard deviations σ_r . The numerical model overpredicts σ_r for the data points with σ_r less than about 1 cm where these data points correspond to the data points with $(\bar{\eta}_r + S) > 18$ cm. The numerical model also underpredicts σ_r for the data points with $\sigma_r > 4$ cm perhaps because Eq. (73) was initially developed for permeable slopes.

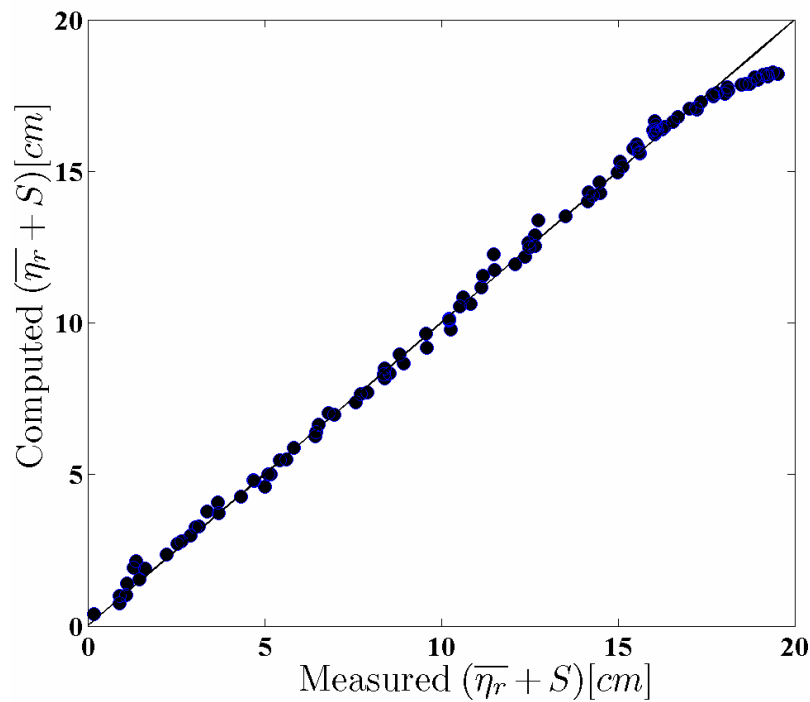


Fig. 8. Measured and computed mean water levels of runup wire for 107 tests.

Fig. 10 compares the measured and empirical rates q_o where q_o is predicted using the empirical formula given by Eq. (85). The formula overpredicts q_o by the factor exceeding 2 for some of the wave overtopping tests.

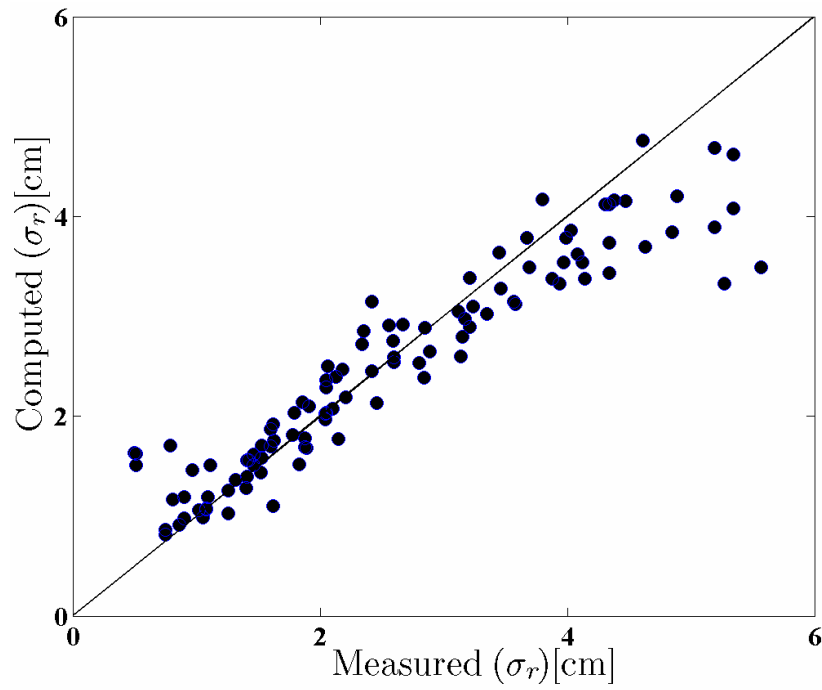


Fig. 9. Measured and computed standard deviations of free surface oscillation along runup wire for 107 tests.

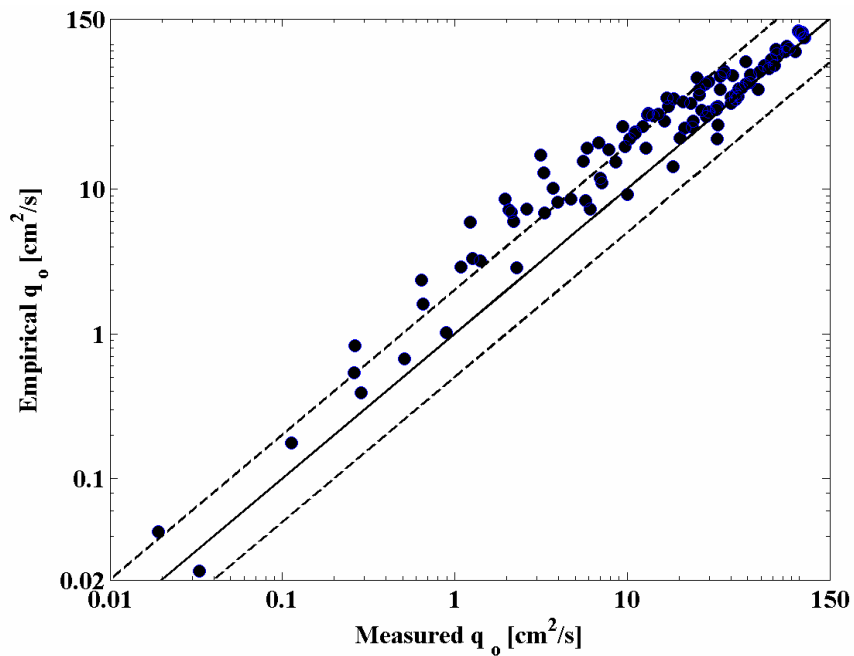


Fig. 10. Measured and empirical wave overtopping and overflow rates for 107 tests.

Fig. 11 compares the measured and empirical overtopping probabilities P_o where P_o is predicted using Eqs. (78) and (84). The formula tends to underpredict P_o for the data points with $P_o < 0.5$. Eq. (78), (84) and (85) could be recalibrated for the present CSHORE but the empirical formulas do not appear to be robust as will be shown in section 9.5.

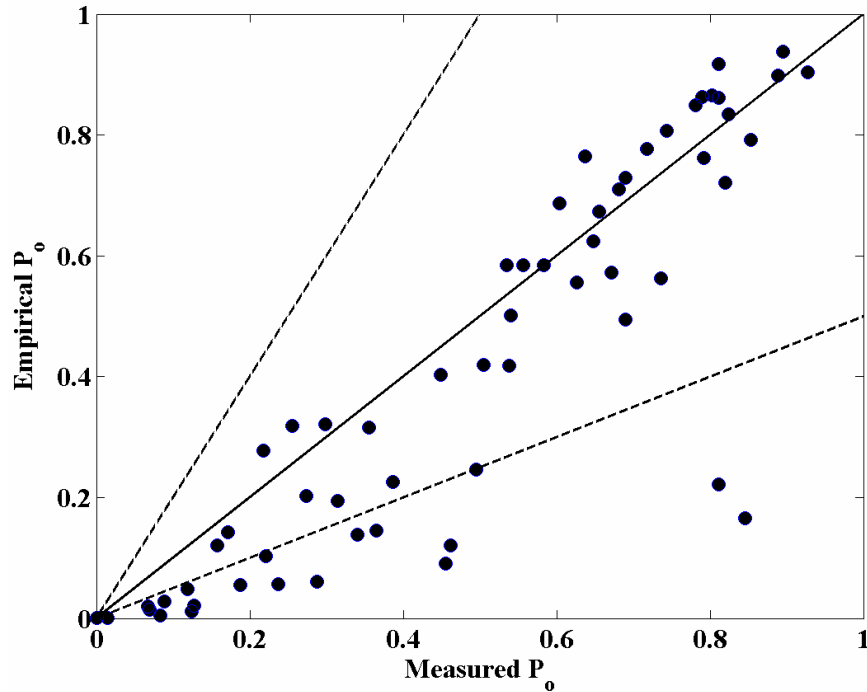


Fig. 11. Measured and empirical wave overtopping probabilities for 107 tests.

9.4 Comparison of CSHORE wet and dry model with present experiments

The wet and dry model in section 8.1 is compared with the 107 tests. The number of nodes with constant nodal spacing from $x = 0$ to the landward end of the levee crest located at $x_c = 12.8$ m in Fig. 6 was 1279. The breaker ratio parameter γ used to estimate the breaker height H_B in Eq. (38) was taken as $\gamma = 0.7$ in the previous comparisons by Kobayashi et al. (2007b) and Kobayashi and de los Santos (2007). For the present 107 tests, $\gamma = 0.8$ yields slightly better agreement for the cross-shore variation of σ_η . The bottom friction factor f_b is calibrated in the

range of $f_b = 0.0 - 0.005$. The computed q_o changed less than 10%. The following computed results are based on $f_b = 0.002$. The computed cross-shore variations of $\bar{\eta}, \sigma_\eta, \bar{U}$ and σ_U are plotted together with the measured values of $\bar{\eta}$ and σ_η at wave gauges G1 – G6 for all the tests (Farhadzadeh et al. 2007).

Wave overtopping test 41 and overflow test 94 are shown in Figs. 12 and 13 as examples. The mean water level $(\bar{\eta} + S)$ above $z = 0$ and the bottom elevation z_b are plotted together in the top panel. The computed wet probability P_w is plotted in the bottom panel where $P_w = 1$ in the wet zone. The computed and measured values vary very little in the region of $0 \leq x \leq 4.5$ m which is omitted in these figures. The agreement between the measured and computed values for $(\bar{\eta} + S)$ and σ_η at wave gauges G1—G3 is excellent because the measured values at $x = 0$ are specified as input. For test 41, the mean water level $(\bar{\eta} + S)$ increases landward due to the increase of the wave setup $\bar{\eta}$. The decrease of the wave height represented by σ_η occurs mostly on the 1/5 levee slope because of little wave breaking on the beach. It is noted that the stepped change of the computed σ_η occurs sometimes in the transition zone in Fig. 5 because σ_η is not matched at $x = x_{swl}$. The offshore (negative) return current \bar{U} is small on the beach and increases on the 1/5 slope before \bar{U} becomes onshore due to the wave overtopping flow. The standard deviation σ_U increases gradually on the beach and rapidly on the 1/5 slope before its decrease in the very small mean depth in the wet and dry zone where the wet probability P_w decreases rapidly on the 1/5 slope and becomes approximately constant on the crest. For test 94,

the computed mean water level $(\bar{\eta} + S)$ exhibits little wave setup due to the water level decrease associated with the overflow. The standard deviation σ_{η} increases on the 1/5 slope due to shoaling and decreases due to wave breaking. The computed value of σ_{η} remains approximately constant on the submerged levee crest where the mean depth \bar{h} is approximately constant. The computed mean velocity \bar{U} is almost zero except near the levee crest where \bar{U} becomes as large as σ_U due to overflow.

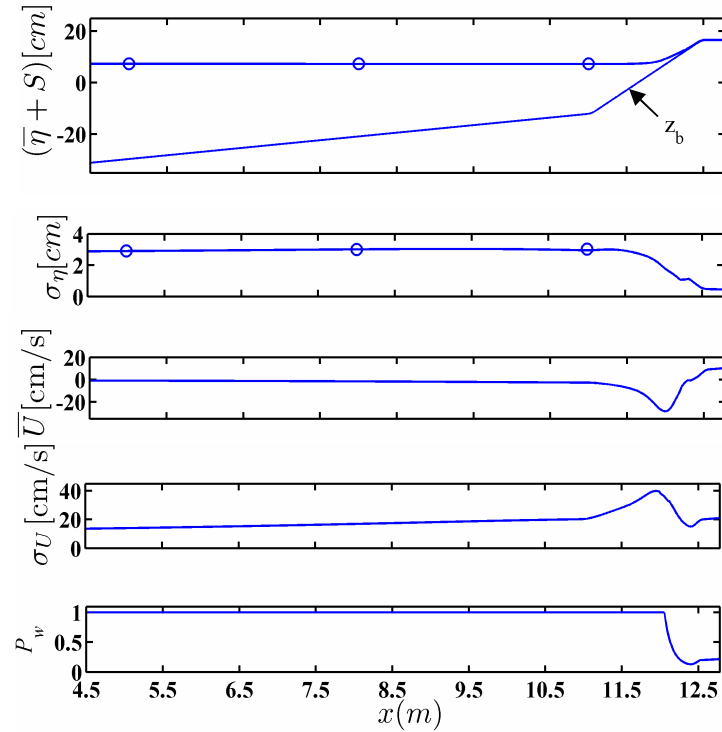


Fig. 12. Measured (circle) and computed (solid line) mean and standard deviation of free surface elevation η and depth-averaged velocity U together with wet probability P_w for wave overtopping test 41 where mean water level $(\bar{\eta} + S)$ and bottom elevation z_b are plotted in top panel.

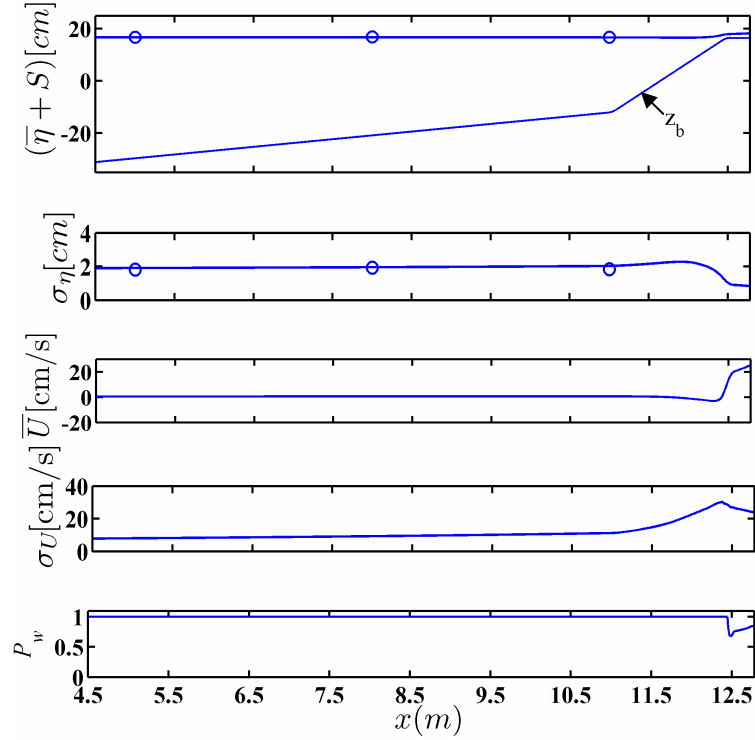


Fig. 13. Measured (circle) and computed (solid line) mean and standard deviation of free surface elevation η and depth-averaged velocity U together with wet probability P_w for overflow test 94 where mean water level $(\bar{\eta} + S)$ and bottom elevation z_b are plotted in top panel.

Fig. 14 compares the measured and computed rates q_o for the 107 tests. The agreement is within the factor of about 2 because of the calibration of the empirical equation (100) using the same tests. Fig. 15 compares the measured and computed probabilities P_o for the 107 tests. The agreement is also within the factor of about 2 because the same tests are used to calibrate the empirical relation between P_o and P_c discussed below Eq. (102). Comparisons with additional experiments are required to verify the numerical model including its capability of predicting the water depth and velocity in the wet and dry zone.

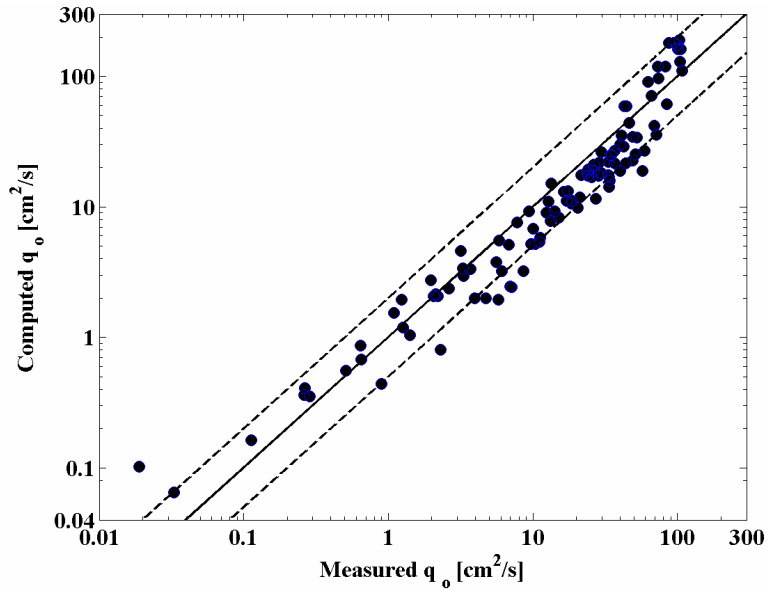


Fig. 14. Measured and computed wave overtopping and overflow rates for 107 tests.

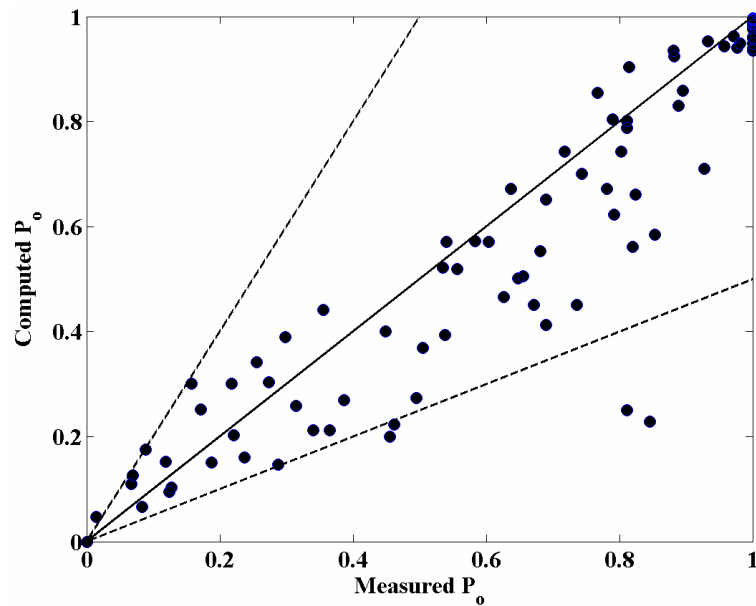


Fig. 15. Measured and computed wave overtopping probabilities for 107 tests.

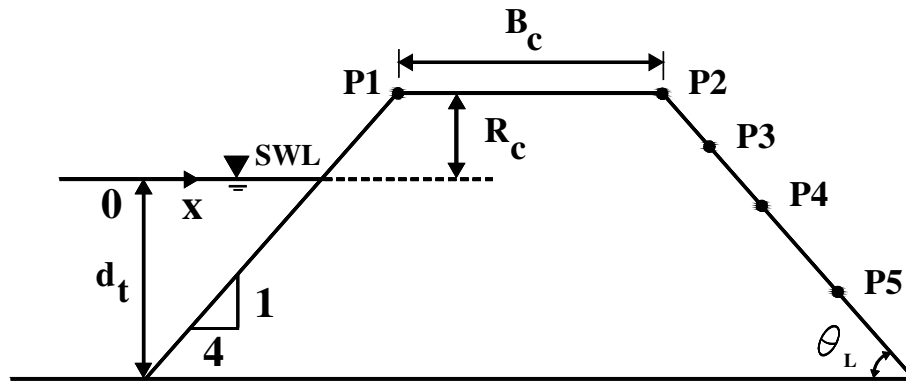
9.5 Comparisons with Dutch Experiments

van Gent (2002b) conducted experiments in a wave flume that was 55 m long, 1.0 m wide, and 1.2 m high. A smooth beach with a 1/100 slope was installed in the flume and 7 series for

different structures were performed as shown in Fig. 16. The seaward slope was 1/4 for all the series. The crest height above the toe of the seaward slope was 0.6 m for series A, B, C, D and D' (dikes) and 0.2 m for series E and F (low-crested structures). The crest width was 0.2 m for series A, B and E and 1.1 m for the rest. The landward slope was 1/2.5 for series A and C and 1/4.0 for the rest. The structure surface was smooth except for series D' for which a single layer of gravel of 4.9-mm diameter was glued on the crest and landward slope. The crest height R_c shown in Fig. 16 was in the range of 10 – 30 cm for series A, B, C, D and D' and 7.5 – 10 cm for series E and F. The 18 irregular waves measured at the toe of the 1/4 slope for series A – D' were characterized by $H_{mo} = 12.6 – 15.3$ cm and $T_{m-1,0} = 1.44 – 2.21$ s. The 14 irregular waves for series E and F were characterized by $H_{mo} = 6.2 – 8.2$ cm and $T_{m-1,0} = 1.73 – 2.97$ s. The mean water level $\bar{\eta}$ above SWL at the toe was not reported by van Gent (2002b) and is assumed to be zero in the following computations.

The computation domain starts from the seaward boundary $x = 0$ at the toe of the 1/4 slope where the measured values of H_{mo} and $T_{m-1,0}$ for each test are available. Its landward end is located at the downward end of the landward slope at the same elevation as the toe elevation. The constant nodal spacing is 0.5 cm. The empirical parameters for the numerical model are kept the same except for the bottom friction factor f_b for the rough crest and landward slope for series D'. Since $f_b = 0.002$ is assumed for the smooth surface, use is made of $f_b = 0.006$ for the rough surface. The differences of the computed q_o and P_o for $f_b = 0.005 – 0.025$ for the rough surface are found to be well within the accuracy (a factor of 2) of the present numerical model.

In short, the calibration of f_b does not improve the agreement noticeably perhaps because the flow through the roughness is not accounted for.



Series	$\cot \theta_L$	B_C (m)	d_t (cm)	R_c (cm)	Roughness
A	2.5	0.2	30 – 50	10 – 30	smooth
B	4.0	0.2	30 – 50	10 – 30	smooth
C	2.5	1.1	30 – 50	10 – 30	smooth
D	4.0	1.1	30 – 50	10 – 30	smooth
D'	4.0	1.1	30 – 50	10 – 30	rough*
E	4.0	0.2	10 – 12.5	7.5 – 10	smooth
F	4.0	1.1	10 – 12.5	7.5 – 10	smooth

Note: $(d_t + R_c) = 60$ cm for series A, B, C, D. and D'
 $(d_t + R_c) = 20$ cm for series E and F

*Roughness on crest and landward slope

Fig. 16. Series A, B, C, D, D', E and F conducted by van Gent (2002).

The empirical formulas for q_o and P_o in the present CSHORE have been compared with the 107 tests in Figs. 10 and 11. These formulas are compared with the 118 tests by van Gent (2002b) in Figs. 17 and 18. The formula given by Eq. (85) overpredicts q_o considerably for series A, B, C, D and D' for relatively low probabilities of wave overtopping. The agreement for series E and F is within the factor of about 2. The formula given by Eqs. (78) and (84) predicts P_o within the factor of about 2 for series A and B but tends to overpredict P_o for series C, D and D' and

underpredict it for series E and F. Figs. 17 and 18 indicate the difficulty in developing robust formulas that predict q_o and P_o within the factor of 2 consistently.

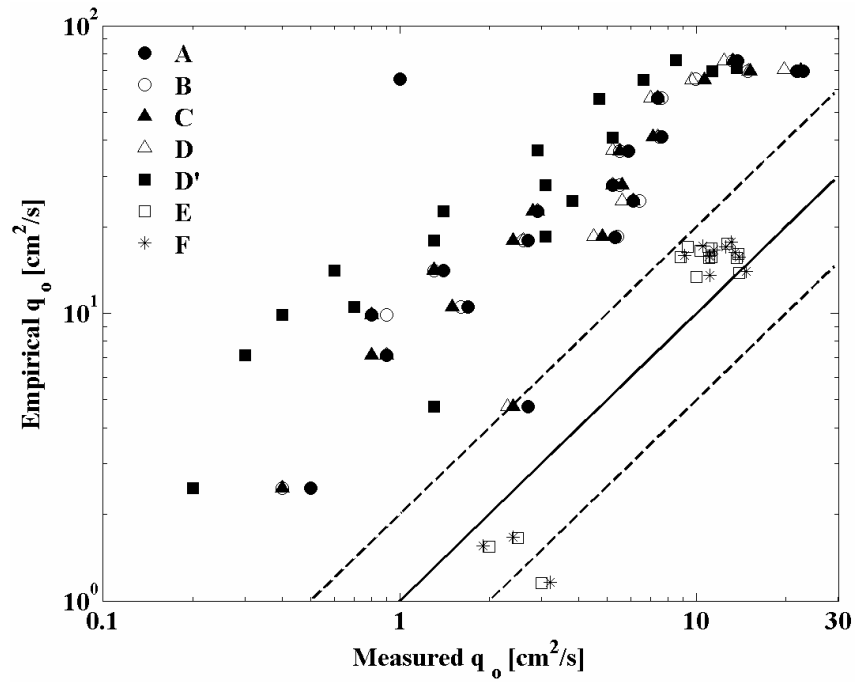


Fig. 17. Measured and empirical wave overtopping rates for 118 Dutch tests.

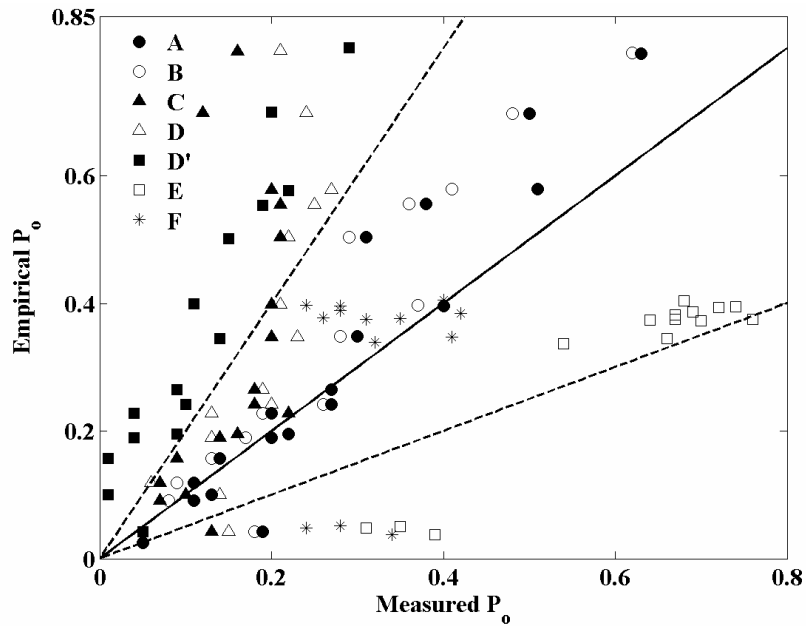


Fig. 18. Measured and empirical wave overtopping probabilities for 118 Dutch tests.

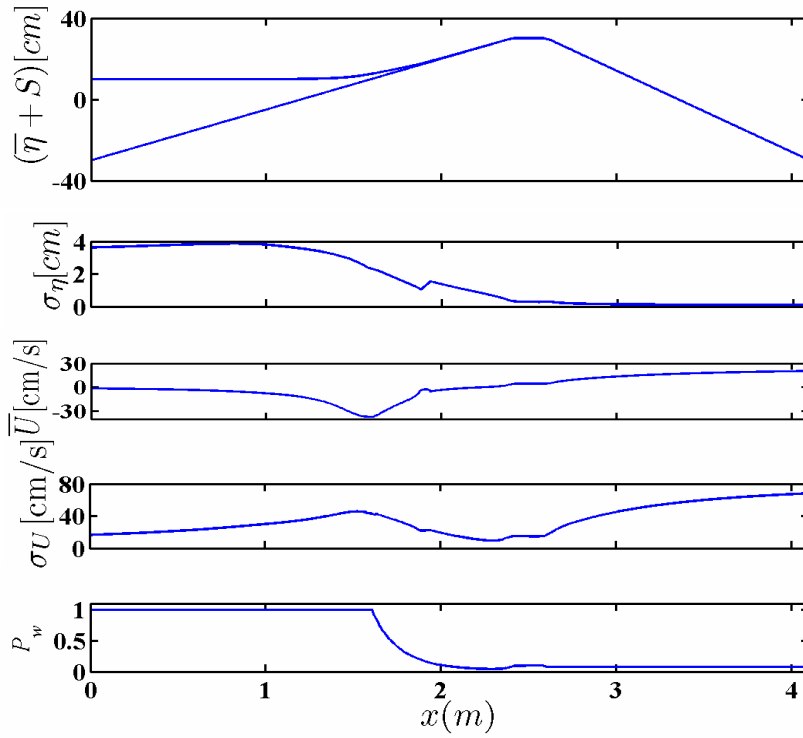


Fig. 19. Computed mean and standard deviation of free surface elevation η and depth-averaged velocity U together with wet probability P_w for series A with wave conditions No. 1.06 where mean water level $(\bar{\eta} + S)$ and bottom elevation z_b are plotted in top panel.

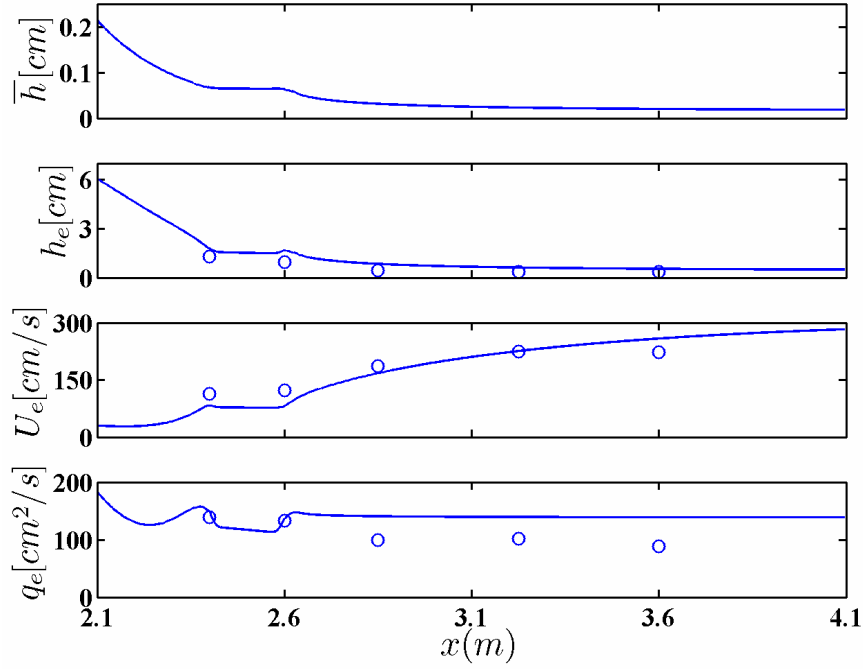


Fig. 20. Computed cross-shore variation of mean depth \bar{h} and comparisons with measured (circle) depth $h_{2\%}$, velocity $U_{2\%}$ and discharge $q_{2\%}$ for series A with wave conditions No. 1.06.

Fig. 19 shows the computed cross-shore variations of the mean water level ($\bar{\eta} + S$) together with the bottom elevation z_b , the free surface standard deviation σ_η , the mean velocity \bar{U} , the velocity standard deviation σ_U , and the wet probability P_w for test 1.06 of series A. Fig. 19 is similar to Fig. 12 except for the computed variations on the landward slope in Fig. 19. The mean depth $\bar{h} = (\bar{\eta} + S - z_b)$ and σ_η are of the order of 0.1 cm or less on the crest and landward slope, whereas \bar{U} and σ_U increase downward on the landward slope and are of the order of 10 cm/s or larger. The wet probability P_w , which is assumed to be constant on the landward slope in Eq. (103), is of the order of 0.1 on the crest and landward slope. Fig. 20 shows the computed cross-

shore variations of \bar{h}, h_e, U_e and q_e in the zone of $x = 2.1 - 4.1$ m in Fig. 19 where h_e, U_e and q_e are the depth, velocity and discharge corresponding to the exceedance probability $e = 0.01$ as explained in the following. The data points in Fig. 20 are the measured values exceeded by 2% of the incident 1,000 waves. The flow in the wet and dry zone in Figs. 19 and 20 is characterized by the small water depth and very large velocity during the short wet duration. The probabilistic model for the wet and dry zone in section 8.1 appears to reproduce the essential aspects of this intermittent flow.

Fig. 21 compares the measured and computed wave overtopping rates q_o for the 7 series consisting of 118 tests. The agreement is mostly within the factor of 2 but for series E and F, the computed q_o is about a half of the measured q_o . The reason for this underprediction is not clear but might be related to the neglected mean water level $\bar{\eta}$ at the toe of the 1/4 slope which may have been located inside the surf zone for series E and F. Fig. 22 compares the measured and computed wave overtopping probabilities P_o for the 7 series. The numerical model tends to overpredict P_o for series C and D' but the agreement is within the factor of 2 for the rest. The comparisons for q_o and P_o do not prove that the numerical model can predict the water depth and velocity which are more directly related to the erosion of a dike (Schüttrumpf and Oumeraci 2005).

van Gent (2002b) measured the water depth and velocity at five points for each test as shown in Fig. 16. Points P1 and P2 were located at the seaward and landward ends of the crest, respectively. Points P3, P4 and P5 were located on the landward slope at elevations of 10, 25

and 40 cm, respectively, below the crest for series A – D'. These elevations were 5, 10 and 18 cm below the crest for series E and F. The measured water depth and velocity at each point were analyzed on the basis of individual wave overtopping events. The values tabulated in his report are the water depth $h_{2\%}$, velocity $U_{2\%}$, and discharge $q_{2\%}$ corresponding to the values exceeded by 2% of the incident 1,000 waves. It is noted that the numerical model is based on the vertical depth h and the horizontal velocity U . The measured depth was the depth normal to the slope and the measured velocity was parallel to the slope. The differences of h and U defined differently are less than 8% on the landward slopes of 1/2.5 and 1/4. These differences are neglected in the following comparisons.

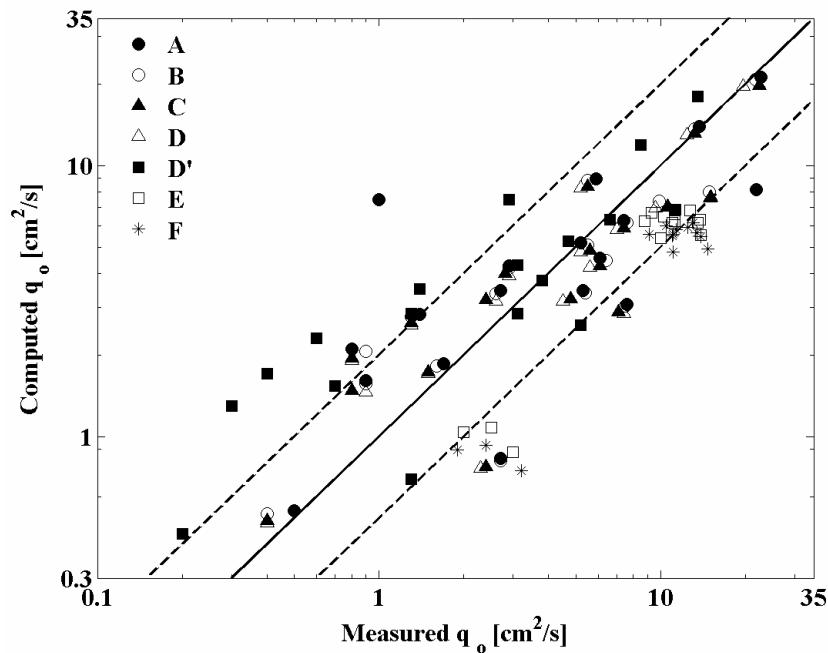


Fig. 21. Measured and computed wave overtopping rates for 118 Dutch tests.

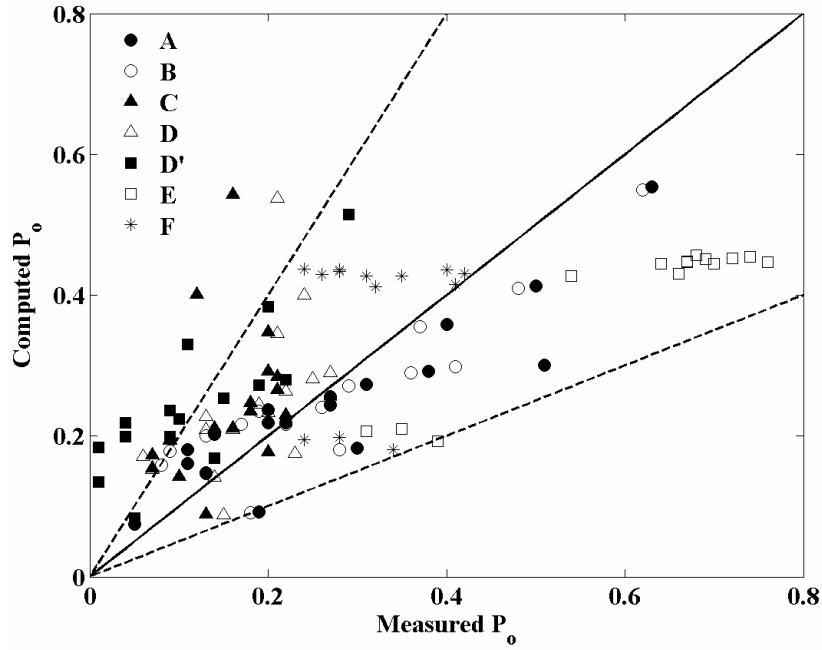


Fig. 22. Measured and computed wave overtopping probabilities for 118 Dutch tests.

For the probability density function $f(h)$ given by Eq. (89), the water depth h_e corresponding to the exceedance probability e is given by

$$h_e = \frac{\bar{h}}{P_w} \ln\left(\frac{P_w}{e}\right) \quad \text{for } P_w > e \quad (120)$$

Using Eq. (92), the velocity U_e and discharge q_e corresponding to the exceedance probability e are expressed as

$$U_e = \alpha\sqrt{gh_e} + U_s \quad ; \quad q_e = h_e U_e \quad (121)$$

The probability e of $h > h_e$ at given x is not directly related to the probability based on individual overtopping events where the exceedance probability 2% used by van Gent (2002b) is normally regarded as an extreme event. It is assumed that $h_e = h_{2\%}, U_e = U_{2\%}, q_e = q_{2\%}$ with $e = 0.01$. The compared results for $e = 0.005, 0.01$ and 0.02 are found to be similar because h_e

given by Eq. (120) is not very sensitive to $e = 0.005 - 0.02$ as long as the wet probability P_w is larger than about 0.1.

Fig. 23 compares the measured and computed water depth $h_{2\%}$ for the 7 series at the five points where $h_{2\%}$ decreases landward on the crest (P1 and P2) and on the landward slope (P3, P4 and P5). The agreement is mostly within the factor of 2 but $h_{2\%}$ is overpredicted by about 50% for series B, C, D and D'. Fig. 24 compares the measured and computed velocities $U_{2\%}$ where $U_{2\%}$ does not change much on the crest and increases downward on the landward slope. The agreement is mostly within the factor of 2 but $U_{2\%}$ is underpredicted at points P1 and P2 and overpredicted at points P4 and P5. Fig. 25 compares the measured and computed discharge $q_{2\%}$. The agreement is good with no systematic deviations for series A, B, C, D and D'. For series E and F, some data points deviate more than the factor of 2.

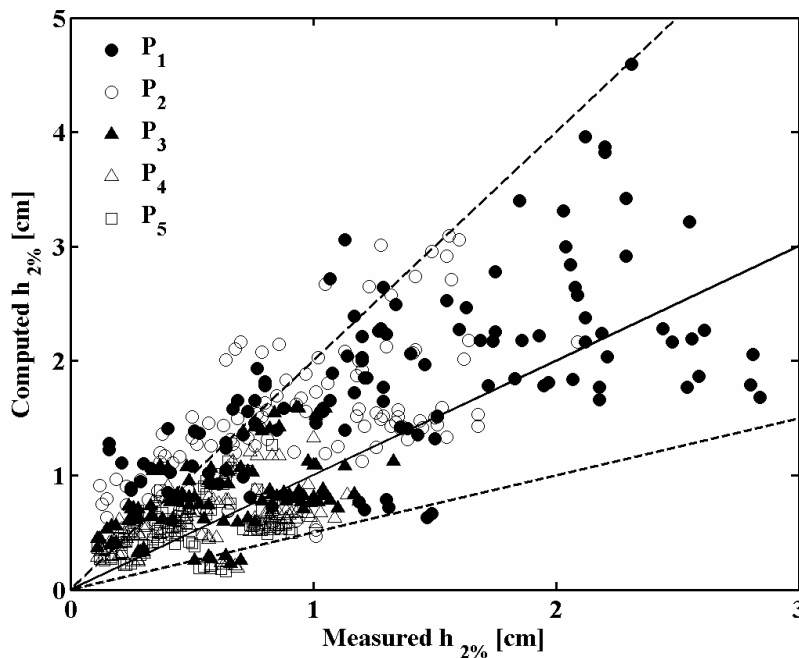


Fig. 23. Measured and computed water depth $h_{2\%}$ at five points.

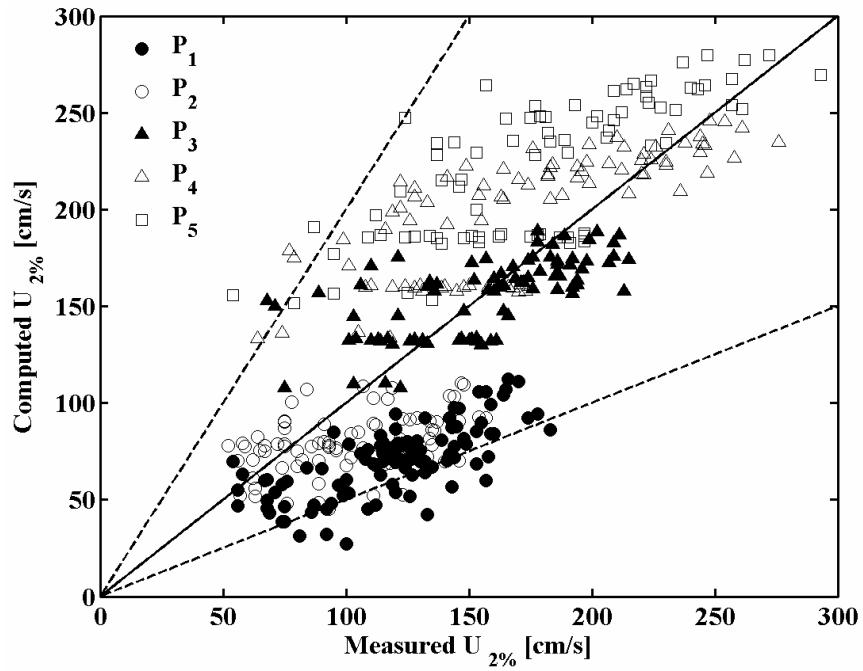


Fig. 24. Measured and computed velocity $U_{2\%}$ at five points.

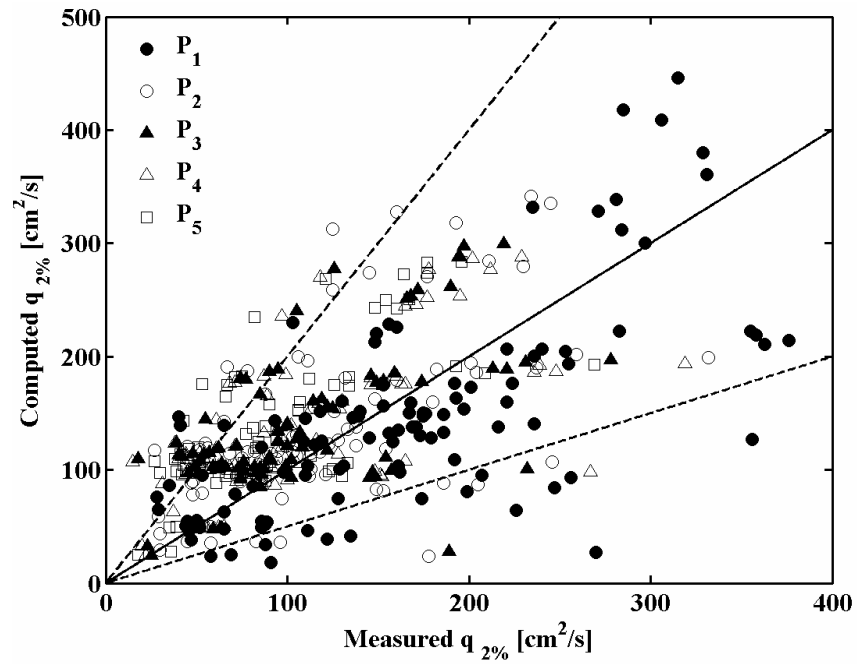


Fig. 25. Measured and computed discharge $q_{2\%}$ at five points.

9.6 Representative wave periods $T_{m-1,0}$ and T_p

The comparisons shown in Figs. 8 – 25 are also made using the measured spectral peak period T_p at $x = 0$ instead of the spectral wave period $T_{m-1,0}$. The compared results for T_p and $T_{m-1,0}$ are almost the same for the present 107 tests and series A, B, C, D and D'. For these tests, the seaward boundary $x = 0$ is located outside the surf zone and the difference between T_p and $T_{m-1,0}$ is small. For series E and F, the toe of the 1/4 slope may have been located inside the surf zone. The ratio of $T_p / T_{m-1,0}$ was less than 0.5 for the four wave conditions at $x = 0$. For these tests with $(T_p / T_{m-1,0}) < 0.5$ the agreement is clearly better for $T_{m-1,0}$

Figs. 26 – 34 based on the representative wave period T_p are presented in the following. The corresponding figure based on the representative wave period of $T_{m-1,0}$ is indicated in each figure so that the two figures can be compared. The spectral peak period T_p in water depth of about 10 m or deeper is normally reported in the U.S. The compared results in Figs. 26 – 34 show that the present CSHORE is not sensitive to the representative wave period as long as the seaward boundary $x = 0$ is located outside the surf zone. Inside the surf zone, the wave characteristics may vary rapidly in space and the difference $\bar{\eta}$ between the mean and still water levels may not be negligible. The present CSHORE does not account for low-frequency waves whose effects seem to be within the accuracy (factor of 2) of this numerical model.

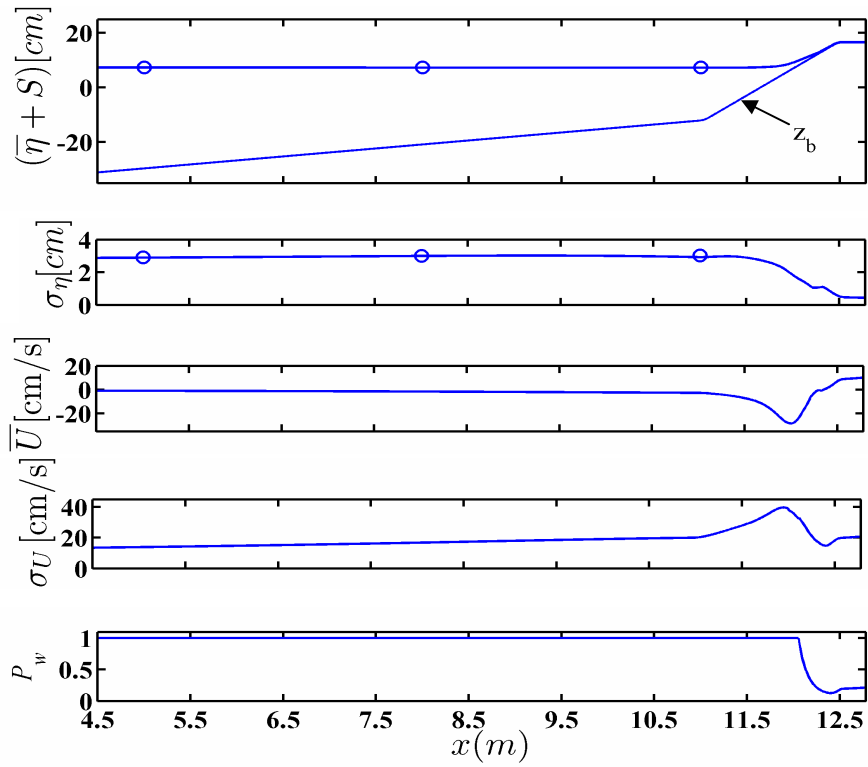


Fig. 26. Measured (circle) and computed (solid line based on T_p) mean and standard deviation of free surface elevation η and depth-averaged velocity U together with wet probability P_w for wave overtopping test 41 where Fig. 12 is based on $T_{m-1,0}$.

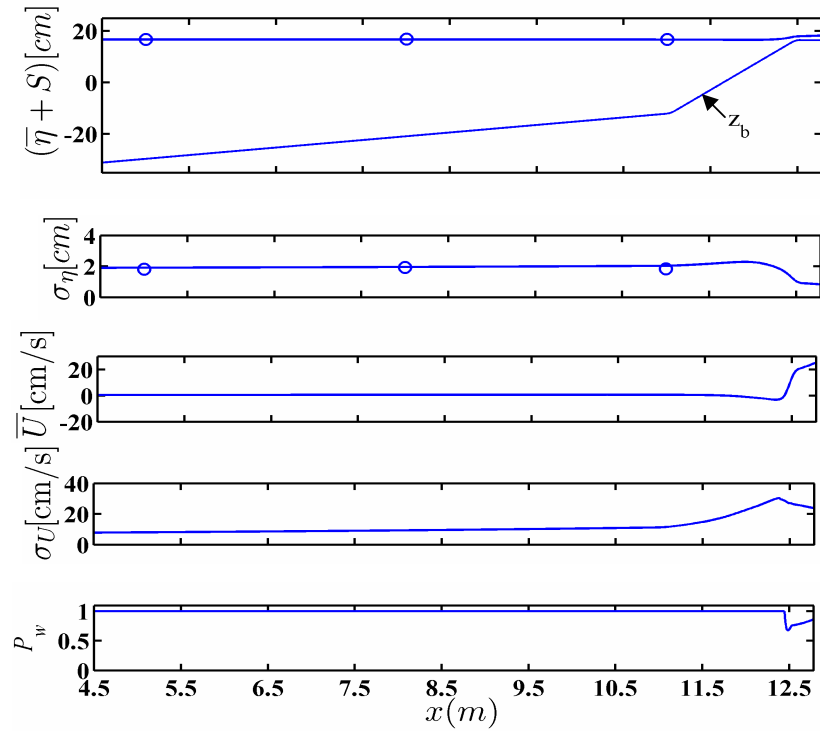


Fig. 27. Measured (circle) and computed (solid line based on T_p) mean and standard deviation of free surface elevation η and depth-averaged velocity U together with wet probability P_w for overflow test 94 where Fig. 13 is based on $T_{m-1,0}$.

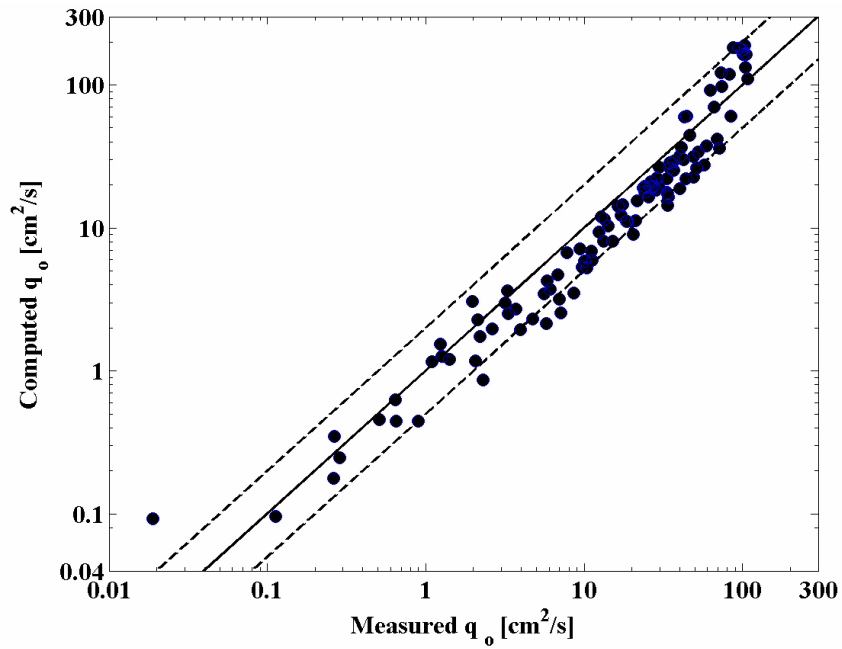


Fig. 28. Measured and computed (based on T_p) wave overtopping and overflow rates in comparison to Fig. 14.

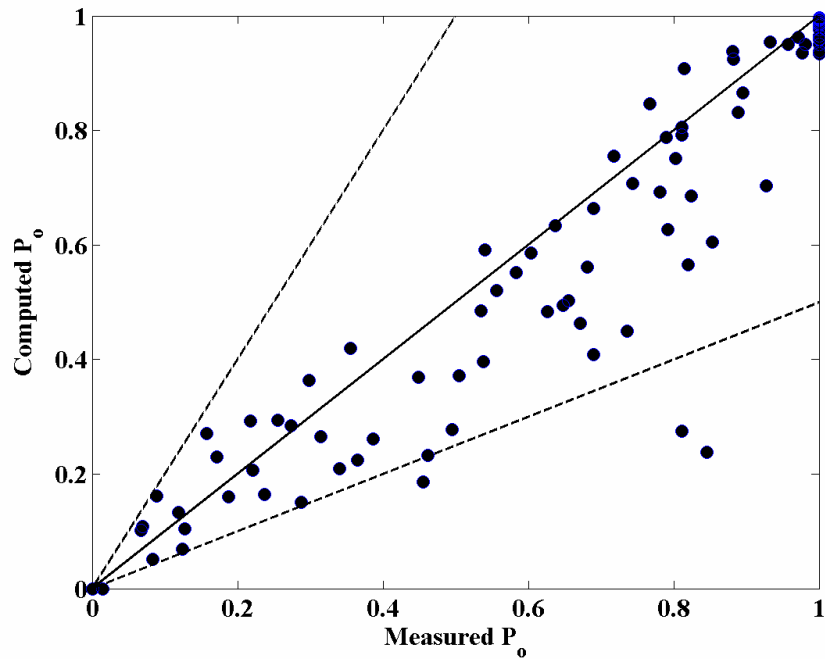


Fig. 29. Measured and computed (based on T_p) wave overtopping probabilities in comparison to Fig. 15.

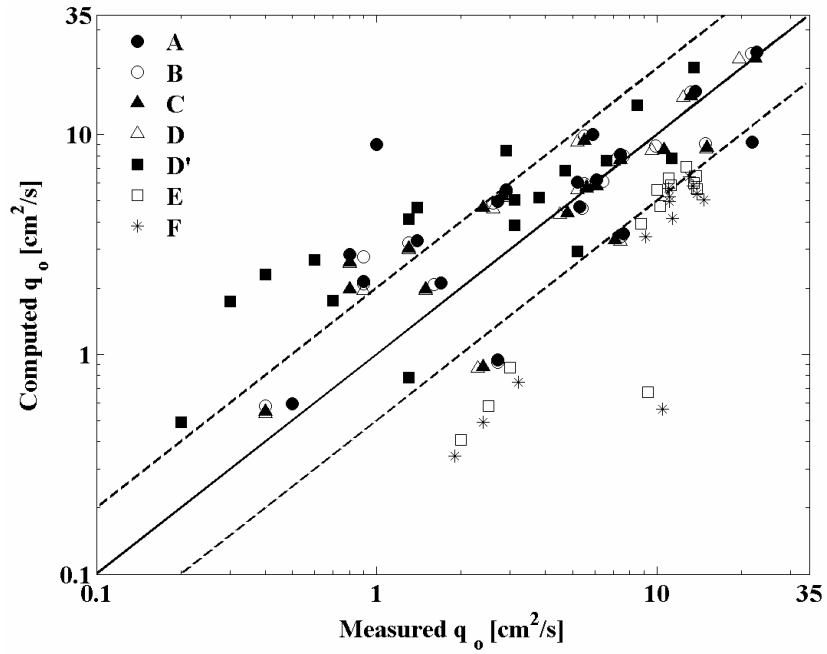


Fig. 30. Measured and computed (based on T_p) wave overtopping rates in comparison to Fig. 21.

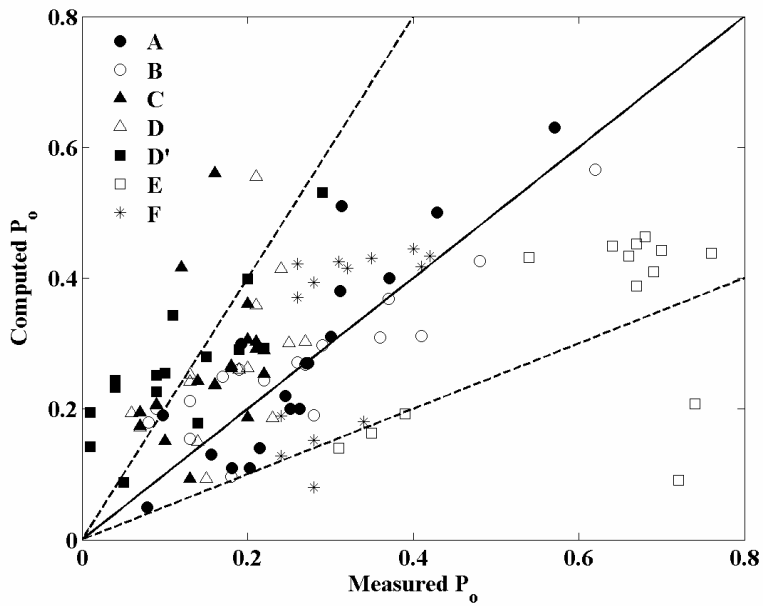


Fig. 31. Measured and computed (based on T_p) wave overtopping probabilities in comparison to Fig. 22.

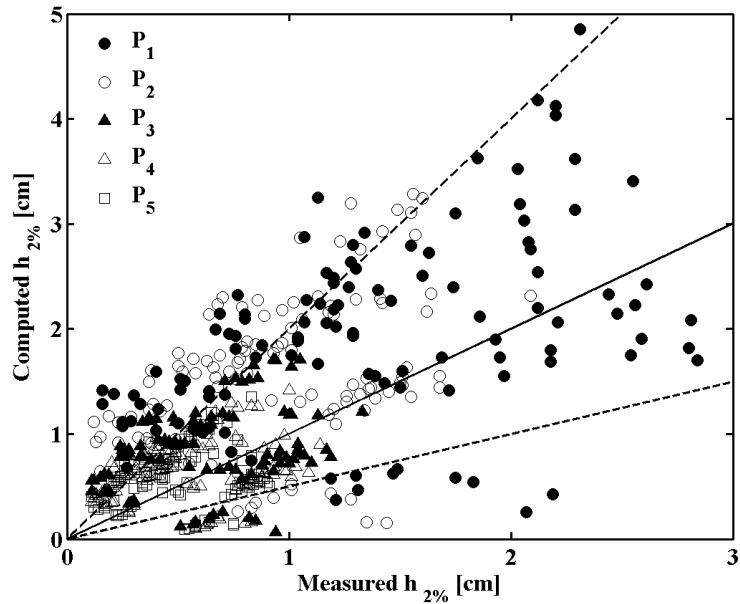


Fig. 32. Measured and computed (based on T_p) water depth $h_{2\%}$ at five points in comparison to Fig. 23.

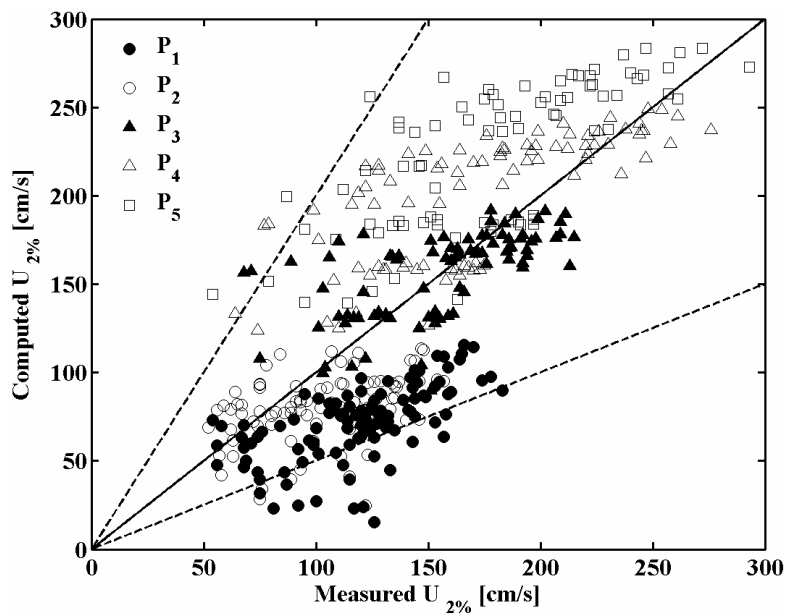


Fig. 33. Measured and computed (based on T_p) velocity $U_{2\%}$ at five points in comparison to Fig. 24.

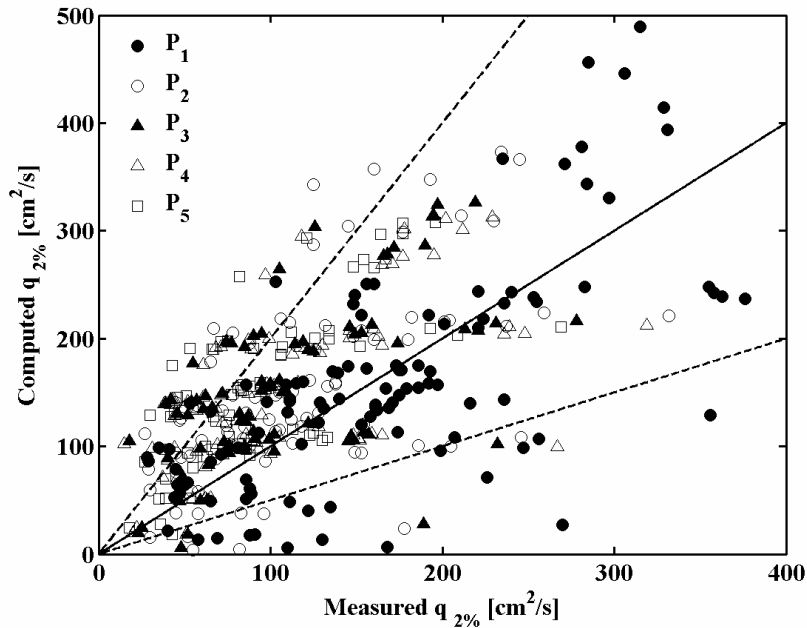


Fig. 34. Measured and computed (based on T_p) discharge $q_{2\%}$ at five points in comparison to Fig. 25.

10. Computer Program CSHORE

The computer program CSHORE is explained sufficiently so that users will be able to use it effectively and modify it if necessary. CSHORE provides various options but only certain combinations of the options have been applied and verified as summarized in section 2. Enough explanations are provided in the computer program so that users will be able to follow the computer program with additional explanations provided in the following. It is noted that the symbols used in this section are based on those used in the computer program rather than those used in the previous sections.

10.1 Main program

The wave action equations (36) or (63), the momentum equations (22) and (23), and the roller energy equation (41) are solved using the finite-difference method with constant nodal spacing Δx of a sufficient resolution in very small water depth. The use of constant small Δx may be justified because CSHORE is very efficient computationally and the use of constant Δx reduces the input preparation time. It is noted that these governing equations divided by ρg are solved in the main program so that the fluid density ρ does not appear in the resulting equations.

The differential equations solved numerically can be expressed in the form

$$\frac{dy}{dx} = f(x, y)$$

where x = cross-shore coordinate, positive onshore; y = unknown variable that needs to be computed; and f = known function of x and y . An improved Euler method of second-order accuracy (e.g., Chaudhry 1993) is used to approximate the above equation as follows:

$$\text{Predictor: } y_{j+1}^* = y_j + f(x_j, y_j) \Delta x$$

$$\text{Corrector: } y_{j+1} = y_j + \frac{1}{2} [f(x_j, y_j) + f(x_{j+1}, y_{j+1}^*)] \Delta x$$

where the subscripts j and $(j+1)$ indicate the nodes located at x_j and $x_{j+1} = (x_j + \Delta x)$ and the superscript star denotes a temporary value of y_{j+1} at node $(j+1)$. The wave action equation (36) or (63) for the free surface standard deviation σ_η , the cross-shore momentum equation (22) for the wave setup $\bar{\eta}$, and the roller equation (41) for the roller volume flux q_r are solved using this Euler method. On the other hand, the longshore momentum equation (23) is approximated by an implicit finite-difference method, which is more stable numerically, to obtain the

longshore bottom shear stress τ_{by} at node $(j+1)$ and the corresponding longshore current \bar{V} at node $(j+1)$.

In reality, the four unknown values of $\sigma_\eta, \bar{\eta}, \bar{V}$ and q_r at node $(j+1)$ involved in the four differential equations are computed in sequence and iteratively. The mean water depth \bar{h} given by Eq. (1) is uniquely related to the wave setup $\bar{\eta}$ for the given storm tide S and bottom elevation z_b . The convergence of the iteration is based on the difference between the computed and guessed values where the metric units are used in the computer program and the gravitational acceleration $g = 9.81 \text{ m/s}^2$. The difference for σ_η (m), \bar{h} (m), and \bar{V} (m/s) must be less than EPS1, whereas the difference for q_r (m^2/s) must be less than EPS2. The maximum number of the iteration is MAXITE. The DATA statement in the main program specifies $\text{EPS1}=10^{-3}$, $\text{EPS2}=10^{-6}$ and $\text{MAXITE}=20$ where double precision is used in the entire program. It is noted that q_r involves the product of the length and velocity.

The only input in the main program is as follows:

```
WRITE(*,*) 'Name of Primary Input-Data-File?'  
READ(*,5000) FINMIN  
5000  FORMAT(A12)
```

where FINMIN corresponds to the name of the input file which will be read later before the computation.

10.2 Subroutines

Subroutines are arranged in numerical order after the main program in order to indicate the location of each subroutine in the computer program. The numerical order approximately corresponds to the chronology of the CSHORE development summarized in section 2.

Subroutine 1 **OPENER** opens all input and output files. The input file with its name = FINMIN is assigned to unit=11 for the READ statement. The names of the output files start with the letter O. The output file ODOC (unit=20 for the WRITE statement) is used to store the input (to check the accuracy of the input file) and the summary of the computed results (to check the overall appropriateness of the computed results and to compare with measurements such as wave runup and overtopping rates). The output file OMESSG (unit=40) stores warning and error messages generated during the computation. These messages must be examined carefully if the computed results appear questionable. The other output files are explained in section 10.4.

Subroutine 2 **INPUT** reads the contents of the input file FINMIN as explained in detail in section 10.3. The gravitational acceleration g is specified as GRAV=9.81 m/s² in the DATA statement.

Subroutine 3 **BOTTOM** calculated the bottom elevation $z_b(x_j)$ with $x_j = (j-1)\Delta x$ at node j using the input bottom elevations specified at a number of cross-shore locations. Use is made of linear interpolation and smoothing to reduce sharp corners that tend to cause numerical irregularity. This subroutine also computes the nodal spacing Δx using the input integer JSWL which is the number of nodes along the bottom below the datum $z = 0$ as well as the cross-shore bottom slope S_{bx} of the smoothed z_b . If the bottom is permeable, the lower boundary elevation

z_p of the permeable layer (see Fig. 2) is calculated in the same way as z_b . The thickness h_p of the permeable layer is obtained using $h_p = (z_b - z_p) \geq 0$.

Subroutine 4 **PARAM** computes constant parameters before the landward marching computation. Eqs. (65) and (66) are used to compute the values of α_p, β_1 and β_2 using the default values of $\nu = 10^{-6} \text{ m}^2/\text{s}$, $\alpha_0 = 1000$ and $\beta_0 = 5$. The default value of $\alpha = 2$ in Eq. (92) for the wet and dry zone is specified and the value of B defined in Eq. (97) and other constant parameters are calculated.

Subroutine 5 **LWAVE** solves the dispersion relation for linear waves given by Eq. (2) which is rewritten in terms of $x = k\bar{h}$

$$x - D \left(1 - \frac{T_p Q}{2\pi \bar{h}^2} x \right)^2 \coth(x) = 0$$

with

$$D = k_o \bar{h} \quad ; \quad Q = Q_x \cos \theta + Q_y \sin \theta$$

where T_p = representative wave period at $x=0$ specified as input; \bar{h} = mean water depth at given node; k_o = deep water wave number given by $k_o = (2\pi)^2 / (gT_p^2)$ calculated in subroutine 4 **PARAM** or at the end of the main program if additional wave conditions are specified as input at the seaward boundary $x=0$. The above equation is solved using the Newton-Raphson method (e.g., Press et al. 1989). After the wave number $k = x/\bar{h}$ is obtained, the linear wave quantities such as those defined in Eq. (3) are computed and the wave angle θ for obliquely incident waves is calculated using Eq. (21). CSHORE provides the option of IWCINT=0 or 1.

IWCINT=0 corresponds to the case of no wave and current interaction, which was assumed in the earlier version of CSHORE developed for the condition of no or little wave overtopping. IWCINT=1 corresponds to the present version of CSHORE which allows considerable wave overtopping and overflow. If IWCINT=0, the terms involving Q_x and Q_y in Eqs. (2), (22), (23) and (36) are neglected and $Q = 0$ in the above equation for $x = k\bar{h}$.

Subroutine 6 **GBXAGF** computes G_{bx} and G_f using the approximate equations (46) and (48) for obliquely incident waves and the exact equations given by Kobayashi et al. (2007b) for normally incident waves. The complementary error function *erfc* involved in the exact equations is computed using Function **ERFCC** given by Press et al. (1989). Subroutine 6 **VSTGBY** computes $V_* = \bar{V} / \sigma_T$ for known G_{by} using Eq. (47). The longshore momentum equation (23) is solved numerically to obtain τ_{by} and the corresponding G_{by} is calculated using Eq. (33).

Subroutine 7 **DBREAK** computes the energy dissipation rate D_B due to wave breaking using Eq. (38) and specifies the upper limit of unity for $\sigma_* = \sigma_\eta / \bar{h}$ in the wet zone of very shallow water. The other limit of σ_* introduced for irregular wave transmission over submerged porous breakwaters by Kobayashi et al. (2007b) has been found to be unnecessary for the other applications of CSHORE discussed in section 2.

Subroutine 8 **OUTPUT** stores most of the computed results in the output files as explained in detail in section 10.4.

Subroutine 9 **POFLOW** computes the standard deviation σ_p of the discharged velocity in a permeable layer using Eq. (72), the mean cross-shore discharge velocity \bar{U}_p using Eq. (70), and the energy dissipation rate D_p due to flow resistance in the permeable layer using Eq. (68). CSHORE provides the option of IPERM = 0 or 1. IPERM=0 implies an impermeable bottom and this subroutine is not called from the main program. IPERM=1 implies that a permeable layer exists in the computation domain where the permeable layer thickness $h_p = 0$ for impermeable segments.

Subroutine 10 **QORATE** is called from the main program after the landward marching computation in the wet zone if the option of IOVER=1 is specified as input to allow wave overtopping and overwash in the computation domain. No wave overtopping is allowed if IOVER=0 and the wave overtopping rate $q_o = 0$ in Eqs. (19) and (62). The combined wave overtopping and overflow rate q_o is obtained by calling subroutine 16 WETDRY. After the convergence of repeated landward computations to obtain q_o , the quantities related to wave runup and overtopping are computed using the equations in section 7. The formulas given by Eqs. (80) and (85) yield the empirical rate q_o in comparison to the rate q_o computed using the present wet and dry model. The uncertainties of the empirical and computed q_o are large (at least a factor of 2) and it is prudent to compare the two values of q_o .

Subroutine 11 **SEDTRA** computes the sediment transport quantities in the wet zone using the equations in section 5 after the landward marching computation of the hydrodynamic quantities

is completed. This subroutine is called from the main program only for the option of IPROFL=1, corresponding to a movable bottom. For a fixed bottom, IPROFL=0 must be specified as input. The computation is performed separately for normally incident waves (integer IANGLE=0) and for obliquely incident waves (IANGLE=1) partly because of the CSHORE development history discussed in section 2 and partly because of no longshore sediment transport for IANGLE=0. The sediment transport quantities in the wet and dry zone are computed using the equations in section 8.2 only for IANGLE=0 and IOVER=1.

Subroutine 12 **CHANGE** computes the bottom elevation change from the present time level to the next time level using Eq. (61) with $\partial q_y / \partial y = 0$. The finite difference equations for the profile change computation given by Tega and Kobayashi (1999) are of second-order accuracy. The time step Δt for the profile change computation is computed using the numerical stability criterion of the adopted explicit finite difference method. The profile change is computed if IPROFL=1.

Subroutine 13 **INTGRL** integrates a function numerically using a modified Simpson's rule (e.g., Press et al. 1989). This subroutine is used in Subroutine CHANGE to ensure that the computed profile change satisfies the conservation of the sediment volume in the entire computation domain.

Subroutine 14 **SMOOTH** smoothes the cross-shore variation of a variable that depends on x . Simple moving averaging is performed using NPT nodes landward and seaward of a specified node. The default value of NPT=5 is given in the DATA statement. NPT=1 corresponds to no

smoothing. The smoothing of certain variables reduces sudden changes and improves numerical stability. Some variables are smoothed before their storage and plotting.

Subroutine 15 **EXTRAPO** called from Subroutine SEDTRA is used to extrapolate a finite sediment transport rate at the landward end node of the computation to zero transport rate on the landward dry zone after the introduction of the scarping algorithm given by Eq. (60). The number of nodes for the extrapolation is specified by NPE. The default value of NPE=5 is given in the DATA Statement. If wave overwash is allowed by choosing the option IOVER=1, this subroutine is not used.

Subroutine 16 **WETDRY** computes the hydrodynamic quantities in the wet and dry zone using the equations in section 8.1. Function GBWD following this subroutine computes the value of $G_b(r)$ for given r using Eqs. (98) and (99).

Subroutine 17 **TRANWD** called from the main program and subroutine SEDTRA connects the computed values by the wet model and the wet and dry model in the overlapping zone because the transition between the two different models is somewhat artificial. The overlapping zone and transition algorithm are discussed at the end of section 8.1.

Subroutine 18 **PROBWD** computes the probabilities of sediment movement and suspension using Eqs. (105), (106) and (107) as well as Eqs. (108), (109) and (110) where only the critical fluid velocities U_{cb} and U_{cs} are different in these equations. Function GDWD computes the

value of $G_d(r)$ for given r using Eqs. (113) and (114). Function GDWD is placed immediately after Subroutine PROBWD.

10.3 Input

A user of CSHORE must read Subroutine 2 **INPUT** and learn how to prepare the primary input data file. Input parameters and variables are read using the FORMAT statements at the end of Subroutine INPUT. A user must follow the FORMAT requirements so that a correct input value is assigned to the specific input parameter or variable. This requirement may not be convenient but the resulting input file is orderly and can be checked easily. In the following, the input parameters and variables are explained in the sequence described in Subroutine INPUT.

- NLINES is the number of lines used to identify a specific input file because a number of input files can become large when CSHORE is compared with a number of data sets with different bottom profiles.
- (COMMEN(J), J=1, 14) read for NLINES lines contains the description of the input file. The comments in these lines do not affect the computed results at all.
- IPROFL = 0 or 1 for a fixed or movable bottom where the profile evolution is computed for IPROFL=1.
- IPERM = 0 or 1 for an impermeable or permeable bottom where the parameters for the permeable layer must be specified later if IPERM=1.

- IOVER = 0 or 1 for no wave overtopping or combined wave overtopping and overflow at the landward end of the computation domain where wave overwash and dune profile evolution are computed if IOVER=1 and IPROFL=1.
- IWCINT = 0 or 1 for no or yes for wave and current interactions where the terms involving Q_x and Q_y in Eqs. (2), (22), (23), (36) and (63) are neglected if IWCINT=0. Wave and current interactions are not negligible if the current velocity becomes as large as the wave phase velocity C .
- IROLL = 0 or 1 for no or yes for roller effects where the roller volume flux $q_r = 0$ and $D_r = D_B$ in Eq. (41) for IROLL=0. The option IROLL=1 improves the prediction of longshore current on a beach and dune erosion but the roller effects have found to be negligible for coastal structures with steeper slopes.
- IWIND = 0 or 1 for no or yes for wind effects where the wind stresses τ_{sx} and τ_{sy} on the sea surface are neglected in Eqs. (22) and (23) if IWIND=0.
- JSWL = number of nodes along the bottom below the datum $z = 0$ used to determine the nodal spacing $\Delta x = x_s / JSWL$ where x_s = cross-shore distance between the seaward boundary $x = 0$ and the shoreline located at the bottom elevation $z_b = 0$. The values of JSWL used in the previous computations were of the order of 1000. The corresponding values of Δx were of

the order of 0.01 m and 1.0 m for laboratory and field data, respectively. The integer NN in the PARAMETER statement specifies the maximum number of nodes allowed in the computation domain. The default value of NN = 200,000 should be sufficient for any CSHORE computation.

- GAMMA = empirical breaker ratio parameter γ in Eq. (38) where the range of $\gamma = 0.5 - 1.0$ has been used to adjust the computed cross-shore variation of the wave height in comparison with the measured wave height variation. If no wave height data is available, use may be made of $\gamma = 0.7$ or 0.8.
- D50, WF and SG = median sediment diameter d_{50} (mm), sediment fall velocity w_f (m/s), and sediment specific gravity s if IPROFL=1. The default values for the sediment in subroutine INPUT are the sediment porosity $n_p = 0.4$ in Eq. (61), the critical Shields parameter $\psi_c = 0.05$ for Eq. (49), the suspension efficiency $e_B = 0.005$ and $e_f = 0.01$ in Eq. (51), the suspended load parameter $a = 0.2$ in Eq. (52), the bedload parameter $b = 0.002$ in Eqs. (56) and (57), and the sediment maximum slope $\tan \phi = 0.63$ in Eqs. (52), (58) and (59).
- RWH = runup wire height $\delta_r(m)$ shown in Fig. 3 only if IOVER=1. If no runup wire is deployed, use may be made of $\delta_r = 0.02$ m for small-scale experiments and $\delta_r = 0.1$ m for prototype beaches and structures. The range of $\delta_r = 0.01 - 0.1$ m is realistic for a runup wire placed above a slope.

- SNP and SDP = porosity n_p and nominal diameter D_{n50} of stone used in Eqs. (65) and (66) only if IPERM=1 and a permeable layer is constructed of stone. If other materials are used for slope protection, formulas corresponding to Eqs. (65) and (66) will need to be developed.
- NWAVE = number of waves and water levels at the seaward boundary $x = 0$. If IPROFL=0 and the bottom is fixed, NWAVE is the number of different waves and water levels at $x = 0$ examined for this specific fixed bottom. If IPROFL=1 and the bottom profile evolves from the specified initial profile, NWAVE is the number of sequential waves and water levels at $x = 0$ during the profile evolution starting from the morphological time $t = 0$. It is noted that NWAVE must not exceed the integer NB in the PARAMETER Statement where NB=30,000 is specified.
- TIMEBC(I+1), TPBC(I), HRMSBC(I), WSETBC(I), SWLBC(I), WANGBC(I) for I=1,2,..., NWAVE where

TIMEBC(I+1) = morphological time in seconds at the end of the I-th wave and water level during the profile evolution starting from TIMEBC(1) = 0.0. The wave conditions and water level during TIMEBC(I) to TIMEBC(I+1) are assumed to be constant. For IPROFL=0, TIMEBC(I+1) = 1.0, 2.0, ..., NWAVE may be used to identify the sequence of the waves and water levels at $x = 0$ used for the computation.

TPBC(I) = spectral peak period T_p (s) used to represent the I-th irregular wave period at $x = 0$ but any representative wave period can be specified.

HRMSBC(I) = root-mean-square wave height $H_{rms} = \sqrt{8} \sigma_{\eta}(m)$ used to represent the I-th irregular wave height at $x=0$. If the spectral significant wave height H_{mo} is known, the corresponding H_{rms} may be obtained using $H_{rms} = H_{mo} / \sqrt{2}$.

WSETBC(I) = wave setup (positive) or set-down (negative) $\bar{\eta}(m)$ at $x=0$ relative to the still water level (SWL). If $\bar{\eta}$ is not measured, use may be made of $\bar{\eta} = 0.0$ at $x=0$ as long as the seaward boundary $x=0$ is located outside the surf zone.

SWLBC(I) = still water level S (m) above the datum $z=0$ as shown in Fig. 2. This value of S corresponds to storm tide (sum of storm surge and tide) during the I-th wave conditions.

WANGBC(I) = incident wave angle θ in degrees at $x=0$ for the I-th wave conditions (see Fig. 1 for the definition of θ). The angle is limited to the range of $\theta = -80^{\circ}$ to 80° because the formula for D_b given by Eq. (38) was originally developed for normally incident waves and may not be valid for large incident wave angles. IANGLE=0 or 1 is used to indicate normally or obliquely incident waves in the computer program.

- NBINP = number of points used to describe the input bottom geometry which is the initial profile if IPROFL=1. The bottom geometry is divided into linear segments of different inclination and roughness starting from the seaward boundary $x=0$. It is noted that NBINP must not exceed NB = 30,000 in the PARAMETER statement.
- XBINP(1) and ZBINP(1) = values (m) of x and z of the bottom point at the seaward boundary in the coordinate system (x,z) shown in Fig. 2 where XBINP(1) = 0.0 at the

seaward boundary and the water depth below the datum $z=0$ is given by $-ZBINP(1)$. If $Iperm=1$, $ZPINP(1) = ZBINP(1)$ is specified in the program because the thickness of a permeable layer is assumed to be zero at the seaward boundary.

- If $Iperm=0$, $XBINP(J)$, $ZBINP(J)$ and $FBINP(J-1)$ for $J=2,3,\dots,NBINP$ where

$XBINP(J)$ = horizontal (landward) distance (m) of the input bottom point J from the seaward boundary $x=0$ with the distance $XBINP(J)$ increasing with the increase of the integer J .

$ZBINP(J)$ = bottom elevation $z_b(m)$ of the point J . If the point J is below the datum $z=0$, $ZBINP(J)$ is negative and $-ZBINP(J)$ is the water depth below the datum. If the point J is above the datum, $ZBINP(J)$ is positive and corresponds to the bottom elevation of the point J above the datum.

$FBINP(J-1)$ = bottom friction factor f_b of the linear segment between the bottom points $(J-1)$ and J . The bottom friction factor can be varied to account for the cross-shore variation of bottom roughness as shown in Fig. 2.

- If $Iperm=1$, $XBINP(J)$, $ZBINP(J)$, $FBINP(J-1)$ and $ZPINP(J)$ for $J=2,3,\dots,NBINP$ where $ZPINP(J)$ = value (m) of the z -coordinate of the lower impermeable boundary z_p of the point J as shown in Fig. 2. The vertical thickness of the permeable layer is given by $h_p = (z_b - z_p)$.

- If $Iwind=1$, $W10(I)$ and $WANGLE(I)$ for $I=1,2,\dots,NWAVE$ where

W10(I) = wind speed W_{10} (m/s) at the elevation of 10 m above the sea surface between the time levels TIMEBC(I) and TIMEBC(I+1) used to specify the waves and water levels at the seaward boundary.

WANGLE(I) = wind direction θ_w in degrees (see Fig. 1) corresponding to the wind speed W10(I).

10.4 Output

A user of CSHORE must examine the contents of the output file **ODOC** (unit=20 for the WRITE statement) to ensure that the input file has been prepared and read correctly. The contents of this file created in Subroutine 8 **OUTPUT** and at the end of Subroutine 10 **QORATE** if IOVER=1 are self-explanatory. The notations that have not been explained previously are explained in the following.

First, **ODOC** stores the input parameters and variables.

RBZERO = lower limit of the wave-front slope β_r in Eq. (10) where RBZERO = 0.1 specified in Subroutine 2 **INPUT** where this typical value has been used to reduce the number of calibration parameters.

JCREST = crest node of the maximum bottom elevation for the input bottom profile $z_b(x)$. If the crest is horizontal, JCREST corresponds to the landward end of the horizontal crest located at $x = x_c$ in Fig. 5. If IPROFL=1, the nodal location of JCREST may change with the evolution of the bottom profile.

RCREST = input bottom elevation (m) at the node JCREST corresponding to the maximum value of the input $z_b(x)$.

AWD = parameter α in Eq. (92) which expresses the horizontal velocity U as a function of the water depth h in the wet and dry zone where $\alpha = 2$ is specified in Subroutine 4 **PARAM** but this specified value could be calibrated if necessary.

EWD = exceedance probability e used in Eq. (120) for the comparison with measured values corresponding to 2% of incident irregular waves where $e = \text{EWD} = 0.01$ in Subroutine 4 **PARAM**.

It is noted that JCREST, RCREST, AWD, and EWD are stored only if IOVER=1.

Second, **ODOC** stores the computed quantities at time = TIMEBC(1)=0.0, TIMEBC(2)=, ..., TIMEBC(NWAVE+1). The stored quantities of the ODOC file include

JR = most landward node reached by the landward marching computation using the wet model in section 4 if IPERM=0 and in section 6 if IPERM=1.

XR = x -coordinate (m) of the node JR where $\text{XR} = x_r$ shown in Fig. 5 for an emerged structure or beach.

ZR = z -coordinate (m) of the node JR corresponding to the bottom elevation above the datum.

H(JR) = mean water depth \bar{h} (m) at the node JR which must be very small for an emerged structure or beach if the landward marching computation does not encounter numerical difficulties.

CSHORE estimates the wave reflection coefficient assuming that the cross-shore wave energy flux F_x defined in Eq. (37) is reflected from the node JSWL of the still water shoreline location at $x = x_{\text{SWL}}$ in Fig. 5 and propagates seaward if $\text{JR} > \text{JSWL}$ (the landward marching computation has reached above the still water shoreline) and $\text{JSWL} < \text{JMAX}$ with $\text{JMAX} =$ most landward

node of the computation domain based on the input bottom geometry. If JSWL = JMAX, the computation domain is submerged and some of the cross-shore wave energy flux is transmitted landward. The wave reflection coefficient REFCOF is estimated as the ratio between σ_{ref} and σ_{η} at $x=0$ where σ_{ref} is the free surface standard deviation due to the wave energy flux propagating seaward at $x=0$. The estimated wave reflection coefficient may not be very accurate (Kobayashi et al. 2005, 2007a) but is useful in assessing the applicability of CSHORE which neglects reflected waves in its governing equations.

If IOVER=1, Subroutine OUTPUT calls Subroutine QORATE with ICALL=1 to store the following quantities in the file **ODOC**:

JWD = most seaward node of the landward marching computation in the wet and dry zone as explained in relation to Eq. (100).

H1 = mean water depth $\bar{h}_1(m)$ at the node JWD.

JDRY = most landward node in the wet and dry zone which is less than and equal to the maximum node number JMAX in the computation domain.

POTF = wave overtopping probability P_o estimated using the wet probability P_c at the node JCREST.

WDN = empirical parameter n introduced in Eq. (100).

QOTF = combined overtopping and overflow rate $q_o(m^2/s)$ computed using Eq. (95) with $U_s = 0$ at the node JCREST where the wet and dry model in section 8.1 is limited to an impermeable bottom at present.

QOS = seepage rate $q_s(m^2/s)$ estimated using Eq. (83).

QONEW = computed total rate (m^2/s) which is the sum of QOTF and QOS.

In addition, the following quantities computed using the more empirical equations in section 7 are stored in the file **ODOC** at the specified time levels:

SWL = still water level S (m) above the datum $z = 0$.

RCREST = structure crest elevation (m) above the datum where the crest height R_c above SWL shown in Fig. 3 is given by $R_c = (\text{RCREST} - S)$.

TSLOPE = seaward slope $\tan \theta$ of the structure in Eq. (75).

XE = x -coordinate x_e (m) of the landward end of the permeable layer shown in Fig. 2 and used in Eq. (83) where x_e corresponds to x_c for an impermeable structure in Fig. 5 but the wet and dry model is limited to an impermeable bottom at present.

ZE = z -coordinate z_e (m) corresponding to $z_p(x)$ at $x = \text{XE}$ shown in Fig. 2 and used in Eq. (83).

RWH = runup wire height δ_r (m).

ITEQO = number of iterations to obtain the convergence of the combined overtopping and overflow rate QO.

ICONV = integer used to check the ITEQO iterations where ICONV=0 implies the convergence and ICONV=1 indicates no convergence probably due to numerical oscillations. If ICONV=1, the file OMESSG must be checked to examine the degree of the numerical oscillations of QO.

ERMEAN = mean shoreline elevation (m) above the datum $z=0$ measured by the runup wire

where $ERMEAN = (\bar{\eta}_r + S)$ and $\bar{\eta}_r$ given in Eq. (73) is the mean shoreline elevation above SWL.

SIGRUN = standard deviation σ_r (m) of the shoreline oscillation measured by the runup wire

where σ_r is estimated using Eq. (73).

RKAPPA = shape parameter κ for the Weibull distribution given in Eq. (77) or (84).

R13 = significant runup height (m) above the datum $z=0$ corresponding to $(R_{1/3} + S)$ where

$R_{1/3}$ above SWL is estimated using Eq. (75) or (84).

R2P = runup height (m) above the datum $z=0$ for the 2% exceedance probability where R2P =

$(R_{2\%} + S)$ and $R_{2\%}$ is given by Eq. (79).

PO = wave overtopping probability P_o estimated empirically using Eq. (78).

QOS = seepage rate q_s (m^2/s) estimated using Eq. (83).

QSWL = wave-induced onshore flux q_{SWL} given by Eq. (81).

QOT = wave overtopping rate (m^2/s) corresponding to the first term on the right hand side of Eq. (80) or (85).

QOF = overflow rate (m^2/s) corresponding to the second term on the right hand side of Eq. (85).

QOEMP = empirical total rate (m^2/s) which is the sum of QOS, QOT and QOF.

If IPROFL=1 and IANGLE=1 (obliquely incident waves), Subroutine OUTPUT integrates the sum of the longshore suspended sediment transport rate q_{sy} (m^2/s) and the longshore bedload transport rate q_{by} (m^2/s) from $x=0$ to $x=x_r$ in the wet zone where q_{sy} and q_{by} are predicted

using Eqs. (52) and (57), respectively. The integrated total longshore sediment transport rate (m^3/s) and the corresponding value of K in the CERC formula (Coastal Engineering Manual 2003) are stored in the file **ODOC**. The breaker location is taken at the cross-shore location of the maximum root-mean-square wave height and the value of K in the CERC formula is supposed to be of the order of 0.8.

The rest of the output files store the cross-shore variations of computed variables at the specified time levels TIMEBC(I) with $I = 1, 2, \dots, (NWAVE+1)$. Each output file stores the number of nodes and the output time level immediately before the computed variables are stored at the given number of nodes. This will facilitate displaying the computed variables using the output files. It is noted that the CSHORE computer program does not contain any plotting routine.

The file **OBPROF** (unit=21) contains the bottom profile variables at all the nodes with $J=1,2,\dots,JMAX$.

$XB(J)$ = cross-shore coordinate x (m) of node J where $XB(J) = (J-1) * \Delta x$ does not change with time.

$ZB(J)$ = vertical coordinate z_b (m) of the bottom elevation at the output time level where the bottom elevation evolves with time if $I\text{PROFL}=1$.

$ZP(J)$ = vertical coordinate z_p (m) of the lower boundary of the permeable layer only if $I\text{PERM}=1$ where z_p has been assumed to be fixed so far.

The file **OSETUP** (unit=22) stores the quantities related to the mean and standard deviation of the free surface elevation η for nodes $J=1,2,\dots,JR$

$\text{XB}(J)$ = cross-shore coordinate x (m) of node J for the plotting convenience.

$(\text{WSETUP}(J)+\text{SWLBC}(\text{IWAVE}))$ = sum of the wave setup $\bar{\eta}$ (m) and storm tide S (m) at node J .

$\text{H}(J)$ = mean water depth \bar{h} (m) at node J .

$\text{SIGMA}(J)$ = free surface standard deviation σ_η (m) related to the root-mean-square wave height

$$H_{rms} = \sqrt{8}\sigma_\eta.$$

If $\text{IOVER}=1$, these variables are also stored at nodes $J=(\text{JR}+1), \dots, \text{JDRY}$ in the wet and dry zone.

The file **OPARAM** (unit =23) stores $\text{XB}(J)$ with nodes $J=1,2,\dots,\text{JR}$ and the following parameters:

$\text{WT}(J)$ = intrinsic wave period $T = 2\pi / \omega$ (s) where the angular frequency ω is computed using

Eq. (2).

$\text{QBREAK}(J)$ = fraction Q of breaking waves computed using Eq. (38).

$\text{SIGSTA}(J)$ = ratio $\sigma_* = \sigma_\eta / \bar{h}$ in Eq. (31) whose upper limit is unity.

The file **OXMOME** (unit=24) stores $\text{XB}(J)$ with $J=1,2,\dots,\text{JR}$ and the following terms in the x-momentum equation (22):

$\text{SXXSTA}(J) = \left[S_{xx} / (\rho g) + Q_x^2 / (g\bar{h}) \right]$ (m^2) where S_{xx} and Q_x are given in Eqs. (24) and (19),

respectively.

$\text{TBXSTA}(J) = \tau_{bx} / (\rho g)$ (m) where τ_{bx} is given in Eq. (33).

If IANGLE=1 (obliquely incident waves), the file **OYMOME** (unit=25) stores XB(J) with J=1,2,...,JR and the following terms in the y-momentum equation (23):

$$\text{SXYSTA}(J) = \left[S_{xy} / (\rho g) + Q_x Q_y / (g \bar{h}) \right] (\text{m}^2) \text{ where } S_{xy}, Q_x \text{ and } Q_y \text{ are defined in Eqs. (24), (19) and (20).}$$

$$\text{TBYSTA}(J) = \tau_{by} / (\rho g) (\text{m}) \text{ where } \tau_{by} \text{ is given in Eq. (33).}$$

The file **OENERG** (unit=26) stores XB(J) with J=1,2,...,JR and the following terms in the wave action equation (36) or (63) with ω being replaced by T^{-1} :

$$\text{EFSTA}(J) = \left[\text{ET} \left(C_g \cos \theta + Q_x / \bar{h} \right) \right] / (\rho g) (\text{m}^3) \text{ where E and } C_g \text{ are given in Eqs. (25) and (3).}$$

$$\text{DBSTA}(J) = D_b / (\rho g) (\text{m}^2/\text{s}) \text{ where } D_b \text{ is given by Eq. (38).}$$

$$\text{DFSTA}(J) = D_f / (\rho g) (\text{m}^2/\text{s}) \text{ where } D_f \text{ is given by Eq. (40).}$$

The file **OXVELO** (unit=27) stores XB(J) with J=1, 2, ..., JR and the following cross-shore velocity statistics:

$$\text{UMEAN}(J) = \text{mean velocity } \bar{U} \text{ (m/s) of the depth-averaged cross-shore velocity } U .$$

$$\text{USTD}(J) = \text{standard deviation } \sigma_U \text{ (m/s) of } U .$$

If IOVER=1, these variables are also stored at nodes $J = (JR+1), \dots, JDRY$ in the wet and dry zone.

If IANGLE=1, the file **OYVELO** (unit=28) stores $XB(J)$ with $J=1, 2, \dots, JR$ and the following longshore velocity statistics:

STHETA(J) = $\sin \theta$ with θ = wave angle as defined in Fig. 1 where $\sin \theta$ is computed using Eq. (21).

VMEAN(J) = mean velocity \bar{V} (m/s) of the depth-averaged longshore velocity V .

VSTD(J) = standard deviation σ_V of V .

It is noted that the present wet and dry model is limited to normally incident waves (IANGLE=0).

If IROLL=1, the file **OROLLE** (unit=29) stores $XB(J)$ with $J=1, 2, \dots, JR$ and

RQ(J) = roller volume flux q_r (m^2/s) computed using Eq. (41).

If IROLL=0, $q_r = 0$ and $D_r = D_B$ in Eq. (41).

If IPROFL=1, the file **OBSUSL** (unit=30) stores $XB(J)$ with $J=1, 2, \dots, JR$ and the following variables related to sediment transport:

PB(J) = probability P_b of sediment movement.

PS(J) = probability P_s of sediment suspension.

VS(J) = suspended sediment volume V_s (m) per unit horizontal bottom area.

If IOVER=1, these variables are also stored at nodes $J = (JR+1), \dots, JDRY$ in the wet and dry zone.

If IPERM=1, the file **OPORUS** (unit=31) stores XB(J) with $J=1, 2, \dots, JR$ and the following variables related to the permeable layer:

UPMEAN(J) = mean velocity \bar{U}_p (m/s) of the cross-shore discharge velocity U_p inside the permeable layer.

UPSTD(J) = standard velocity σ_p (m/s) of the discharge velocity computed using Eq. (72).

DPSTA(J) = $D_p / (\rho g)$ (m^2/s) where the energy dissipation rate D_p due to flow resistance in the permeable layer is computed using Eq. (68).

If IPROFL=1, the file **OCROSS** (unit=32) stores XB(J) with $J=1, 2, \dots, JMAX$ and the following cross-shore sediment transport rates:

QBX(J) = cross-shore bedload transport rate q_{bx} (m^2/s).

QSX(J) = cross-shore suspended sediment transport rate q_{sx} (m^2/s).

(QBX(J) + QSX(J)) = cross-shore total sediment transport rate q_x (m^2/s).

It is noted that the transport rates are stored at all the nodes but the rates are zero in the completely dry zone.

If IPROFL=1 and IANGLE=1, the file **OLONGS** (unit=33) stores XB(J) with J=1,2, ... JMAX and the following longshore sediment transport rates:

QBY(J) = longshore bedload transport rate q_{by} (m^2/s).

QSY(J) = longshore suspended sediment transport rate q_{sy} (m^2/s).

(QBY(J) + QSY(J)) = longshore total sediment transport rate q_y (m^2/s).

If IOVER=1 and JR < JMAX (the wet and dry zone exists in the computation domain), the files **OSWASH** (unit=34) and **OSWASU** (unit=35) store XB(J) with the nodes J=JWD, ..., JDRY only in the wet and dry zone and the computed hydrodynamic variables in this zone. The additional variables stored in **OSWASH** are

PWET(J) = wet probability P_w at node J corresponding to the ratio between the wet duration and the total duration at this node.

H(J) = mean water depth \bar{h} (m) during the wet duration only.

HEWD(J) = water depth h_e (m) corresponding to the exceedance probability $e = \text{EWD}$ where

$\text{EWD} = 0.01$ specified in Subroutine 4 PARAM. Eq. (89) yields $h_e = \left(\bar{h} / P_w\right) \ln(P_w / e)$ for

$$P_w > e.$$

The additional variables stores in **OSWASU** are

UMEAN(J) = mean cross-shore velocity \bar{U} (m/s) during the wet duration only.

UEWD(J) = cross-shore velocity U_e (m/s) corresponding to the exceedance probability $e =$

EWD where Eq. (92) yields $U_e = \left(\alpha \sqrt{gh_e} + U_s\right)$ because U increases with the increase of h

monotonically in the wet and dry zone.

QEWD(J) = cross-shore volume flux $q_e = h_e U_e$ (m^2/s) corresponding to the exceedance

probability $e = \text{EWD}$.

A user of CSHORE may not be interested in the computed results in all the output files but should examine all the appropriate output files and ensure that the computed results are realistic physically. This is especially true if CSHORE is applied to new problems where the previous applications of CSHORE have been summarized in section 2.

11. CONCLUSIONS

The horizontally two-dimensional model C2SHORE and the cross-shore model CSHORE are presented. The numerical model C2SHORE is based on the spectral wave model STWAVE (Smith et al. 2001) for the prediction of the directional wave transformation, radiation stresses, and wave-induced volume fluxes and the circulation model, which is a simplified version of SHORECIRC (Svendsen et al. 2002) for irregular waves, for the prediction of the wave setup and depth-averaged current velocities. An efficient finite difference method used for the circulation computation has reduced the computation time significantly. The combined wave current model CSHORE based on the time-averaged continuity, cross-shore momentum, longshore momentum, wave action and roller energy equations predicts the cross-shore variations of the mean and standard deviation of the free surface elevation and depth-averaged cross-shore and longshore velocities under normally or obliquely incident irregular breaking waves. Both models use the same sediment transport formulas for the cross-shore and longshore transport rates of suspended sediment and bedload on sand beaches. These formulas are relatively simple and require the hydrodynamic input variables which can be predicted efficiently and fairly accurately using existing wave and current models. The numerical model C2SHORE has been compared only with one set of field data partly because of its complexity and partly because of lack of bench mark data. The much simpler model CSHORE has been compared with a number of small-scale and large-scale laboratory data and is ready for practical applications. CSHORE has been extended to the intermittently wet and dry zone for the prediction of wave overwash, levee erosion and deformation of a low-crested stone structure.

The computer program CSHORE has been developed with collaboration of a number of graduate students and visiting scientists for the last 10 years. The essential parts of CSHORE and the details of the input and output are described in this report in order to facilitate the use of CSHORE by the broad coastal community. CSHORE based on the time-averaged governing equations is much easier to apply than the corresponding time-dependent model developed by the first author of this report (e.g., Kobayashi and Wurjanto 1990, 1992). A user of CSHORE for a specific problem should read references in section 2 that are related to the specific problem because the user will need to interpret the computed results. CSHORE provides various options but only certain combinations of the options have been examined in the previous computations in section 2. Finally, CSHORE will be extended to predict dune overwash and breaching, levee erosion and breaching, and damage progression of coastal stone structures. These extensions are necessary for the performance and risk-based design of a coastal protection system that may consist of dunes, earthen levees and stone structures on sand beaches.

REFERENCES

- Bagnold, R.A. (1966). "An approach to the sediment transport problem from general physics."
U.S. Geol. Surv., Prof. Paper 422-I.
- Bailard, J.A. (1981). "An energetics total load sediment transport model for a plane sloping beach." *J. Geophys. Res.*, 86, 10,938-10,954.
- Battjes, J.A., and Stive, M.J.F. (1985). "Calibration and verification of a dissipation model for random breaking waves." *J. Geophys. Res.*, 90(C5), 9159-9167.

- Becker, J.M., Firing, Y.L., Aucan, J., Holman, R., Merrifield, M., and Pawlak, G. (2007). "Video-based observations of nearshore sand ripples and ripple migration." *J. Geophys. Res.*, 112, C01007, doi10.1029/2005JC003451.
- Chaudhry, M.H. (1993). *Open-channel Flow*. Prentice Hall, Englewood Cliffs, NJ.
- Coastal Engineering Manual. (2003). Coastal and Hydraulics Lab, US Army Engineer Research and Development Center, Vicksburg, Miss.
- Dalrymple, R.A. (1988). "Model for refraction of water waves." *J. Waterway, Port, Coastal, Ocean Eng.*, 114(4), 423-435.
- Dean, R.G. (1991). "Equilibrium beach profile: Characteristics and applications." *J. Coastal Res.*, 7, 53-84.
- D'Eliso, C., Oumeraci, H., and Kortenhaus, A. (2006). "Breaching of coastal dikes induced by wave overtopping." *Coastal Engineering 2006, Proc. 30th Coastal Engineering Conf.*, World Scientific, Singapore, 2844-2856.
- Dohmen-Janssen, C.M., and Hanes, D.H. (2002). "Sheet flow dynamics under monochromatic nonbreaking waves." *J. Geophys. Res.*, 107(C10), 3149, doi:10.1029/2001JC001045.
- Dohmen-Janssen, C.M., Kroekenstoel, D.F., Hassan, W.N., and Ribberink, J.S. (2002). "Phase lags in oscillatory sheet flow: Experiments and bed load modeling." *Coastal Eng.*, 47, 295-327.
- EurOtop Manual (2007). "Wave overtopping of sea defences and related structures: Assessment manual." www.overtopping-manual.com.
- Farhadzadeh, A., Kobayashi, N., Melby, J.A., and Ricottilli, C. (2007). "Experiments and numerical modeling of wave overtopping and overflow on dikes." Research Rep. No. CACR-07-02, Center for Applied Coastal Research, Univ. of Delaware, Newark, Del.

- Feddersen, F., Guza, R.T., Elgar, S., and Herbers, T.H.C. (2000). "Velocity moments in alongshore bottom stress parameterization." *J. Geophys. Res.*, 105(C4), 8673-8686.
- Gallagher, E.L., Elgar, S., and Guza, R.T. (1998). "Observations of sand bar evolution on a natural beach." *J. Geophys. Res.*, 103, 3203-3215.
- Henderson, S.M., Allen, J.S., and Newberger, P.A. (2004). "Nearshore bar migration predicted by an eddy-diffusive boundary layer model." *J. Geophys. Res.*, 109, C06024, doi:10.1029/2003JC02137.
- Hoefel, F., and Elgar, S. (2003). "Wave-induced sediment transport and sandbar migration." *Science*, 299, 1885-1887.
- Holland, K.T., Holman, R.A., and Sallenger, A.H., Jr. (1991). "Estimation of overwash bore velocities using video techniques." *Proc. Coastal Sediments'91*, ASCE, Reston, Va., 489-497.
- Kamphuis, J.S. (1991). "Alongshore sediment transport rate." *J. Waterway, Port, Coastal, Ocean Eng.*, 117(6), 624-640.
- Kobayashi, N. (1999). "Wave runup and overtopping on beaches and coastal structures." *Advances in Coastal and Ocean Engineering*, World Scientific, Singapore, 5, 95-154.
- Kobayashi, N., and de los Santos, F.J. (2007). "Irregular wave seepage and overtopping of permeable slopes." *J. Waterway, Port, Coastal, Ocean Eng.*, 133(4), 245-254.
- Kobayashi, N., and Johnson, B.D. (2001). "Sand suspension, storage, advection, and settling in surf and swash zones." *J. Geophys. Res.*, 106, 9363-9376.
- Kobayashi, N., and Otta, A.K. (1987). "Hydraulic stability analysis of armor units." *J. Waterway, Port, Coastal, Ocean Eng.*, 113(2), 171-186.

- Kobayashi, N., and Tega, Y. (2002). "Sand suspension and transport on equilibrium beach." *J. Waterway, Port, Coastal, Ocean Eng.*, 128(6), 234-248.
- Kobayashi, N., and Wurjanto, A. (1990). "Numerical model for waves on rough permeable slopes." *J. Coastal Res.*, SI(7), 149-166.
- Kobayashi, N., Cox, D.T., and Wurjanto, A. (1990). "Irregular wave reflection and runup on rough impermeable slopes." *J. Waterway, Port, Coastal and Ocean Eng.*, 116(6), 708-726.
- Kobayashi, N., and Wurjanto, A. (1992). "Irregular wave setup and run-up on beaches." *J. Waterway, Port, Coastal, Ocean Eng.*, 118(4), 368-386.
- Kobayashi, N., DeSilva, G.S., and Watson, K.D. (1989). "Wave transformation and swash oscillation on gentle and steep slopes." *J. Geophys. Res.*, 94(C1), 951-966.
- Kobayashi, N., Zhao, H., and Tega, Y. (2005). "Suspended sand transport in surf zones." *J. Geophys. Res.*, 110, C12009, doi:10.1029/2004JC002853.
- Kobayashi, N., Agarwal, A., and Johnson, B.D. (2007a). "Longshore current and sediment transport on beaches." *J. Waterway, Port, Coastal, Ocean Eng.*, 133(4), 296-304.
- Kobayashi, N., Farhadzadeh, A., and Melby, J.A. (2007c). "Structures of storm surge disaster prevention." *Proc. 4th International Workshop on Coastal Disaster Prevention, Yokohama, Japan*, 41-49.
- Kobayashi, N., Payo, A., and Schmied, L. (2008a). "Cross-shore suspended sand and bedload transport on beaches." *J. Geophys. Res.*, 113, C07001, doi:10.1029/2007JC004203.
- Kobayashi, N., de los Santos, F.J., and Kearney, P.G. (2008d). "Time-averaged probabilistic model for irregular wave runup on permeable slopes." *J. Waterway, Port, Coastal, Ocean Eng.*, 134(2), 88-96.

- Kobayashi, N., Payo, A., and Johnson, B.D. (2008b). "Suspended sand and bedload transport on beaches." Handbook of Coastal and Ocean Engineering, World Scientific, Singapore (in press).
- Kobayashi, N., Pozueta, B., and Melby, J.A. (2003). "Performance of coastal structures against sequences of hurricanes." J. Waterway, Port, Coastal, Ocean Eng., 129(5), 219-228.
- Kobayashi, N., Herrman, M.N., Johnson, B.D., and Orzech, M.D. (1998). "Probability distribution of surface elevation in surf and swash zones." J. Waterway, Port, Coastal, Ocean Eng., 124(3), 99-107.
- Kobayashi, N., Meigs, L.E., Ota, T., and Melby, J.A. (2007b). "Irregular breaking wave transmission over submerged porous breakwaters." J. Waterway, Port, Coastal, Ocean Eng., 133(2), 104-116.
- Kobayashi, N., Buck, M., Payo, A., and Johnson, B.D. (2008c). "Berm and dune erosion during a storm." J. Waterway, Port, Coastal, Ocean Eng. (in press).
- Kriebel, D.L., and Dean, R.G. (1985). "Numerical simulation of time-dependent beach and dune erosion." Coastal. Eng., 9, 221-245.
- Large, W.G., and Pond, S. (1981). "Open ocean momentum flux measurements in moderate to strong winds." J. Phys. Oceanography, 11, 324-336.
- Lentz, S., Guza, R.T., Elgar, S., Feddersen, F., and Herbers, T.H.C. (1999). "Momentum balances on the North Carolina inner shelf." J. Geophys. Res., 104(C8), 18,205-18,226.
- Losada, I.J., Lara, J.L., Guanche, R., and Gonzalez-Ondina, J.M. (2008). "Numerical analysis of wave overtopping of rubble mound breakwaters." Coastal Eng., 55, 47-62.

- Madsen, O.S., and Grant, W.D. (1976). "Quantitative description of sediment transport by waves." *Coastal Engineering* 1976, Proc. 15th Coastal Engineering Conf., ASCE, Reston, Va., 1093-1112.
- Madsen, O.S., Chisholm, T.A., and Wright, L.D. (1994). "Suspended sediment transport in inner shelf waters during extreme storms." *Coastal Engineering* 1994, Proc. 24th Coastal Engineering Conf., ASCE, Reston, Va., 1849-1864.
- Masselink, G., Austin, M.J., O'Hare, T.J., and Russell, P.E. (2007). "Geometry and dynamics of wave ripples in the nearshore zone of a coarse sandy beach." *J. Geophys. Res.*, 112, C10022, doi:10.1029/2006JC003839.
- Mei, C.C. (1989). *The applied dynamics of ocean surface waves*. World Scientific, Singapore.
- Melby, J.A., and Kobayashi, N. (1998). "Progression and variability of damage on rubble mound breakwaters." *J. Waterway, Port, Coastal, Ocean Eng.*, 124(6), 286-294.
- Nairn, R.B., and Southgate, H.N. (1993). "Deterministic profile modelling of nearshore processes. Part 2. Sediment transport and beach profile development." *Coastal Eng.*, 19, 57-96.
- Neves, M.G., Reis, M.T., Losada, I.J., and Hu, K. (2008). "Wave overtopping of Póvoa de Varzin breakwater: Physical and numerical simulations." *J. Waterway, Port, Coastal, Ocean Eng.*, 134(4), 226-236.
- Phillips, O.M. (1977). *The dynamics of the upper ocean*. Cambridge Univ. Press, Cambridge, U.K.
- Powell, M.D., Vickery, P.J., and Reinhold, T.A. (2003). "Reduced drag coefficient for high wind speeds in tropical cyclones." *Nature*, 422, 279-283.

- Press, W.H., Flannery, B.P., Teukolsky, S.A., and Vetterling, W.T. (1989). Numerical recipes. The art of scientific computing. Cambridge Univ. Press, New York, NY.
- Ribberink, J.S. (1998). "Bed-load transport for steady flow and unsteady oscillatory flows." Coastal Eng., 34, 59-82.
- Ribberink, J.S., and Al-Salem, A.A. (1994). "Sediment transport in oscillatory boundary layers in cases of rippled beds and sheet flow." J. Geophys. Res., 99, 12,707-12,727.
- Ruessink, B.G., Miles, J.R., Feddersen, F., Guza, R.T., and Elgar, S. (2001). "Modeling the alongshore current on barred beaches." J. Geophys. Res., 106(C10), 22,451-22,463.
- Seymour, R., Guza, R.T., O'Reilly, W., and Elgar, S. (2005). "Rapid erosion of a small southern California beach fill." Coastal Eng., 52, 151-158.
- Shi, F., Kirby, J.T., and Hanes, D.M. (2007). "An efficient model-splitting method for a curvilinear nearshore circulation model." Coastal Eng., 54, 811-824.
- Shi, F., Johnson, B., and Kobayashi, N. (2008). "2DH modeling of waves, currents and sediment transport at FRF during Hurricane Isabel." 2008 Ocean Sciences Meeting, American Geophysical Union, Orlando, Florida.
- Smith, J.M., Sherlock, A.R., and Resio, D.T. (2001). "STWAVE: Steady-state spectral wave model user's manual for STWAVE, version 3.0." ERDC/CHL SR-01-1, Coastal and Hydraulics Laboratory, US Army Corps of Engineers, Vicksburg, Miss.
- Schüttrumpf, H. (2001). "Wellenüberlaufströmung bei Seedeichen – Experimentelle und theoretische untersuchungen." Ph.D. thesis, Leibniz-Institute for Hydraulics, Technical Univ. of Braunschweig, Braunschweig, Germany.
- Schüttrumpf, H., and van Gent, M.R.A. (2003). "Wave overtopping at sea dikes." Proc. Coastal Structures'2003, ASCE, Reston, Va., 431-443.

- Schüttrumpf, H., and Oumeraci, H. (2005). "Layer thickness and velocities of wave overtopping flow at sea dikes." *Coastal Eng.*, 52, 473-495.
- Svendsen, I.A., Haas, K., and Zhao, Q. (2002). "Quasi-3D nearshore circulation model SHORECIRC version 2.0." Res. Rep. No. CACR-02-01, Center for Applied Coastal Research, Univ. of Delaware, Newark, Del.
- Tega, Y. and Kobayashi, N. (1996). "Wave overwash of subaerial dunes." *Coastal Engineering* 1996, Proc. 25th Coastal Engineering Conf., ASCE, Reston, Va., 4148-4160.
- Tega, Y., and Kobayashi, N. (1999). "Numerical modeling of overwashed dune profiles." Proc. Coastal Sediments'99, ASCE, Reston, Va. 1355-1370.
- Thornton, E.G., Humiston, R.T., and Birkemeier, W. (1996). "Bar/trough generation on a natural beach." *J. Geophys. Res.*, 101, 12,097-12,110.
- Trowbridge, J., and Young, D. (1989). "Sand transport by unbroken water waves under sheet flow conditions." *J. Geophys. Res.*, 94, 10,971-10,991.
- van der Meer, J.W., Bernardini, P., Snijders, W., and Regeling, E. (2006). "The wave overtopping simulator." *Coastal Engineering* 2006, Proc. 30th Coastal Engineering Conf., World Scientific, Singapore, 4654-4666.
- van Gent, M.R.A. (1995). "Porous flow through rubble-mound material." *J. Waterway, Port, Coastal, Ocean Eng.*, 121(3), 176-181.
- van Gent, M.R.A. (2001). "Wave runup on dikes with shallow foreshores." *J. Waterway, Port, Coastal, Ocean Eng.*, 127(5), 254-262.
- van Gent, M.R.A. (2002a). "Wave overtopping events at dikes." *Coastal Engineering* 2002, Proc. 28th Coastal Engineering Conf., World Scientific, Singapore, 2203-2215.

- van Gent, M.R.A. (2002b). “Low-exceedance wave overtopping events: Measurements of velocities and the thickness of water-layers on the crest and inner slope of dikes.” Delft Cluster Report DC030202/H3803, Delft Hydraulics, Delft, The Netherlands.
- van Gent, M.R.A., Coeveld, E.M., Walstra, D.J.R., van de Graaff, J., Steetzel, H.J., and Boers, M. (2006). “Dune erosion tests to study the influence of wave periods.” Coastal Engineering 2006, Proc. 30th Coastal Engineering Conf., World Scientific, Singapore, 2779-2791.
- van Rijn, L.C., Walstra, D.J.R., Grasmeijer, B., Sutherland, J., Pan, S., and Sierra, J.P. (2003). “The predictability of cross-shore bed evolution of sandy beaches at the time scale of storms and seasons using process-based Profile models.” Coastal Eng., 47, 295-327.
- Wurjanto, A., and Kobayashi, N. (1993). “Irregular wave reflection and runup on permeable slopes.” J. Waterway, Port, Coastal, Ocean Eng., 119(5), 537-557.